UNIVERSITÀ DEGLI STUDI DI PALERMO

Dottorato di Ricerca in Scienze Fisiche

Dipartimento di Fisica e Chimica - DiFC

SSD FIS/07

# Statistical Characterization and Agent-Based Modelling of the Air Transportation Socio-technical Complex System

PHD CANDIDATE

**CHRISTIAN BONGIORNO**

COORDINATOR

**PROF. GIOACCHINO MASSIMO PALMA**

TUTOR

**PROF. SALVATORE MICCICHÈ**

CICLO XXIX

2017

# Contents

# 1 Introduction

## 1.1 Overview

In the course of my studies I conducted empirical analysis on real-life complex systems; specifically, I focused on agent-based models and complex networks. The aim of the present dissertation is to provide both a complete perspective of the results I achieved and an overview of the tools necessary to approach these systems. In this introduction, I will, firstly, explore the concepts of complexity and emergence from a general point of view; then, I will proceed to present an introductory description of the real systems that I studied; finally, I will present a short overview of the work I have done on these systems.

## 1.2 Complexity and Emergence

In recent years, some physicists have developed an interdisciplinary approach to their work; the development of statistical physics, in particular, has proved extremely useful in analysing social [1], biological [2] and socio-technical systems [3]. The first moves away from classical physics and towards an interdisciplinary approach occurred when researchers faced complexity. Describing complexity is, of course, a hard task as a unique definition of it does not exist. Researchers usually talk about complexity when a system exhibits a new form of organization, more specifically complexity occurs when the relationship between the parts of a system give rise to a collective behaviour [4, 5].
Although an emerging behaviour is typically observed in social or biological systems, physical systems can also exhibit such properties. A well known example from the physical field is water [6]; water's properties can be considered as an emerging phenomenon as

they are unpredictable even after exhaustive studies of its constituents i.e. hydrogen and oxygen. Another physical example of emergent phenomena is friction; friction being the force that resists the relative motion of two surfaces sliding against one another. Such force emerges from the microscopic complex texture of the surfaces, whose interaction by sliding converts mechanical energy into heat energy.
This construct of emergent behaviour can equally be applied to human organization. Among many examples, the complexity of the urban environments in which humans live [7] is incontrovertible evidence for emergent behaviour in human organization. Even in the absence of predefined planning, the social interactions of people in urban areas, over time, will lead to an efficient organization of these areas. Emergence is, therefore, a universal concept that transcends almost all branches of knowledge and science, grounded always in the idea that microscopic heterogeneous interactions can produce surprising macroscopic behaviour.
As a consequence, when researchers deal with emerging behaviours, the reductionist approach widely used in classical physics – that a phenomenon can be kept apart from the rest of the system – must, in many cases, be abandoned. In fact, the removal of the object of study from the environment in which it exists might imply the disappearance of the emerging phenomenon. New tools and methodologies, beyond what classical physics offered, are therefore necessary to study such open and intrinsically self-interacting systems.

Despite the common presence of emerging phenomena both in social and thermodynamic systems, the expression "complex system" is typically reserved for those systems whose behaviour *crucially depends upon tiny details* [8].
To highlight this difference let us think about thermodynamics. Originally, the study of thermodynamics focused on probabilistic and macroscopic descriptions of the states of the system, since the extremely high number of particles involved makes it practically impossible to write down the equations of motion. Even if these equations were possible, producing the solution, given the extremely high number of coupled equations, would be a huge task.
Despite these analytical issues, the observation of a particular collective state in some

thermodynamic conditions is possible and such thermodynamic states can be fully and uniquely understood in terms of the main thermodynamic parameters: pressure, volume, temperature and number of particles. Let us think, for example, about water that is boiling at 100 degrees. Such collective state is essentially always verified in our experience. Which means that, it is definitively independent by the configurations of the water particles. On the contrary, in a complex system, a negligible difference of some boundary conditions can produce a totally different final state.

To understand better the peculiarities of complex systems, let us now consider Dynamical Systems. A Dynamical system is a system in which a *known* function describes the time dependence of an object in a state space. That means that the knowledge of the current state implies the knowledge of the future states. However many systems, characterized by a significant number of heterogeneous interacting entities, and sometimes also extremely simple ones with a non-linear coupling of the variables, like the double pendulum [9], have in certain conditions shown surprisingly unpredictable dynamics: they are chaotic [10]. The physics of a chaotic system is deterministic, however in a chaotic system a long-range prediction cannot be done with accuracy. The initial appearance of disorder is grounded in the unpredictability of the system. The intrinsically unpredictable nature of the system dynamic is shown by trying to reproduce exactly the same set up of the experiment, which is impossible. Such surprising behaviour is in part caused by the strong sensitivity of small initial conditions to variation. Obviously, in theory, perfect knowledge of such initial conditions[1] could permit us to make predictions; however, the presence of errors, no matter how small, is inevitable, and the strong sensitivity of the initial conditions leads to an intrinsic unpredictability of the system dynamic [11]. As a consequence in many real systems the paradigm of the perfect prediction has been undermined.
Similarly to what happens in the case of thermodynamic, whilst the huge amount of heterogeneous information has limited the predictive power of the micro-structure, the aggregation, in many cases, seems predictable and it has typical patterns among very different systems, like powerlaw tails [12], community structures [13] and hierarchical or-

[1] combined with infinite computational power and the knowledge of the dynamical equations

ganization [14]. Therefore the interest of scientists in such systems has moved from the lower unpredictable level to the higher aggregate level, which shows non-trivial emerging properties. A remarkable example is the Omori law of earthquakes [15], that is: the empirical prediction of the intensity of the aftershock subsequent to a primary strong earthquake. Although it is not possible to forecast when or where they will occur, their intensity show a powerlaw decay over time.

The current interest in complex systems has caused physicists to move away from classical models to deal with open systems. In natural science, an open system allows the environment to exchange both matter and energy with it. A closed system, on the other hand, can exchange only energy with the environment, not matter. For this reason, a complex system requires a different approach; new techniques have been developed to do this. These techniques ensure that external interactions with the environment can be considered. Many of these new methodologies were transposed from other disciplines, such as sociology or biology, in which dealing with open systems is the norm; a social or biological system can almost never be isolated from its environment. When dealing with social complex systems, computer simulations are usually the preferred method of analysis because analytical resolutions are inapplicable. In particular, a class of computational algorithms, named Agent-Based Models (ABM), has gained a primary position in modelling emerging phenomena in social systems. The use of such computational methods allows researchers to overcome two big problems of complex systems in the following ways: first, they permit the inclusion of heterogeneous entities; and, second, they allow the modelling of the interaction between such entities and the environment without a perfect formal knowledge of the fundamental equations that rule the dynamics. A more detailed discussion of ABM will be undertaken in the following section.

## 1.3 Agent-Based Models in Statistical Physics

To face complexity physicists have developed specific tools designed to highlight the collective behaviour of such systems. In particular in my research activities, I focused

my interest on complex networks and Agent-Based Models (ABM). In the following I will briefly describe agent-based models that are the central part of this dissertation.

A popular way to investigate emerging phenomena observed in reality is agent-based modelling [16, 17]. The main advantage of an ABM is that it can model interactions among autonomous agents, mainly by computational simulation. It is worth noting that an ABM is conceptually different from the simulator approach widely used in engineering science. In fact, an ABM should be designed bearing in mind the parsimony principle[18], i.e. just few specific characteristics of the agent interactions are included in the model whereas most of the environmental or individual peculiarities are kept apart. A simulator, on the contrary, tries to reproduce in detail the dynamic of each component of the system. ABMs have drawbacks: the simplicity of them can limit their predictive power. However, there are also great advantages, for example: the observation of an emerging phenomenon in such a simple controllable toy system represents strong clues about the real causes of the emergence[19]. A historical example of this approach is the segregation model of Schelling[20], which shows a critical transition to segregation in a very basic modelling of interactions. More specifically, Schelling modelled two types of entities/agents, let us say "black" and "white" that lay on a bidimensional grid. Starting from a random initial condition with a homogeneous distribution of the two colors, at each time-step some agents could be moved to another position on the grid according to a predefined rule. Such a rule is the "intolerance to diversity". In fact, if an agent has a fraction of neighbours $p$ of an opposite color, then he will decide to move to another place of the grid. Surprisingly even for a small probability of the intolerance of diversity $p \simeq 0.37$, the collective stationary states will be composed of segregated groups of agents of the same color. For a lower value of $p$ no segregated groups will be present in the system.

Later the development of ABMs became more and more refined. At present, they often include some social peculiarities like learning processes or heterogeneous agents. In modern ABMs, agents usually hold the following features [21]: i) perception i.e. agents can perceive their environment and also the other agents in their neighbourhood; ii) performance i.e. they have a set of actions that they can perform; iii) memory i.e. they

have a memory storing a set of information; iv) policy i.e. they have a set of heuristic rules that control their response to external stimulus.

Another specific and fundamental characteristic of ABMs is the level of abstraction that can be used to build them: the lower the level of abstraction, the more detailed the modelling; the higher level of abstraction, the more simplified the modelling will be – this is usually done by describing the dynamic through aggregate variables/entities[22]. An example of a highly abstract ABM is the Schelling model[20] that we have just described above, or the one in Ref.[23]. In that paper the authors proposed an ABM approach to solve the problem of molecular self-assembly by using a heuristic set of rules. Those rules are applied to rigid tetris-shape objects. Despite the simplicity of the model, it showed both near optimal aggregates and require less computer processing than Monte-carlo simulations, commonly used in literature[24]. At the low level of abstraction, in Ref.[25], an ABM was used to map the spreading of a disease in Italy. Such a model takes into account the very detailed structure of social interactions, including differences between households, schools and workplaces, movement between different cities and vaccine supplies. The results of this ABM were broadly similar to epidemic patterns historically [26].

Once the optimal setup for the ABM is chosen, a computational investigation is performed and the experiment can be repeated many times even varying the environment or behavioural parameters, which is of course impossible for a real social system. Indeed, the possibility to include "what-if" experiments in the analysis makes the ABM approach much more similar to methods of investigation used in the field of physics, rather than those used in the field of social science.

Historically agent-based modelling has been commonly used in the domain of sociology. Recently, physicists have become increasingly interested in it. The stochastic motion of diffusing particles can be described by Langevin equations, however, to explain their ability to react chemically, the introduction of a self-consistent field for the particles is required. That field induces a self-adaptive process which produces the structural formation. This is called active Brownian motion[27]. Unlike standard Brow-

nian particles, active particles can take energy from the environment by local or global coupling. Agent-based modelling was used to describe such systems[28]. The authors showed that the complex collective motion observed can be explained as the result of the active motion of the agents with their mutual interactions. Then the resulting complex behaviour of the swarm of particles emerged from two opposite influences: the active motion of the particle/agents that drives the swarm to disperse, and the local attraction of the particles/agents that drives to concentrate into a swarm. The swarm intelligence [29] is, indeed, a self-organized collective behaviour observed both in natural and artificial systems, for example animal herding. Typically the observation of such peculiar behaviour needs the presence of interacting autonomous agents that can be easily modelled by ABMs [30, 31].

Another important contribution that physicists introduced to agent-based modelling was to mix a physical framework with social or biomedical one. For example, Ref.[32] studied the transport of nano particles in blood flow with an ABM based around fluid dynamic equations. Another example is in Ref.[33] where the authors described urban evacuation planning again using fluid dynamic equations.

Even if the rules of the micro-structure were not modelled as physical equations, the statistical mechanic approach was crucial in many cases to understand the underlying rules governing those systems, for example in minority games[34]. The minority games are an extension of the El Farol bar problem. This problem, proposed by Brian Arthur in Ref.[35], sets out the following scenario: suppose one wants to listen to music every Thursday in the El Farol bar. If the bar is too crowded one can no longer listen to the music. A paradoxical result is produced by supposing that all customers in the bar are informed in the same way. In fact, if all the customers think that just a few people will go to the bar, then the bar will be crowded; on the other hand, if all the people think that the bar will be crowded, then nobody will go to the bar. Consequently, only mixed strategies, with not all the actors thinking in the same way, could provide solutions to the problem. In the minority game the agents have the further ability to make decisions according to previous knowledge of the subject, meaning that they can take advantage of

the available public information concerning recent bar attendance history. The adaptive agents, so defined, are shown to react according to mechanisms that are similar to those encountered in statistical mechanics. In fact, their stationary state is not the expected Nash equilibrium, with all the agents maximizing their utility function, but instead is the ground state of a disordered spin model that presents a richer dynamic [36], much like metastable states. Evidently, there is a similarity between this model and many other systems in which the active entities/particles interact with an external entity/field. For example in economics, where investors interact with the market basing their decisions on their previous knowledge. It is worth noting that this approach is opposed to the classic representative agent of macro-economic theory, which, by assuming all the agents are identical, produces a necessarily unique agent theory. In the minority games, as we have seen above, the agents heterogeneity is an essential condition to avoid frustrated behaviour.
Ultimately, the great advantage of an agent-based model is its wide applicability. In fact when just a small number of individuals participate in the dynamic, a deterministic approach, as mean-field, could be no more suitable; whereas an ABM can also show emerging phenomena when there is a small number of participants involved.

## 1.4 The Air Transportation System

As I mentioned above, in the course of my research I dealt with real-life complex systems. More specifically, I conducted an empirical statistical analysis and agent-based modelling of the Air Transportation Management (ATM). In the following section I will describe first the ATM system, focusing the attention to the main issues concerning its complexity, then I will summarise my approach.

### 1.4.1 General Description

Complex system theory has recently been used to try to better understand Air Transportation Management. One prominent example is a series of studies where the network topology of the airport network was investigated [37, 38, 39, 40, 41, 42]. Another study

focused its attention on the navigation points (NVPs) network [43]. NVPs are fixed bidimensional points in the airspace that are used in the ATM system to direct air traffic flow. This works in the following way: a few hours before departure flight plans are released that consist of sequences of NVPs that the aircraft must follow en route to the destination airport. An important aspect of airway infrastructure is its "inefficient" topology. In fact, an aircraft trajectory, for safety reason, is typically different from the shortest path between origin and destination airport. This is because an NVP-based systems is considered more controllable than a free-routing one because it allows the air traffic controllers (ATC) to focus their attention on a limited number of special NVPs where the routes intersects. A key figure of the ATM system are these ATCs. The main mission of the ATCs is to guarantee the safety of aircraft by maintaining a safe distance among them. They have the additional task to enhance the efficiency of the system, allowing the aircraft to follow the shortest path locally, only when air-traffic conditions permit it.
The growth of the ATM system – both the free routing and the increment of flight connections – are therefore constrained by the limits of human control of the system.

In 2012, around 9.5 million flights crossed European airspace and this number is expected to increase by 50% in the next 20 years [44]. Due to this traffic increase, without significant changes in the way air transport is currently managed, flying in Europe could lead to increased costs for the airlines, due to greater delays, and for the environment, due to higher $CO_2$ emissions. To tackle these challenges, the European Commission created in 2007 the SESAR JU (Single European Sky ATM Research Joint Undertaking) with the aim of coordinating all relevant research and development efforts in the sphere of aerospace in Europe. Since its inception SESAR has been working on defining, exploring, testing, and implementing new solutions to cope with the predicted increase in air traffic. The concepts of free-routing and 4D trajectories, for example, have been proposed [45, 46, 47] and are already implemented in some areas of the European Airspace [48]. In the future, or in what we call in the following, SESAR scenario, all airspace users will be allowed to plan an optimal trajectory, in space and time, from departure to arrival. This is a radical shift from the current practice whereby aircraft need to stick to the structure of the airspace network and follow pre-defined

airways which are often not the most direct routes. In this environment, air traffic controllers have the role of avoiding conflicts in some specific areas that are mainly located where airways intersect. The implementation of free-routing poses, therefore, some challenges in terms of the safety of the operations and the complexity of the situation that controllers have to manage. For instance, conflicts may become harder to detect due to the spread and increased number of possible conflicting points. Moreover, methods used to solve conflicts (i.e. direct routes) may not be applicable any longer since aircraft will be already flying the most direct trajectory.

### 1.4.2 Our Contribution

Although Free Route Airspace is already implemented in some parts of Europe [49], its application is still limited to conditions where traffic load is quite low. Therefore, it is relevant to assess its impact in the higher traffic conditions foreseen in the next 20 years, specifically, in relation to the safety of the operations and to the complexity that controllers will have to manage. To this end, we have developed an ABM to evaluate the implementation of some of the features foreseen by SESAR within the ELSA "Empirically grounded agent-based model for the future ATM scenario" project co-financed by EUROCONTROL on behalf of the SESAR Joint Undertaking in the context of SESAR Work Package E. The ELSA agent-based model is a two layer multi-agent model: the first layer is strategic, where the airline companies negotiate their flight plans with a Network Manager, taking into account that the flight plans must comply sector capacities. The outcome of the strategic layer is a flight plan that becomes the input of the second layer, the tactical one. In the tactical layer, pilots and controllers interact with each other, in particular pilots follow the released flight plans and controllers modify the aircraft trajectory to both solve potential conflicts and to enhance the system efficiency i.e. allowing aircraft to follow a free route locally if such a choice does not imply an increment of complexity. Within the ELSA project I developed the ABM of the tactical layer.

The specific scientific questions that I investigated are: *(i)* what are the issues that affect the predictability of the last filed flight-plan within the ATM system? How is the predictability affected by these issues? *(ii)* Can sectors capacity be improved by a more

efficient management of conflicts? *(iii)* What are the impacts of the changes foreseen by SESAR on the airspace management and on the controllers' workload? *(iv)* Are these changes able to accommodate efficiently the foreseen traffic increase?

### The characterization of the deviations from the planned trajectory

During the early phases of the development of the ABM, we performed a preliminary investigation of the ATM system with the aim of highlighting the ATC operations [50]. In this work we observed several regularities by comparing the planned flight plans (so called M1 files) with the radar tracked ones (so called M3 files) of the German airspace. At a global level we observed an important deviation from the Gaussian behaviour of the percentage increment of planned trajectory length, moreover these deviations are more pronounced during night-time. Another empirical observation regards the "angle to destination" hold by a flight when a deviation from planned trajectory occurs, this angle is typically of 20 degrees and it is significantly different with respect to a random null expectation. Both these facts suggest that optimization is an important task of the ATC and it can be revealed from data. Subsequently we focused our attention on a local NVP level, and we observed that only few NVPs are involved in flight trajectory deviation, and those NVPs are systematically over-deviated along different time-periods. The results achieved in Ref.[50] were useful to outline the development and the calibration of the ELSA ABM.

### Modelling the Tactical ATM: an Agent-Based Model Approach

ABMs are a consolidated tool in the Air Traffic Management domain. In our opinion, we can track down essentially three big research areas of applications of ABMs in ATM. In fact, we can have ABMs: (i) for the conflict detection and resolution [51], (ii) for the management of the traffic flow [52] and (iii) for the investigation of the aspects related to the role of human operators [53].

ABMs for the conflict detection and resolution intervene at a tactical or pre-tactical level and provide methods for detecting and solving (multiple) conflicts on a pairwise or global basis. In Ref.[51] a set of categories has been proposed for the categorization of the different modeling approaches. For example, these categories include the

dimensions at which the model works (vertical, horizontal or both), the method of conflict resolution (optimization, brute force, force field, etc.) and the type of maneuvers adopted by aircraft to avoid the conflict (vectoring, flight level changes and velocity changes). Among others, the work in Ref.[54] has received much attention, although it was not used at an operational level: it proposed a global method for conflict resolution based on genetic algorithms and taking into account future velocity uncertainties. The conflict detection and resolution algorithm of Ref.[55] is based on a local geometrical resolution of conflicts involving a combination of velocity changes and re-routings. Using the geometric characteristics of aircraft trajectories and intuitive reasoning, closed-form analytical solutions have been developed for optimal heading and/or speed commands. The conflict resolutions are optimal in the sense that they minimize the velocity vector changes required for conflict resolution, resulting in minimum deviations from the nominal trajectory. Another interesting approach is the conflict detection and resolution algorithm of Ref.[56] that is based on a potential field approach that in its original and simplistic version assumes that aircraft are like charged particles interacting in an external electric potential field. In Ref.[52] a multi-agent model is proposed where two features are implemented: agent are endowed with reinforcement learning algorithms and they are individually (rather than globally) rewarded in terms of their contribution to the overall performance of the system. This will ensure a better managing of congestion issues obtained by issuing ground delays, re-routings and setting separation between aircraft. The input to the model is given by a set of trajectories generated by FACET [57]. FACET is a simulation and analysis tool that provides flight trajectories that follow a set of navigation points between the origin and destination airport. The trajectories can be made conflict free by using an additional module that performs aircraft self-separation by using either the algorithm of Ref.[55] or the algorithm of Ref.[56]. The model proposed in Ref.[58] proposed a global optimization of the system by taking advantage of the capabilities of specific causal models, namely the Colored Petri Network models. The detection of conflicts is followed by a geometrical local resolution of conflicts [55] that is iterated until all secondary possible conflicts are resolved. The optimal or suboptimal solutions thus proposed for each aircraft are then used to feed the considered causal model that will select the ones that solve simultaneously all conflicts

through a certain scoring procedure. However, the model works on idealized trajectories connecting the departure and arrival airports in a rectilinear way.

The agents of our agent-based model are aircraft pilots and air traffic controllers who are active within Area Control Centers (ACC) in the European airspace. The pilots are passive entities: they follow a flight plan, or the instructions of the ATCs; ATCs, on the other hand, are active entities and monitor, control and modify the flight plan. ATCs' actions are influenced by the current workload of the sectors they manage and by the workload of neighbouring sectors. Furthermore, the local geometry of the flight plans indirectly influences their actions. In the tactical phase of the air traffic management, we model and simulate the events of a planned flight plan, transforming it into an actual one. Therefore we are in the tactical phase of the air traffic management. The model we propose here provides a conflict detection module based on the computation of the pairwise distances between all aircraft present in a certain airspace and also provides a module for the pairwise local resolution of conflicts at a tactical level [59]. The approach of Ref.[55] is very close in spirit to the one presented here, where, however, the resolution algorithm works on the basis of numerical simulations. We also implemented a module for the issuing of directs. When possible, directs are issued by controllers at a tactical level in order to speed up the passage of aircraft within a certain airspace and therefore to facilitate the airline operations. We believe that this is one of the novelties of our model, not present in the ABMs we have recalled above.
Our model performs a local conflict detection and resolution procedure mainly based on geometric considerations and mainly working at the level of an ACC. Subsequently, once trajectory has been made conflict-free, it searches for possible improvements of the system efficiency by issuing directs. The issuing of directs is the place where the controllers behavior is most evident. Indeed, the way we implement the strategies adopted by controllers to issue directs is based on information relative to each specific sector in the airspace as well as information relative to the entire considered airspace. This is done having in mind that controllers of a certain ACC all work in the same physical place and therefore that induces the emergence of "best practices" shared by the controllers of the entire ACC.

Once the model was developed, a calibration procedure was performed. The aim of the calibration was to reproduce the stylized facts illustrated above, in particular we focused in the intra-day dynamic of the flight deviation rate. We calibrated the model with respect to three parameters: the first two refer to the direct operations and they are respectively an unconditional probability of direct and a sensitivity to sector traffic congestion, the third parameter is the lookahead of the ATC, used in his forecast to guarantee the minimum safety separation between aircraft.
We showed that a calibrated model can be used to discover zones of the airspaces that require a significant activity of the ATC. In the same work we showed that the spatial heterogeneity of the ATC operations can be observed also from data. However, differently from the ABM simulations, in real data the real compositions of the ATC operations cannot be discovered, in fact an horizontal deviation can occur either for network optimization (direct) or for safety reasons(re-routing). As a second step we showed that the exploration of the range of parameters can be used to perform scenario simulations, for example we relaxed the sensitivity on the traffic congestion of our ATC, and we showed how it can impact on safety. In particular we observed weak but significant linear relations between direct and safety operations, moreover this relation is still present also in condition of noisy forecast of the ATC.
The useful results obtained in this work let us believe that the ELSA ABM will be a valid tool to test the inefficiency of the air transportation network for the present and for the future scenarios.

### The free route scenario

One of the strongest interests of the Airport Transport Management (ATM) community is the development of a free-routing system, i.e. an air transportation system where the routes of the aircraft coincide with the shortest geodetic path. The ELSA ABM was used to implement this concept on simulated trajectories that preserve the same statistical regularities observed in real trajectories [60]. Our analysis was first focused on the Italian ACC LIRR. Later we extended our results to a set of 15 different European ACCs. Specifically, we implemented two concepts of the new SESAR scenario: the free-

routing and de-conflicted flight plans. In order to explore the free-routing concept, we introduced a new technique that performs a slow transition of the current ATM network towards the SESAR scenario. Our approach was based on a local uniform correction of the flight plans, controlled by a network efficiency parameter, taking the value of 1 only in the SESAR scenario.

Furthermore, as mentioned above, we implemented the concept of de-conflicted flight plans on our simulated trajectories. This was done by a brute force algorithm, that recursively shifted in time the flight departures until no conflict was detected by our module. It is worth noting that if the flight plans in this scenario are precisely executed, no conflicts will be detected by our ABM. However the real-life execution of a flight plan must take into account several variables that can affect our result. We modelled such uncertainty with a random uniform delay of the aircraft departure. As a result, the delayed flight plans could not be de-conflicted any longer.
The aim of the investigation is to test the resilience of the de-conflicted flight plan concept on different networks. Such networks are defined by ranging the efficiency parameter from the current scenario towards the new SESAR scenario. Our ultimate goal is to identify, from a safety and predictability point of view, which scenario is most suitable to accommodate inevitably unforeseeable events.

After performing numerical simulations with the model, we have shown that in a free-routing scenario the controllers perform less operations although these operations are dispersed over a larger portion of the airspace. This can potentially increase the complexity of conflict detection and resolution for controllers. Furthermore, by investigating all the intermediate scenarios, we observed two different regimes, which are regulated by two linear laws. These laws connect the observed number of ABM operations with the number of operation that we should expect. Specifically the slope of such linear law becomes 5 times bigger when the efficiency parameter approaches the SESAR scenario. Another important aspect that we investigated is the relationship between conflicts and traffic demand. We observed that the operations performed by the ABM increase with the square of the number of aircraft. This observation is very robust along all the transition to the free-routing. However we have highlighted that such scaling can be modified by a severe constraint on the sectors capacity.

## 1.5 Outline of the Thesis

This dissertation is organized as follow: in chapter 2 we discuss an empirical investigation of the ATM system performed with the aim of highlighting the ATC operations from data, the results obtained here were published in Ref.[50]. The results achieved in chapter 2 were useful to outline the development and the calibration of the ELSA ABM. In chapter 3 we describe each module of our ABM in detail, in particular we focus on the time-step configuration, the conflict detection and resolution module, and the direct module. In chapter 4 we describe the procedure that we used to generate the input data necessary in order to perform the simulations both of current and SESAR scenario. Finally in chapter 5 we discuss the results of ABM simulations. In particular, in section 5.1 we show the calibration activities performed, in section 5.2 we show that a calibrated model is able to reproduce stylized facts of the ATM system, and in section 5.3 we characterize the behavioural parameters of our ATC agents, such work was used to write the pre-print of Ref.[61]. In chapter 5.4 we show our prediction on the future SESAR scenario based on our ABM simulations, part of this work was published in Ref.[60].

# 2 Statistical Characterization of Flight Deviations

In the recent literature it is possible to find many examples where network science has been applied to the air transportation system (for a review, see [37, 3]). Many studies have focused on the topological aspect of the airport network [38, 39, 40, 41, 42, 62, 63, 64, 65, 66, 67, 68], but network science techniques can also be used to study topics more related to air traffic management [69, 70, 71, 72, 73, 74, 75, 76, 77, 78, 79]. In particular, one can consider different elements of the airspace like sectors and navigation points and build networks which are informative about the air traffic management [43]. In fact, differently than the airport network, navigation point networks are more related to air traffic management problems and to safety issues.

In this chapter, we present a study of the air traffic management procedures controlling the flow of flights occurring on top of the navigation point network. Navigation points are fixed two dimensional points in the airspace specified by latitude and longitude. The airlines must use this grid to plan each flight trajectory from departure to destination. Navigation points are also of reference for air traffic controllers who use them to solve conflicts and problems originated by unforeseen events and to rationalize and decrease the complexity of the aircraft flow. The navigation points can be viewed as a guide for airlines, but also as a burden, because flights cannot fly straight and have to find a path on this predefined grid. In fact, it is foreseen by the SESAR project [80] that navigation points will slowly disappear to allow smooth trajectories, the so-called "business" trajectories. However, in the present air transportation system they are crucial for air traffic controllers. It is worth mentioning that some areas of ECAC have implemented free-routes already, for example Maastricht ACC, although such ACCs cover just a small

amount of ECAC airspace.

In our study we investigate how the planned flight trajectories are modified by controllers in relationship with unforeseen events or pilots' requests. Our study is based on a metric called directional-fork, or *di-fork*, comparing planned flight trajectories with deviated flight trajectories. By using this metric we obtain a quantitative description of the deviations of planned flight trajectories called by air traffic controllers at the level of single navigation point pairs. The activity of air traffic controllers usually concerns two main aspects: on one side they are responsible for loss of safety and for making the aircraft trajectories conflict-free. On the other side, whenever possible, they can issue directs that $(i)$ shorten trajectories, thus allowing for lower fuel consumption, and $(ii)$ can improve the predictability of the system. In our investigations we show that directs are the main determinants for the probability of flight trajectory deviations.

We perform a statistical validation of the navigations point pairs by comparing the observed values of the di-fork metric with the values expected under a null hypothesis of deviations occurring at randomly distributed navigation point pairs. In other words, we investigate how the different navigation points present in a given airspace are used by air traffic controllers over the day. Specifically, we detect navigation point pairs where trajectories $(i)$ are most likely to be deviated with respect to the planned ones, thus providing a "destabilization" of the planned trajectory, or $(ii)$ are most likely not to be deviated with respect to the planned ones, thus providing a "stabilization" of the planned trajectory.

The chapter is organized as follows: in section 2.1 we describe the database used in our investigation. Section 2.2 deals with the statistical investigation of planned flight trajectories. Section 2.3 focuses on the statistical properties of flight deviations observed from the planned flight trajectories. Section 2.4 introduces the di-fork and the statistical validation method used to detect a set of over-expressed and under-expressed navigation point pairs.

## 2.1 Data

Our database contains information on all the flights that, even partly, cross the ECAC airspace. Data are collected by EUROCONTROL (http://www.eurocontrol.int), the European public institution that coordinates and plans air traffic control for all Europe and were obtained as part of the *SESAR Joint Undertaking* WP-E research project ELSA "Empirically grounded agent based model for the future ATM scenario". [1]

Data come from two different sources. First, we have access to the Demand Data Repository (DDR) [81] database containing all the trajectories followed by any aircraft in the ECAC airspace during 15 months – from the $8^{th}$ of April 2010 to the $27^{th}$ of June 2011. Each 28 day time period is termed AIRAC cycle. A planned or realized trajectory is made by a sequence of navigation points crossed by the aircraft, together with altitudes and timestamps. The typical time between two navigation points lies between 1 and 10 minutes, giving a good time resolution for trajectories. In this work we use the "last filed flight plans", i.e. the so-called M1 files, which are the planned trajectories – filed from 6 months to one or two hours before the real departure. We also use the real trajectories, i.e. the so-called M3 files, because we will compare planned and actual trajectories in order to investigate the air traffic controllers role. It is worth mentioning that the last filled flight plans (M1 files) already incorporate airline preferences. In fact, we have also checked that M1 and M3 files do not show dramatic differences. Indeed, we do not have access to data relative to the initial flight plan, and that prevented us from performing a rigorous study on the way airline preferences affect the overall performances of the system. We might only recall that the issue of airline preferences was touched upon in Ref.[60].

In our study we are considering commercial flights. For this reason we have selected only scheduled flights – excluding, in particular, military flights – using land-plane aircraft, i.e. no helicopter, gyrocopter, etc. This gives, in first approximation, the full set of commercial flights. We also excluded all flights having a duration shorter than 10 minutes and a few other flights having obvious recording data errors.

[1] Data can be accessed by asking permission to the legitimate owner (EUROCONTROL). The owners reserve the right to grant/deny access to data.

The database includes all flights in the enlarged ECAC airspace [2] even if they departed and/or landed in airports external to the enlarged ECAC airspace.

The other source of information are the NEVAC files. NEVAC files [3] contain all the elements allowing the definition (borders, altitude, relationships, time of opening and closing) of the elements of airspaces, namely airblocks, sectors, airspaces (including Flight Information Region, National Airspace, Area Control Center, etc.). The active elements at a given time constitute the configuration of the airspace at that time. Thus, they give the configuration of the airspaces for an entire AIRAC cycle. Here we only use the information on sectors, airspaces and configurations to rebuild the European airspace. Specifically, at each time we have the full three dimensional boundaries of each individual sector and airspace in Europe. All this information have been gathered in a unique database, using MySQL, in order to allow fast crossed queries. The last filled flight plans (M1 files) are released a few hours before departure. Therefore they already incorporate the fact that some sectors might be closed due to military operations. This is why we did not consider them in our analysis at all. In any case, the way we might treat sudden closures of sectors caused by military operations is essentially the same we use to consider disruptions due to extreme weather events. Therefore, having the information about what are the portions of airspace closed for military operations, we might consider such situation with very minor modifications of our model.

Our investigations are mainly performed considering the flights relative to the AIRAC 334, i.e. the AIRAC starting on May 6, 2010 and ending on June 2, 2010. Data relative to other AIRACs are considered in order to check the stability of our results. We only consider flights that cross the German airspace, which is one of the European regions

[2] Countries in the enlarged ECAC space are: Iceland (BI), Kosovo (BK), Belgium (EB), Germany-civil (ED), Estonia (EE), Finland (EF), UK (EG), Netherlands (EH), Ireland (EI), Denmark (EK), Luxembourg (EL), Norway (EN), Poland (EP), Sweden (ES), Germany-military (ET), Latvia (EV), Lithuania (EY), Albania (LA), Bulgaria (LB), Cyprus (LC), Croatia (LD), Spain (LE), France (LF), Greece (LG), Hungary (LH), Italy (LI), Slovenia (LJ), Czech Republic (LK), Malta (LM), Monaco (LN), Austria (LO), Portugal (LP), Bosnia-Herzegovina (LQ), Romania (LR), Switzerland (LS), Turkey (LT), Moldova (LU), Macedonia (LW), Gibraltar (LX), Serbia-Montenegro (LY), Slovakia (LZ), Armenia (UD), Georgia (UG), Ukraine (UK).

[3] `http://www.eurocontrol.int/eec/public/standard_page/NCD_nevac_home.html`

with the highest levels of air traffic. Specifically, we select from our database all airspace portions labeled with an ICAO code starting with ED. This would imply that small portions of the airspace of Belgium and Netherlands, mainly at high altitudes, are also included in our analyses. The boundaries of the considered airspace are shown in Fig. 2.9 below. Moreover, to focus our analysis on the en-route phase of each flight, we filter the trajectories retaining only the portion at an altitude higher than 240 FL. Time of the day is always expressed in UTC. Finally, data do not include Saturdays and Sundays in order to avoid weekly seasonality effects. The selected time period partly overlaps with the major disruption of the European airspace occurred during the Eyjafjallajokull volcano eruption. Such disruption ended on May 9, 2010. Considering that in our investigations we eliminated Saturdays and Sundays, the overlap lasts for two days only. We decided to perform our analysis with AIRAC 334 because it was far away from Easter holydays and Summer holydays, thus allowing us to discard seasonality effects. In any case we checked that the results obtained with AIRAC 334 are not significantly different from those obtained for successive AIRACs.

In the left panel of Fig. 2.1 we show the box plot of the daily number of active flights in the different hours of the day. An intraday pattern is clearly recognizable, with many flights during day-time and almost ten times less flights during the night. In the right panel of Fig. 2.1 we show the number of active navigation points in the planned trajectories at different hours of the day. A navigation point is active in a given time interval if at least one flight is scheduled to pass through it in that interval. Also in this case one can see that significantly less navigation points are used during the night.

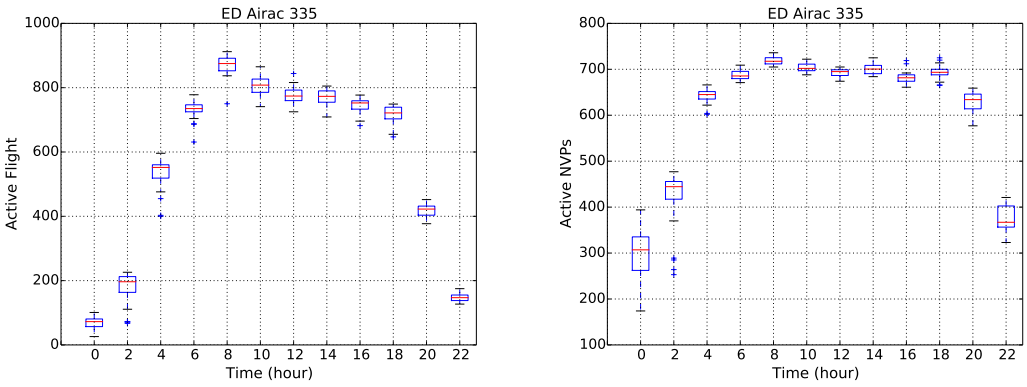


Figure 2.1: Box plots of the daily number of flights (left panel) and number of active navigation points of the planned flight trajectories (right panel) for different time windows of the day. Data refer to the whole 334 AIRAC and the German (ED) airspace and are binned in two hour intervals.

## 2.2 Statistical properties of the length of planned and actual trajectories

When planning their flights, the airlines have to take into account many different constraints that give rise to trajectories quite different the one from the other, even for the same origin-destination airport pair in the same day. As a result, any investigation of flight trajectories aiming at detecting statistical regularities in the deviations occurring in the actual flight trajectories with respect to the planned ones, must take into account such heterogeneity. To this end, we present first some simple statistical facts aiming at having an overview of the data. This is the starting point of our analysis. We seek to understand under which conditions the controllers are using specific navigation points with respect for instance to the traffic conditions.

First, we associate each flight trajectory with a timestamp defined as $(i)$ the entrance time in the German airspace for flights coming from different airspaces or $(ii)$ the first time when the aircraft reaches 240 FL for flights departing inside the ED airspace. In this way, we are able to see that different types of flights are present during day and night. To show this, Table 2.1 displays the mean and the 2.5% and 97.5% percentile

of the distribution of flight length (in km) during day (6:00 am - 9:00 pm) and night (9:00 pm - 6:00 am). The values shown in Table 2.1 refer to the whole flight trajectory. We consider separately planned flight trajectories and actual flight trajectories. The first observation is that night-time flights have flight trajectories that are typically much longer than day-time flights, both for planned and actual trajectories.

| | Planned (km) | actual (km) |
|---|---|---|
| Day | 2831 (627, 12983) | 2822 (616, 12954) |
| Night | 3698 (655, 13030) | 3687 (628, 13037) |

Table 2.1: Average length of the planned and actual flight trajectories during day (6:00 am - 9:00 pm) and night (9:00 pm - 6:00 am). The numbers in round brackets are the values corresponding to the 2.5% and 97.5% percentile of the length distribution. All values are expressed in km. Data refer to the whole 334 AIRAC and the German (ED) airspace.

This claim is confirmed by comparing the distribution function of the planned length trajectories during day and night time shown in Fig. 2.2. Similar results are observed when investigating the actual trajectories.

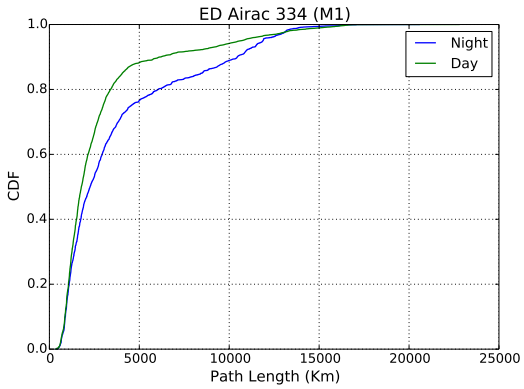


Figure 2.2: Cumulative distribution function of the length of planned flight trajectories in the 334 AIRAC during day (green line) and night (blue line). Data refer to the whole 334 AIRAC and the German (ED) airspace.

We then compare the difference in length between planned and actual trajectory,

considering separately day and night. Table 2.1 shows no appreciable difference, but this is mainly due to the large heterogeneity of flight length. To have a comparison for each flight, in Figure 2.3 we show the probability density function of the fractional difference between the length of planned (labeled as *L(M1)*) and actual (labelled as *L(M3)*) flight trajectories during day (left) and night (right) time. For comparison we also show a normal distribution with the same mean and variance as the data. During day-time the distribution is almost symmetric, even if the left tail is slightly fatter than the right one, indicating a larger probability of *longer* actual trajectories (*L(M1)* < *L(M3)*). On the contrary, for night-time flights, actual trajectories are more likely to be *shorter* than the planned trajectories (*L(M1)*> *L(M3)*), as indicated by the fatter right tail. In any case, empirical data show tails much fatter than Gaussian ones.

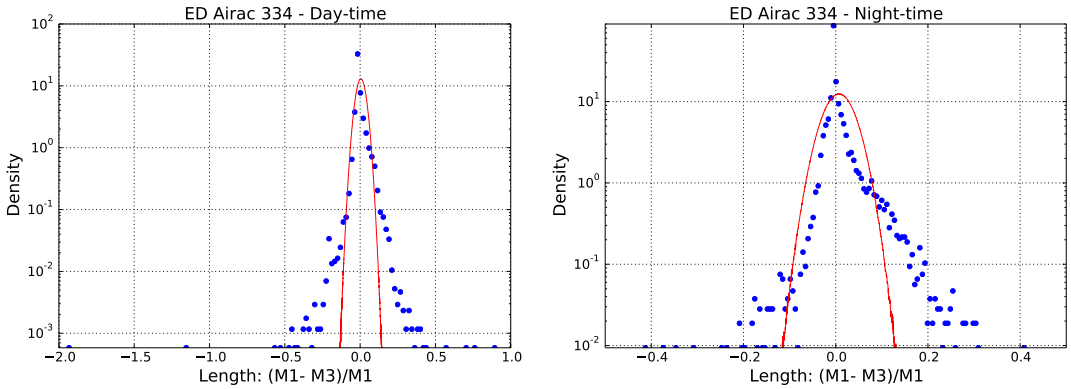


Figure 2.3: Semilogarithmic plot of the probability density function of the relative difference between the length of the planned and actual trajectory of flights in the German airspace during the 334 AIRAC for different parts of the day: day-time from 6:00 am to 9:00 pm (left panel), and night-time from 9:00 pm to 6:00 am (right panel). The red lines are Gaussian density with mean and variance matching those of the data.

These results indicate that the difference in planned and actual flight length has different characteristics during day and night. We now investigate whether this difference is associated with a better management of the traffic during night-time due, for example, to the presence of minor constraints in low traffic conditions.

In order to do this, we use the "flight efficiency" Key Performance Indicator, as defined

by the Performance Review Commission in [82].However, while the efficiency values presented in [82] are computed over the en-route portion of trajectory, we here compute efficiency by taking into account the whole trajectory. This efficiency is related to the best path that a flight can follow in theory, without taking into account winds. Indeed, the efficiency is obtained by comparing the planned or actual length of the $i$-th flight trajectory with the length of the shortest path between its origin airport ($O^i$) and destination airport ($D^i$). Specifically, the Efficiency for a single flight $i$ is:

$$E_i = \frac{\ell_i}{\ell_i^{nvp}} \tag{2.1}$$

where $\ell_i$ is the shortest distance between origin and destination (i.e. the grand circle) associated with the flight $i$, while $\ell_i^{nvp}$ is the length measured along its planned or actual trajectory specified by the series of successive navigation points crossed and defining the flight trajectory. This variable takes positive values smaller than or equal to unity. In Table 2.2 we show the average $\mu_E$ (third and sixth columns), confidence intervals (fourth and seventh columns) and standard deviations $\sigma_E$ (fifth and eighth columns) of the efficiency computed in different time windows of the day, and considering planned and actual flight trajectories separately. Averages are taken across all investigated flights. The confidence intervals are evaluated with a bootstrap procedure [4]. An important result is that for all time windows the average efficiency of the planned trajectories is always smaller than the efficiency of actual trajectories. This suggests that the air traffic controllers play an important role in increasing the system's performances. Night-time flights (in particular during the time interval from 8:00 pm to 4:00 am) are on average more efficient than day-time flights. Moreover, the gain of average efficiency obtained in the actual trajectories is systematically larger during night-time. It is worth mentioning that the definition of Eq. 5.4.1 is a standard definition also used in Ref. [82]. However, while we reported in the table the averages and standard deviations of the efficiency

[4]For each two-hour time window, we store the efficiency values computed for each flight in an $E_t$ array. We therefore obtain 12 $E_t$ arrays. To compute the confidence interval of the average efficiency for each $E_t$ we create 1000 bootstrap copies $E_t^*$ by a sampling with replacement of the element of $E_t$. For each bootstrap replica of data we compute the average thus obtaining a distribution of average values $\langle E_t^* \rangle$. The confidence intervals correspond to 95% respectively associated with the 2.5 and 97.5 percentile of the average and standard deviation distributions.

ratios, in the ATM domain it is more customary to deal with the ratio between the average values $\langle \ell_i \rangle$ and $\langle \ell_i^{nvp} \rangle$.

The difference of the average flight trajectory efficiency between night and day and between planned and actual trajectories shows the relevance of the navigation points structure in determining the choices of both the airlines and the air traffic controllers in the planning and management of flight trajectories. Hereafter we investigate the statistical regularities associated with the modifications of planned flight trajectories originated by the interactions between air traffic controllers and pilots. In fact, we believe that a sound statistical characterization of the deviations occurring in the actual flight trajectories might be better performed focusing on the modifications occurring at the level of navigation points.

## 2.3 Statistical characterization of flight trajectory deviations

Starting from this section we perform our investigations by considering the en-route phase of the flight trajectories only. We consider as en-route the portion of trajectory ranging from the first navigation point when the ascending aircraft reaches FL 240 to the last navigation point when the descending aircraft leaves FL 240. Indeed our definition of en-route phase is different from the one reported in Ref. [82]. European airspaces are usually vertically divided into two portions: FL 240 is considered to be the upper limit of the lowest portion in the vast majority of the European airspaces.

We first study whether the deviations from the planned flight trajectory occur in specific regions of the trajectories or if rather they are uniformly distributed over the trajectory. To this end, for each flight $f^i$ scheduled between the origin airport $O^i$ and the destination airport $D^i$ and for each navigation point $P_j^i$ of the planned flight trajectory, we compute the distance $d_j^i$ of the navigation point $j$ from the destination airport $D^i$. Such distance is computed along the planned flight trajectory. We then normalize such distance dividing it by the total planned length $\ell^i$ of the flight, i.e. the distance from $O^i$ to $D^i$ measured along the flight trajectory. The normalized distance $\hat{d}_j^i$ is obtained as $\hat{d}_j^i = d_j^i/\ell^i$.

| Time | # Flight | $\mu_E$ (Planned) | CI (Planned) | $\sigma_E$ (Planned) | $\mu_E$ (Actual) | CI (Actual) | $\sigma_E$ (Actual) |
|---|---|---|---|---|---|---|---|
| $(0, 2)$ | 1324 | 0.9271 | $(0.9236, 0.9305)$ | 0.0640 | 0.9382 | $(0.9358, 0.9406)$ | 0.0446 |
| $(2, 4)$ | 3509 | 0.9382 | $(0.9365, 0.9398)$ | 0.0497 | 0.9434 | $(0.9420, 0.9448)$ | 0.0425 |
| $(4, 6)$ | 10122 | 0.9194 | $(0.9180, 0.9208)$ | 0.0730 | 0.9239 | $(0.9226, 0.9253)$ | 0.0673 |
| $(6, 8)$ | 11650 | 0.9131 | $(0.9118, 0.9144)$ | 0.0707 | 0.9189 | $(0.9171, 0.9212)$ | 0.1131 |
| $(8, 10)$ | 14252 | 0.9196 | $(0.9184, 0.9207)$ | 0.0687 | 0.9234 | $(0.9223, 0.9245)$ | 0.0670 |
| $(10, 12)$ | 12663 | 0.9239 | $(0.9228, 0.9250)$ | 0.0631 | 0.9271 | $(0.9260, 0.9282)$ | 0.0651 |
| $(12, 14)$ | 12526 | 0.9206 | $(0.9193, 0.9218)$ | 0.0693 | 0.9239 | $(0.9228, 0.9250)$ | 0.0647 |
| $(14, 16)$ | 12485 | 0.9208 | $(0.9197, 0.9220)$ | 0.0655 | 0.9252 | $(0.9242, 0.9263)$ | 0.0600 |
| $(16, 18)$ | 11550 | 0.9187 | $(0.9174, 0.9200)$ | 0.0707 | 0.9220 | $(0.9208, 0.9232)$ | 0.0656 |
| $(18, 20)$ | 11770 | 0.9120 | $(0.9107, 0.9133)$ | 0.0722 | 0.9188 | $(0.9176, 0.9200)$ | 0.0662 |
| $(20, 22)$ | 6026 | 0.9189 | $(0.9170, 0.9208)$ | 0.0736 | 0.9300 | $(0.9285, 0.9315)$ | 0.0602 |
| $(22, 24)$ | 1857 | 0.9226 | $(0.9194, 0.9256)$ | 0.0683 | 0.9325 | $(0.9298, 0.9352)$ | 0.0586 |

Table 2.2: Average $\mu_E$ and standard deviation $\sigma_E$ of the planned and actual flight trajectories together with their 95% confidence intervals (CI) during different time windows of the day. Confidence intervals are obtained with a bootstrap procedure. See the text for more details about the bootstrap procedure. The values reported within round brackets refer to the 2.5 and 97.5 percentile of the average and standard deviation distributions, respectively. Data refer to the whole 334 AIRAC and the German (ED) airspace.

We call *deviation* the event in which an aircraft passing over a certain navigation point present in the planned M1 trajectory does not go to the next one as specified in the planned (M1) trajectory. In Fig. 2.4 we show the probability density function of $\hat{d}^i_j$ for all the navigation points and for those where we detect deviations from the planned flight trajectory[5]. One can see by direct inspection that the two distributions are quite different from each other thus suggesting the idea that the navigation points where deviations occur are not randomly distributed along the trajectory. In particular, the figure shows that there are more deviations far from the destination airport. The figure thus shows that deviations frequently occurs close to the beginning of the flight trajectory, thus indicating that they might not occur to recover from accumulated en-route delay. The fact that the two distributions of Fig. 2.4 have different shapes indicates that ATCO decisions are not randomly distributed along the trajectories.

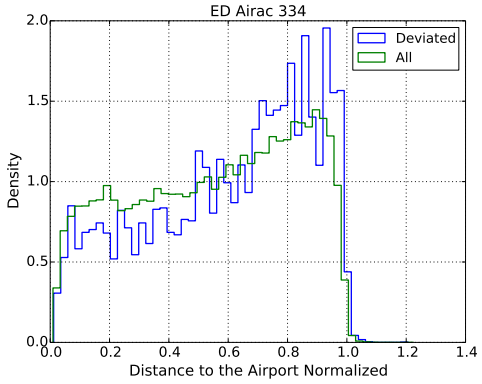


Figure 2.4: Probability density function of the normalized distance from the arrival airport of the navigation point where a deviation occurs (blue line). As a comparison, the green line is the probability density function of the normalized distance from the arrival airport of all navigation points crossed by the flight. Normalization is obtained by dividing the distance along the trajectory by the flight length, thus 0 corresponds to the arrival airport and 1 to the departing airport. Data refer to the whole 334 AIRAC and the German (ED) airspace.

[5]To be more precise, if an aircraft after being deviated returns back to its planned trajectory and subsequently it is deviated again, then for such flight trajectory we count two deviations.

We perform a similar analysis on an angle-to-destination estimator. Specifically, for each flight $f^i$ planned between the origin airport $O^i$ and the destination airport $D^i$ the angle-to-destination of a navigation point $P_j^i$ is the angle $\alpha_j^i$ between the segment connecting the two consecutive navigation points $P_j^i$ and $P_{j+1}^i$ and the segment connecting $P_j^i$ with $D^i$, see the left panel of Fig. 2.5. In the right panel of Fig. 2.5 we show the probability density function of $\alpha_j^i$ for (i) all the navigation points and (ii) conditioned on navigation points where we detect deviations from the planned trajectory. Also in this case the two distributions are quite different from each other, thus supporting the conclusion that the navigation points where deviations occur are not randomly distributed along the flight trajectory. It is also worth mentioning that, differently from the case of flight length, there exists a typical angle of $20° - 25°$ for which deviations occur preferentially. One can view this angle as the typical angle after which a deviation is needed, since the aircraft is following a direction not in line with the destination airport. Note also that small angles are not represented, probably because flights in line with the destination airport do not need to be deviated. Hence, this fact advocates a major role of the directs in the cause of deviations, rather than traffic regulations.

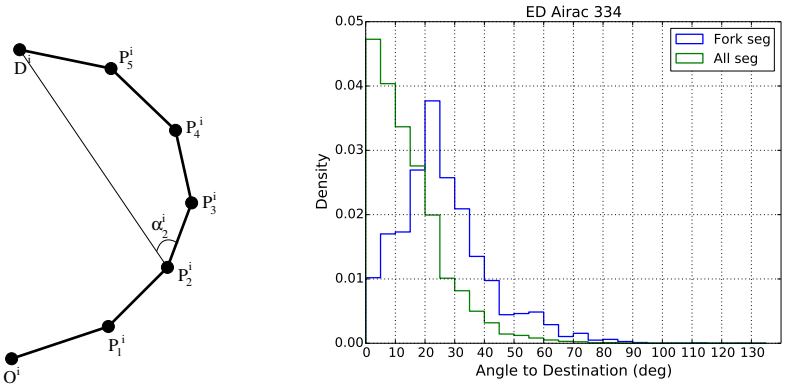


Figure 2.5: The left panel illustrates our definition of angle-to-destination. The right panel shows the probability density function of the angle-to-destination variable estimated at a navigation point where a deviation occurs (blue line) and for all navigation points (green line). Data refer to the whole 334 AIRAC and the German (ED) airspace.

A third aspect we want to emphasize is that trajectory deviations do not occur in a

uniform way throughout the day. Rather, we observe an intraday pattern, as shown in the left panel of Fig. 2.6. The figure shows the ratio between the observed deviations and the possible deviations in the airspace[6]. Consistently with the definition of deviations given above, the possible deviations are defined as the number of navigation points that in each M1 trajectories ($i$) are actually crossed by the aircraft and are therefore also present in the M3 trajectories and ($ii$) irrespective of the fact that the next planned navigation point is crossed or not. As a result the number of possible deviations coincide with the number of navigation points that are present both in the M1 and M3 flight plans. This is therefore a global metric that is not attached to a single navigation point, rather it is relative to the considered airspace. We show such ratio as a function of the time of the day in the left panel and as a function of the number of active flights in the right panel. Interestingly, the ratio of deviations is higher during night-time than during day-time.

This observation, as well as the observation on the angles, suggests that, since traffic is lower during night, the main motivation for deviations is not the need of dealing with safety issues, but rather the possibility of issuing directs that will shorten the flight trajectories. Such observation is in agreement with ATCs interviewed with ELSA project and it is confirmed by the results summarized in the right panel of Fig. 2.6 where we plot the fraction of deviations as a function of the total number of aircraft present in the considered time window, averaged over an entire AIRAC. Each point refers to an hourly time-window and different symbols refer to different AIRACs. Specifically: 334 (circle), 335 (square), 336 (triangle), 337 (diamond) 338 (star).

An inverse relation between the fraction of deviated flights and the number of active

[6]Error bars are given by the Wilson score interval [83] used to associate a confidence interval to a proportion in a statistical population. The Wilson interval is an improvement over the normal approximation interval. In fact, it is more accurate even for a small number of trials and for extreme probabilities. It can be derived from Pearson's chi-squared test with two categories and it is defined as:

$$\frac{1}{1+\frac{1}{n}z^2}\left[\hat{p}+\frac{1}{2n}z^2 \pm z\sqrt{\frac{1}{n}\hat{p}\left(1-\hat{p}\right)+\frac{1}{4n^2}z^2}\right] \tag{2.2}$$

where $\hat{p}$ is the sample proportion observed, $n$ is the number of the trials, and $z$ is the level of significance.

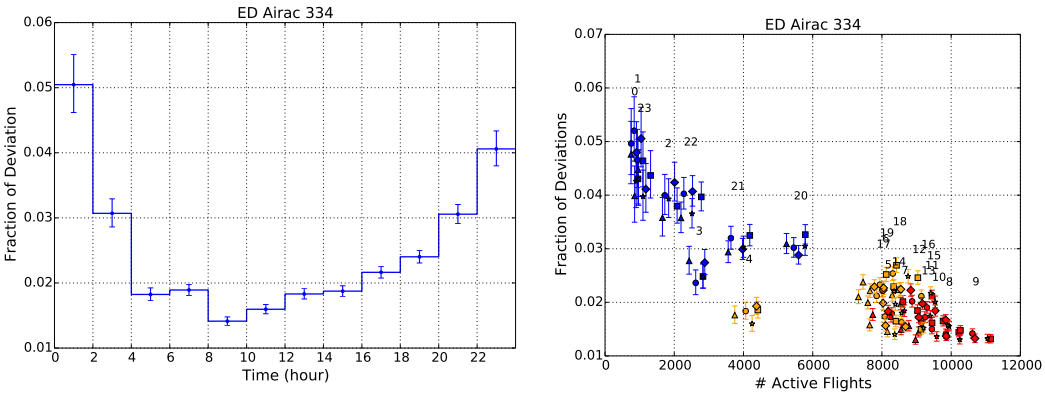


Figure 2.6: In the left panel it is shown the ratio between the number of deviations from the planned trajectory and number of possible deviations as a function of the hour of the day. The vertical error bars represent the Wilson score interval. See the text for more details. The right panel shows such fraction of deviations from the planned trajectory as a function of the number of active flights in different hours of the day. The number indicate the hour of the day. Different symbols refer to different AIRACs, from AIRAC 334 to AIRAC 338. Data refer to the German (ED) airspace.

flights is observed. During night-time (blue points) the traffic is lower and the fraction of deviations is larger, while the opposite is true during day-time. The figure therefore indicates that there exists an negative correlation between fraction of deviations and traffic. When using the Pearson correlation coefficient we estimate a statistically significant (p-value ¡ 0.01) correlation of -0.88, only slightly different from the value -0.83 obtained when we consider the Spearman correlation coefficient. This fact confirms that most of the deviations are actually directs, because safety issues are very few during the night.

Finally, Fig. 2.7 shows the point-biserial correlation between the angle-to-destination for a navigation point, that is a quantitative variable, and the presence or absence of a flight deviation at the same navigation point, that is a categorical one [7]. The figure

[7]The point-biserial is nothing but the Pearson correlation coefficient between a vector with real entries and a boolean vector made of [0, 1]. As in Fig. 2.2 the error bars are computed by using a bootstrap replica of data and considering a 95-percentile confidence interval.

shows that the correlation is statistically different from zero. The aim of this analysis is to assess the controllers behavior in optimizing the trajectories. In fact, the stronger the correlation, the higher the tendency of the controller in deviating aircraft. The observed intraday dynamics indicates an higher point-biserial correlation during night (from 8:00 pm to 4:00 am) rather than during the day. Again this result can be explained in terms of air traffic controllers-pilots interaction to optimize flight paths rather than interventions due to solve safety issues.

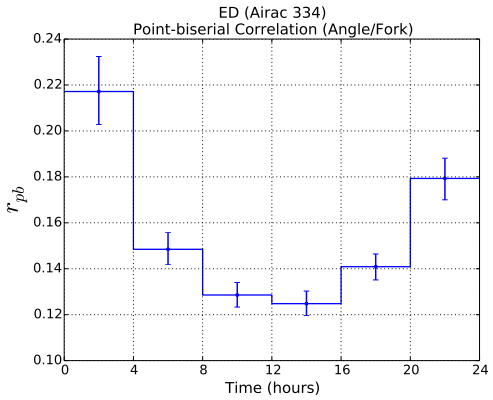


Figure 2.7: Point-biserial correlation between the angle-to-destination and the categorical variable indicating the presence of a deviation of the planned flight trajectory as a function of the hour of the day. Data refer to the whole 334 AIRAC and the German (ED) airspace.

The conclusion of the previous statistical facts is the importance of pro-active deviations rather than reactive ones. In other words, controllers usually modify the horizontal trajectories in order to speed the flights up. This leads to deviations starting early in the trajectory, triggered by high angles-to-destination and low traffic condition, usually during night. We are now interested in studying the temporal heterogeneities of the deviations, focusing on single navigation point pairs, i.e. trajectory segments.

## 2.4 Over-expression and under-expression of flight deviations at navigation points ordered pairs

We are now interested in studying the temporal heterogeneities of the deviations, focusing on single navigation point pairs, i.e. trajectory segments. We want to verify whether deviations occur randomly over the considered airspace or rather if they exhibit some statistical regularities that can be characterized in space and time.
To this end, in section 2.4.1 we will introduce the metric, called di-fork, that we will use to characterize deviations at a local level. In section 2.4.2 we will use the di-fork metric in order to make clear, in a statistically robust way, that deviations follow specific patterns, both in space and time. Such patterns are characterized by the fact that in certain times and in certain portions we have either more or less deviations than expected. The statistical procedure that will give us this information is briefly illustrated in the worked example illustrated in Fig. 2.8.

Let us preliminarily discuss a metric, called fork, that was first introduced in Ref. [84]. Such metric is used for characterizing the differences between planned and actual flight trajectories at the level of each single navigation point. Let us first provide a qualitative description of it. For each flight, we consider the last navigation point which is common to the planned and the actual flight trajectory. At this point, we consider that a "fork" happens when the flight trajectory is deviated from the planned one. By counting the number of flights which are deviated from the considered navigation point and by dividing it by the total number of flights flying through the navigation point in the selected time interval, we obtain a quantitative indicator of how much the navigation point is a "source" of deviations for the planned flight trajectories. This quantity varies between 0 and 1 and is computed for each navigation point.

Hereafter we are providing a more formal definition. Let us consider a certain time window $\Delta t$. Let us consider a generic navigation point $P$ appearing in at least one of the actual flight trajectories. Let us call $pF_{\Delta t}(P)$ the number of flights passing through $P$ as observed in the planned flight trajectories. Let us call $dF_{\Delta t}(P)$ the number of flights passing through $P$, as observed in the actual flight trajectories, and missing the next navigation point as indicated in the corresponding planned flight trajectory. The

fork $F_{\Delta t}(P)$ is defined as the ratio $F_{\Delta t}(P) = dF_{\Delta t}(P)/pF_{\Delta t}(P)$. By construction, this metric aggregates the information on the different flight trajectories that in a certain time window $\Delta t$ are passing through $P$.

This metric already produced some interesting results presented in [84]. However, its weakness relies in the heterogeneity of trajectories which can cross a single navigation point. Indeed, controllers are managing flows, i.e. ensemble of trajectories, and for them the navigation point is a support to the flow. As a consequence, different flows crossing at a given navigation point can be managed differently. We therefore introduce a slightly different metric, where we take into account the direction of the flow as well as the navigation point itself.

### 2.4.1 The directional fork

Let us consider pairs $C(P_j, P_k) = (P_j, P_k)$ of navigation points that are consecutively crossed according to a certain flight plan. The navigation point pairs we consider are ordered and therefore $(P_j, P_k)$ and $(P_k, P_j)$ are different pairs describing flights passing through the same pair of navigation points but moving in the opposite direction.

Similarly to the previously mentioned fork metric, the directional fork (or *di-fork*) $\Phi_{\Delta t}(C)$ associated with an ordered navigation point pair $C$ is defined as the ratio $\Phi_{\Delta t}(C) = DF_{\Delta t}(C)/PF_{\Delta t}(C)$ where $PF_{\Delta t}(C)$ is the number of flights planned to flow through $P_j$ and $P_k$ in the direction from $j$ to $k$ and $DF_{\Delta t}(C)$ is the number of flights actually crossing $P_j$ and then deviated to a navigation point different from $P_k$ in the considered time window $\Delta t$. In other words, the first navigation point is the one crossed by the aircraft and the second one is the navigation point present in the planned flight trajectory but not present in the actual flight trajectory. This definition allows us to investigate the deviations as a function of the different directions, and to have a more flow-based metric. It is worth emphasizing again that the di-fork metric refers to navigation point pairs, while the fork metric of Ref. [84] refers to single navigation points.

Below we investigate the capabilities of the di-fork metric in providing a statistical characterization of the deviations occurring in the flight trajectories. More specifically, we are interested in seeing how the statistical facts we found in section 2.3 are present at the microscopic level, i.e. at the navigation point pair level.

### 2.4.2 Navigation point pairs with over-expressed and under-expressed values of the di-fork metric

Here we investigate whether the flight trajectory deviations are randomly distributed over the day or rather if they are over-expressed or under-expressed for specific navigation point pairs. This type of investigation cannot be done only in terms of the occurrence of the flight trajectory deviations because the number of flights passing through a specific navigation point pair in a given time interval is a quite heterogeneous variable. We therefore estimate the over-expression and under-expression of flight trajectory deviations by considering navigation point pairs and trying to compare the occurrences of flight trajectory deviations observed in this pair with an appropriate null model.

In this section we investigate the navigation point pairs $C(P_j, P_k)$ for which the air traffic flow is from $P_j$ to $P_k$. Suppose that during a specific day we have $PF_{day}$ flights with planned flight trajectories connecting $P_j$ to $P_k$ in a step. Suppose also that $DF_{day}$ is the number of flights passing through the first navigation point $P_j$ and deviating from the successive navigation point $P_k$ in the same day. Let us now define $PF_{\Delta t}$ the flights that are planned to fly through $P_j$ and $P_k$ during an intraday time interval $\Delta t$. We can estimate what is the probability of observing a number $DF_{\Delta t}$ of flights flying through $P_j$ and then deviating from $P_k$ during the same time interval. By assuming that for each navigation point pair, the flight trajectory deviation events are independent the one from the other, a good approximation of the probability of detecting $DF_{\Delta t}$ is given by the hypergeometric distribution[8]:

$$H(DF_{\Delta t}|PF_{day}, DF_{day}, PF_{\Delta t}) = \frac{\binom{DF_{day}}{DF_{\Delta t}}\binom{PF_{day}-DF_{day}}{PF_{\Delta t}-DF_{\Delta t}}}{\binom{PF_{day}}{PF_{\Delta t}}}. \tag{2.3}$$

By using this value of the probability of observing $DF_{\Delta t}$ deviated flight trajectories we can obtain for each navigation point pair $C(P_j, P_k)$ a p-value for the over-expression or the under-expression of $DF_{\Delta t}$. The probability of Eq. (2.3) allows us to associate a $p$-value $p(DF_{\Delta t})$ with the actual number $DF_{\Delta t}$ of detected deviation. Specifically, for

[8]It is worth mentioning that using the hypergeometric distribution is equivalent to performing an one tail Fisher's exact test [85] starting from a $2 \times 2$ contingency table whose entries are $DF_{\Delta t}$ and $PF_{\Delta t} - DF_{\Delta t}$ in the first column and $DF_{day} - DF_{\Delta t}$ and $(PF_{day} - DF_{day}) - (PF_{\Delta t} - DF_{\Delta t})$ in the second column [86].

over-expression (OE) we have

$$p_{OE}(DF_{\Delta t}) = 1 - \sum_{X=0}^{DF_{\Delta t}-1} H(DF_{\Delta t}|PF_{day}, DF_{day}, PF_{\Delta t}), \tag{2.4}$$

whereas for under-expression (UE) we have

$$p_{UE}(DF_{\Delta t}) = \sum_{X=0}^{DF_{\Delta t}} H(DF_{\Delta t}|PF_{day}, DF_{day}, PF_{\Delta t}). \tag{2.5}$$

Since we are performing this test for all possible navigation point pairs $C(P_j, P_k)$, we have to use a correction for multiple hypothesis test comparison. The most restrictive correction is given by the Bonferroni correction that prescribes to select only the p-values smaller than $P = \alpha/2N_{pair}N_t$ where $\alpha$ is the univariate p-value significance level usually set to $\alpha = 0.01$, $N_t = 12$ is the number of used time bins and $N_{pair}$ is the number of possible pairs we tested. Such number changes depending on the specific investigation. As an example, when testing the 334 AIRAC only we use $N_{pair} = 29076$ and therefore we have $P = 2.43\,10^{-8}$. In the analysis presented below, where we test for over- and under-expressions over five consecutive AIRACs we will consider $N_{pair} = 146112$ and therefore $P = 2.85\,10^{-9}$. The factor 2 is taken into account because we consider both over- and under-expressions. Rather than the Bonferroni correction, we will instead use the Holm-Bonferroni multiple hypothesis test correction [87]. This is uniformly more powerful than the Bonferroni correction, as it controls the family-wise error rate for every hypothesis test in a strong sense. Let $p_1 < p_2 < p_3 < \cdots < p_M$ be all p-values sorted from smallest to largest, where $M = 2N_{pair}N_t$ is the number of performed tests. Let $k$ be the smallest value such that $p_k < \alpha/(M - k + 1)$. All p-values $p_i$ such that $i \leq k$ are considered to be statistically significant in the Holm Bonferroni approach.

In the results presented hereafter, we aggregate the number of temporally over-expressed and under-expressed navigation point pairs relative to the different days of an AIRAC.

### 2.4.3 Worked example

In Fig. 2.8 we illustrate an example of the two possible outcomes of the statistical validation procedure associated to the hypergeometric distribution described above. The left panel indicates a situation where we have an over-expressed navigation point pair

(thick red segment). The first navigation point is crossed by 90 aircraft. However only 48 of them reach the other navigation point of the pair. This results in a di-fork value of $(90 - 48)/90 = 0.467$ which leads to an over-expression as a result of the comparison with the average daily behavior characterized by a di-fork value of $(987 - 785)/987 = 0.205$, see the central panel. The right panel shows the same pair in a different time window. Now there are many more aircraft crossing the two navigation points. However, the pair results to be under-expressed, given that only $135-131 = 4$ out of 135 aircraft do not cross the second navigation point of the pair. The example shows that having an over-expressed or under-expressed pair does not necessarily indicate that the pair is more frequently used. Rather, the statistical validation procedure associated to the hypergeometric distribution selects the pairs where the occurrence of deviations is statistically different from the daily average.

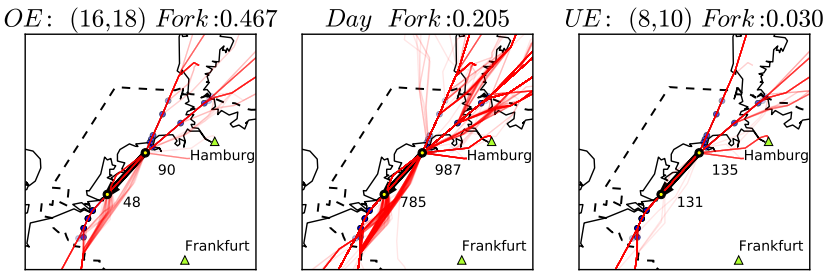


Figure 2.8: The left panel shows a navigation point pair (thick red segment) where the first navigation point is crossed by 90 aircraft. However only 48 of them reach the other navigation point of the pair. This results in a di-fork value of $(90-48)/90 = 0.467$. The right panel shows a navigation point pair (thick red segment) where the first navigation point is crossed by 135 aircraft. and 131 of them reach the other navigation point of the pair. This results in a di-fork value of $(135 - 131)/135 = 0.030$. The central panel shows the daily behavior of the considered pair. The first navigation point is overall crossed by 987 aircraft, with 785 of them reaching the other navigation point of the pair. Therefore the average daily behavior is characterized by a di-fork value of $(987 - 785)/987 = 0.205$.

In Table 2.3 we show the number of over-expressed (second column) and under-

expressed (third column) navigation point pairs in the 334 AIRAC. The fourth and fifth column show the number of navigation point pairs with at least one and five planned flights, respectively. The number of over-expressed navigation point pairs is larger in the night than during day-time, while the opposite is true for under-expressed pairs. Time windows of early morning (e.g. the 6:00 am 8:00 am time window) and of early afternoon (e.g. the 2:00 pm 4:00 pm time window) present a roughly balanced number of over-expressed and under-expressed navigation point pairs. The fifth and sixth columns indicate the number of OE and UE observed in at least one of the 5 AIRACs from 334 to 338.

For illustrative purposes, in Fig. 2.9 we show the localization of the under-expressed pairs and over-expressed pairs in the 12 bi-hourly time-windows occurring in a day. The different colors are proportional to the measured di-fork value in the considered time-window, according to the color code on the right of the figure. Although there seem to be a predominance of segments with colors belonging to upper and lower part of the color bar, in some case we can also see, see panel (2, 4) for instance, some segment with colors belonging to the central part of the color bar. Once again, this indicates that the statistical validation procedure associated to the hypergeometric distribution selects the pairs where the occurrence of deviations is statistically different from the daily average, rather than pairs with higher or lower di-fork values.

In fact, in the left panel of Fig. 2.10 we show all navigation point pairs of the considered airspace in the 12 bi-hourly time-windows occurring in a day. As in the above case, the different colors are proportional to the measured di-fork value in the considered time-window, according to the color code on the right of the panel[9]. The comparison of such panel with Fig. 2.9 clearly shows that navigation point pairs with larger di-fork values are not over-expressed as well as navigation point pairs with small di-fork values are not under-expressed. In the right panel of Fig. 2.10 we show again all navigation point pairs of the considered airspace in the 12 bi-hourly time-windows occurring in a day. However, here the colors are proportional to the number of aircraft traveling across the navigation

[9]In this graphical representation the navigation point pairs $C = (a, b)$ and $\overline{C} = (b, a)$ are considered together. In other words, the di-fork value represented here is defined as $(DF(C)+DF(\overline{C}))/(PF(C)+PF(\overline{C}))$. Moreover, we only show the segments such that $(PF(C) + PF(\overline{C})) \geq 5$

| | # of OEs 334 AIRAC | # of UEs 334 AIRAC | # of pairs with at least 1 flight | # of pairs with at least 5 flights | # of OEs in at least 1 AIRAC | # of UEs in at least 1 AIRAC |
|---|---|---|---|---|---|---|
| $[0, 2]$ | 10 | 1 | 876 | 510 | 19 | 1 |
| $[2, 4]$ | 12 | 0 | 977 | 667 | 34 | 0 |
| $[4, 6]$ | 1 | 0 | 1316 | 1003 | 6 | 2 |
| $[6, 8]$ | 3 | 2 | 1386 | 1108 | 6 | 6 |
| $[8, 10]$ | 1 | 6 | 1442 | 1157 | 5 | 17 |
| $[10, 12]$ | 0 | 2 | 1426 | 1160 | 1 | 11 |
| $[12, 14]$ | 1 | 1 | 1408 | 1110 | 5 | 13 |
| $[14, 16]$ | 1 | 0 | 1400 | 1116 | 6 | 0 |
| $[16, 18]$ | 4 | 0 | 1391 | 1068 | 13 | 1 |
| $[18, 20]$ | 6 | 0 | 1395 | 1099 | 18 | 1 |
| $[20, 22]$ | 14 | 1 | 1306 | 1024 | 33 | 2 |
| $[22, 24]$ | 19 | 0 | 957 | 537 | 35 | 1 |

Table 2.3: Number of over-expressed (second column) and under-expressed (third column) navigation point pairs observed in the 334 AIRAC during different time windows of the day. The fourth and fifth column show the number of navigation point pairs with at least one or five planned flights, respectively. The fifth and sixth columns indicate the number of OE and UE observed in at least one of the 5 AIRACs from 334 to 338. Data shown in this table were obtained by using the FDR correction for multiple test comparison with $N_{pair} = 146112$. Data refer to the German (ED) airspace.

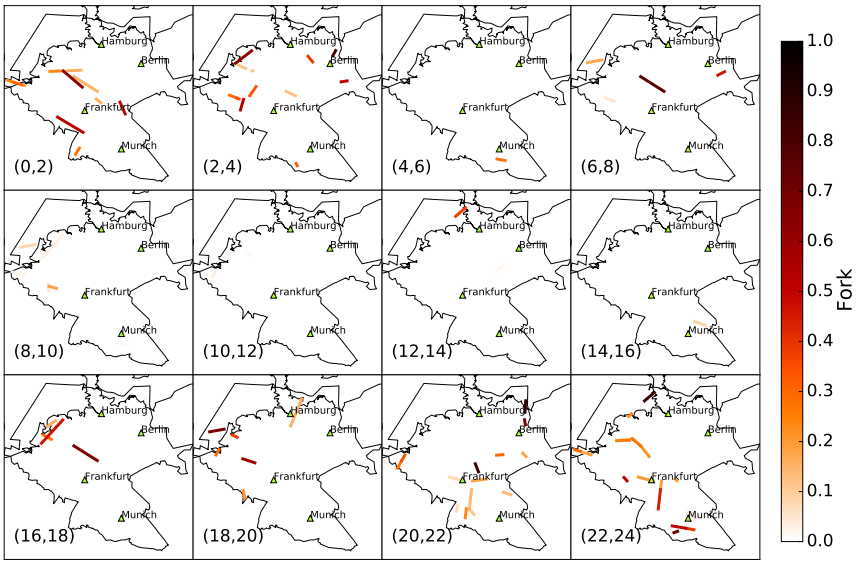


Figure 2.9: Spatial localization of the under-expressed pairs and over-expressed pairs over the day. The different colors are proportional to the measured di-fork value in the considered time-window.

point pair in the considered time window[10]. By comparing such panel with Fig. 2.9 one can clearly see that highly travelled segments are not necessarily over-expressed while poorly travelled segments are not necessarily under-expressed.

The spatial localization of the over-(under-)expressed navigation point pairs might change for different time-intervals. Again this is not surprising because the di-fork metric not only takes into account the topology of the navigation point network which has a slow dynamics over the day, but it also takes into account the flow of aircraft over the network, which is instead pretty variable over the day. However, stable patterns can be detected. In fact, we investigated the temporal persistence of the over-expression and under-expression of flight deviations at navigation point pairs in Fig. 2.11. This is a

[10]In this graphical representation the navigation point pairs $C = (a, b)$ and $\overline{C} = (b, a)$ are considered together. Accordingly, the number of aircraft shown in the figure is the sum of the number go flights traveling from one navigation point to the other in both directions.

color coded figure showing for each investigated time window of the day and for each statistically validated navigation point pairs of the AIRAC 334 whether each navigation point pair turns out to be also over-expressed or under-expressed in the 4 AIRACs successive to AIRAC 334. In the figure a value of 5 (labeled as a red cell) indicates that the navigation point pair is over-expressed in all five considered AIRACs. Negative numbers indicate under-expression. It is worth mentioning that a pair over-expressed (under-expressed) in a certain AIRAC never happens to be under-expressed (over-expressed) in the other 4 AIRACs. For comparison, in the fifth and sixth column of Table 2.3 we indicate the number of OE and UE observed in at least one of the 5 AIRACs from 334 to 338. One can see that there are only a few navigation point pairs that are over-expressed during the 5 AIRACs both during day time and during night-time. The two periods of the day show a quite different general pattern suggesting again different underlying reasons for the deviations of the planned flight trajectories. In fact, the figure is consistent with our previous findings and gives us more information. It seems that during the night, controllers are consistently deviating some of the flows in the airspaces, probably to shorten the corresponding trajectories. During the day on the other hand, controllers are stabilizing the horizontal deviations, especially some flows, which are probably more complex than the others. This also complements the results of [84], in which we were only able to see that some navigation points were consistently over-used for deviations.

As a result, the di-fork metric seems able to show in quantitative way that the fraction of deviations occurring at the level of single navigation point pairs during the day is not a random variable. Rather it follows patterns that reveal to be stable over different AIRACs. Therefore it provides an useful instrument for a “microscopic” statistical characterization of the deviations from planned flight trajectories in the air traffic management procedures. This metric might reveal useful to identify the specific portions of the airspace in which modifications of the current structure are needed in order to make the whole ATM system more efficient. On one side, such modifications might regard the infrastructure, i.e. the navigation point network structure, the route structure and the sectors dynamic configuration [88]. On the other side, modifications might occur also at the level of the strategic 4D trajectory planning [89, 90]

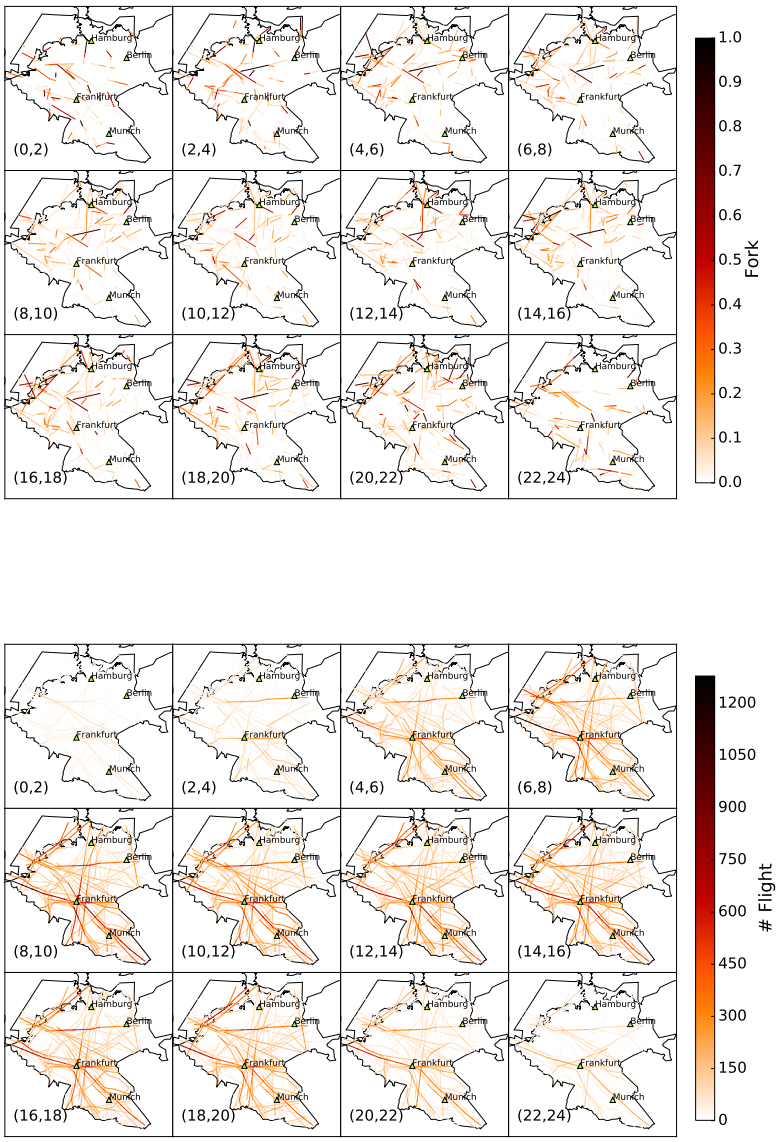


Figure 2.10: Spatial localization of the navigation point pairs over the day. In the left panel the different colors are proportional to the measured di-fork value in the considered time-window. In the right panel the different colors are proportional to the number of aircraft traveling across the navigation point pair in the considered time window.

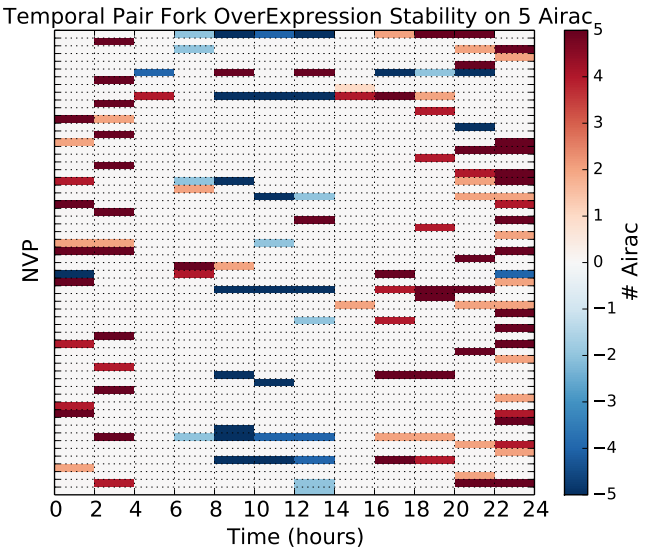


Figure 2.11: Color code summary of the persistence of over-expressed and under-expressed navigation point pairs statistically validated during AIRAC 334 and during the successive 4 AIRACs. On the $x$ axis we report the time window of the day and each horizontal line parallel to the $x$ axis represents a navigation point pair statistically validated at least once during AIRAC 334. Positive values (red cells) indicate that the navigation point pair is repeatedly over-expressed during different AIRACs at the considered time window. Negative values (blue cells) indicate repeated under-expression. Data refer to the five AIRACs from 334 to 338 and to navigation point pairs of the German (ED) airspace. Data shown in this table were obtained by using the FDR correction for multiple test comparison with $N_{pair} = 146112$.

# 3 The ELSA Agent-Based Model

Our agent-based model involves aircraft/pilots and air traffic controllers who are active within an *Area Control Center* (ACC) in the European airspace. At the most elementary level, the airspace is divided in 3-D airspace volumes, termed *elementary sector*, or *collapsed sector* (called simply *sector* in the following). A sector is handled by two controllers: one (*executive*) is responsible of keeping the adequate separation between aircraft in the sector (making sure they do not infringe the separation minima), while the other one (*planner*) is responsible for the coordination with the adjacent sectors and the planning of the modified trajectories. The sectors are dynamic entities, which can be split or aggregated depending on the air traffic load. Moreover, the sectors can be roughly divided in two types: the en-route sectors, controlling the planes in their en-route trajectory, and the Terminal Maneuvering Areas (TMA) or the Control Zones (CTR), managing the take-off and landing phases. The first important level of aggregation of sectors is given by the ACC, where all the sectors are physically controlled from the same room (control center).
In our ABM, the pilots are passive entities, in fact they follow the flight plan, or the instructions of the ATC if they were different. The ATCs shall monitor the execution of the flight plan. The ATC actions are influenced by the current workload of their own sector and by the workload of the neighboring sectors, as well as by the local geometry of the flight plans. The model is able to work on the whole 3-D volume of the airspace, while all results presented here are considering only the portion of airspace above FL 240.

We model and simulate the events that make a planned flight trajectory, recorded in the so-called M1 files, transform into an actual one, recorded in the so-called M3 files.

The aim is that of investigating the issues that affect the predictability[1] of the last filed flight-plan within the ATM system, and what are the changes brought by SESAR in terms of airspace management and controllers' workload.

## 3.1 General features of the model

The interaction between the agents considered in our ABM is needed in order to manage the tactical changes occurring in the system due to unforeseen events, i.e. weather events, congestions, limitation of sectors capacity, etc. Moreover, the ATC sectors are the places where flight trajectories are made conflict free.

The model takes into account that M1 trajectories are not conflict free. Thus one main task to be performed within the model is to deconflict trajectories. Moreover, we can simulate disruptions in the system and see how the system reacts to them[2]. We assume that the disruption lasts for a certain time window. Operationally, this means that for a certain time window a certain area of the sector or ACC can not be crossed by flights. This might correspond to a situation where an extreme weather event occurs and therefore the air traffic must be deviated [91, 92]. As a result, another task of the model is to modify one or more flight trajectories in order to avoid these disruption areas. The way we model this step is to deviate the flight trajectories along new navigation points that are external to the restricted area and with the constraint that (i) we want to minimize the length of the deviated trajectory and (ii) the deviated trajectory must be conflict free.

In general we will take into account two critical situations: (i) there is a possible conflict of trajectories that nevertheless do not intersect one with each other and (ii) there is a possible conflict of trajectories that intersect with each other. These two cases are essentially the same from an operative point of view. We keep this case distinct from the previous one to emphasize that the last case usually occurs mainly in the planned trajectories, while the previous one usually occurs mainly when one of the two conflicting trajectories have already been deviated. In any case the way our ABM treats these three

[1] Predictability is here intended as a comparison of the actual flight arrival time to the scheduled flight arrival time.

[2] However we will not show in this dissertation experiments concerning disruptions

different situations is the same. Starting form the planned trajectory, we identify the navigation point(s) involved in the critical situation and try to select new navigation point(s) for each flight trajectory such that the new trajectory has the minimal length and it is conflict free. This algorithm is therefore essentially based on "re-routing" and the possibility of performing flight level changes.

The model also performs another important task which is related to the issuing of directs. They are given within the ACC in order to speed up the passage of the aircraft within the ACC, provided that no conflict is created. The algorithm we have implemented looks for a new shorter trajectory that allows the aircraft to come back to its planned trajectory within the considered ACC. In general an aircraft in sector $S_A$ can be directly sent to another sector $S_B$ if such choice is preferable in terms of trajectory length. However, if sending the aircraft to a new sector $S_B$ would infringe the capacity of that sector, the algorithm searches for a sub-optimal modified trajectory trying to send the aircraft back to the planned trajectory within the same sector $S_A$.

We have constructed the code in a modular way that allows to swap the priority of the strategies adopted by the controllers. In fact, as a default controllers first check for the possibility of doing re-routings and then change the flight altitude. However, if necessary, we can easily modify the code in such a way that the two strategies mentioned above are swapped or that, if needed, no direct is issued.

The modules described below implement a local resolution of conflicts. However, this way of solving conflicts (i) can be slow from a computational point of view and (ii) provides solutions that are not optimized at a global level, thus making it necessary to "adjust" trajectories several times as long as an aircraft travels across the ACC. We are fully aware of this limitation in our model. Indeed, we implemented such solution because we had indications that this is close to the way controllers work in reality. Moreover, we also believe that our solution might be quite effective in the SESAR scenario simulations. In fact, we might simulate a scenario where controllers have a role less preeminent than in the current scenario and some basic conflict-resolution actions are left to the single aircraft. In this respect, our model might mimic a scenario where pilots, that clearly have not a global vision of the system, endowed with a set of policy rules assigned by their airlines, will perform an *active* conflict resolution at a tactical level, thus realizing

a sort of self-organization amongst aircraft.

## 3.2 Overview of the Model

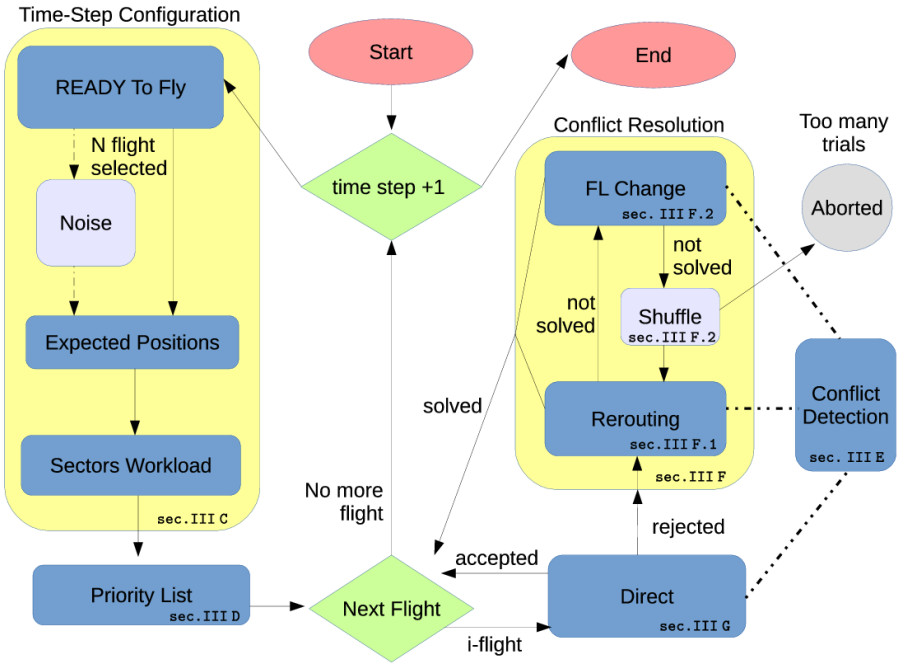


Figure 3.1: Schematic block diagram of the tactical ABM model. Oval red blocks identify the start and the end of the code. Rectangular cyan box are used to indicate the different modules of the model where operational steps are performed. Larger rectangular yellow areas are used to identify different logical areas of the model: the one on the left devoted to the set up of aircraft trajectories and sector configuration and the one on the right devoted to the actual management of trajectories. Rhomboidal green blocks identify the logical nodes where choices are done. Solid lines with arrows are used to logically connect the different blocks. Dashed lines are logical connectors used to highlight the fact that a module is dialoging with the *Conflict Detection* module. For each block we indicate the section where it is described.

A schematic block diagram of the model is given in Fig. 3.1. The logical blocks reported in the left part of the figure are described in sections 3.4 and 3.5. They are relative to

the set up of aircraft trajectories and sector configuration. In these modules the model computes the position of the aircraft with a certain look-ahead, the sectors workload and defines the pairs of aircraft to be checked the one against the other in order to check for possible conflicts. The logical blocks reported in the right part of the figure are described in sections 3.6 and 3.8. They are relative to the actual management of the trajectories needed either to solve possible conflicts or to issue directs in order to shorten the passage of an aircraft in a sector. Here the model computes the distances between aircraft pairs in order to identify the ones that are below the safety threshold and, when needed, modifies the trajectories in order to solve the conflicts. It also tries to shorten the aircraft trajectories, by checking that safety requirements and capacity constraints are not infringed.

We have designed the code in a modular way that allows to swap the priority of the strategies adopted by the controllers. In fact, as a default controllers first check for the possibility of doing re-routings and then change the flight altitude (FL change). Therefore, due to the modularity of the code, the sequence among the different modules can be changed by the user of the code.

The code that implements the model presented here is written in C [93] and it is available at the following URL: `http://ocs.unipa.it/software.html:ELSA Tactical Layer`[3].

## 3.3 Navigation Points

The planned flight trajectories are sequences of specific points of the airspace called navigation points to be crossed by the aircraft at specific times, flight levels, and within a specific sector. The velocity of each aircraft during the flight interval between two navigation points is assumed to be constant and its value is estimated from the schedule of the flight plan. In our simulations all navigation points present in the last-filed flight-plans are used. When trajectory changes are required by the controllers these changes involves temporary navigation points that are selected by the program or that can be externally provided. In the simulations we present in this thesis the temporary

[3] A previous version of the code specifically dedicated for performing simulations in the SESAR scenario is available at the following URL: `http://ocs.unipa.it/software.html:ELSA SESAR Simulator`

navigation points are randomly uniformly distributed within the west Italian ACC.

It should be noted that not all temporary navigation points will be used in the flight deviations. Only a set of them will be selected, as we will explain below. All the not used ones will be eliminated from the analysis after all the flights in the ACC will be managed. As we will explain in section 3.7.1, they are generated to allow the aircraft to deviate from the planned trajectories without necessarily passing over a predefined navigation point which might be too far.

## 3.4 Time-step configuration

The ABM is a discrete-time model. At each time-step the *ReadyToFly* module selects the active aircraft, then the *Expected Position* module computes the expected dynamical evolution of all trajectories within a look-ahead. The look-ahead assumes the value $\Delta t_d$ when the ATCO checks the trajectories for possible safety issues when he tries to issue a direct, see section 3.8. The look-ahead assumes a smaller value $\Delta t_l$ when the ATCO performs the routinary checks for conflict detection, see section 3.6. At time $t_0$ suppose that the position of all aircraft is known. The elementary time step of the model is $\delta t$. At time $t$ the time evolution of the system is computed with $\delta t$ time resolution until the time $t + \Delta t_d$ where $\Delta t_d$ is the look-ahead time of air traffic controllers. On the basis on the estimated time evolution air traffic controllers release their decisions to the aircraft and a new iteration starts. To minimize the computational cost of the simulation the initial time of the next iteration of the model is performed at time $t + \Delta t_s$ where $\Delta t_s$ is a time interval ranging between $\delta t$ and $\Delta t_l$. The values used in our simulations after calibration were $\delta t = 10$ seconds, $\Delta t_l = 7.5$ minutes, $\Delta t_s = 3$ minutes and $\Delta t_d = 15$ minutes, see Fig. 3.2.

Indeed, in the basic setup, the controller forecast of the aircraft position is exact within its time look-ahead. Our ABM allows to introduce some errors in the forecast of the controller. This is done by setting a parameter $l_\epsilon \neq 0$ which is controlling the uncertainty in the estimation of the velocity of the aircraft. Specifically, the uncertainty in the controller's forecast is introduced by the following procedure: (i) between time $t$ (current time) and $t+\Delta t_s$, the model that the aircraft maintains the planned velocity, (ii)

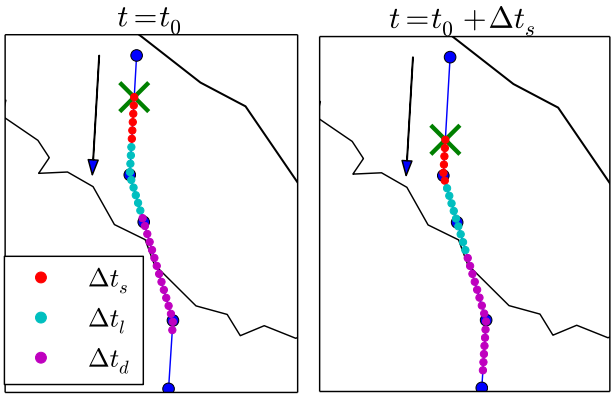


Figure 3.2: Illustration of the time discretization used in the model. In the two panel we show a flight trajectory sampled at a discrete times with an elementary time interval of $\delta t = 30$ sec. The dots indicate the aircraft positions sampled at each $\delta t$. Red dots are the aircraft positions evaluated within a time step $\Delta t_s = 3$ min for the flight trajectory evaluated at $t = t_0$ (left panel) and at $t = t_0 + \Delta t_s$ (right panel). Red and cyan dots are the aircraft positions evaluated within the time interval of the look-ahead $\Delta t_l = 7.5$ min whereas red, cyan and magenta dots are the aircraft positions evaluated within the time interval of the look-ahead used to issue directs $\Delta t_d = 15$ min. Blue circles are navigation points of the flight plan. The cross indicates the initial position of the aircraft at the initial time of the time step. The arrows indicate the directions travelled by the aircraft.

between $t + \Delta t_s$ and $t + \Delta t_l$, the model introduces an uncertainty in the aircraft velocity. The velocity used by the controller is $v(1 + \epsilon_v)$, where $\epsilon_v$ is drawn at random from a uniform distribution in the range $-l_\epsilon$ and $l_\epsilon$. With this choice the controller makes bigger errors on positions on longer times. The choice of considering a uniform distribution is done for the sake of simplicity. That gives us the opportunity of exploring the impact of uncertainty in the ATCOs management procedures. Hereafter, we will consider two rather different cases: $l_\epsilon = 0$ (no uncertainty) and $l_\epsilon = 0.1$ (10 % of maximal percentage error).

It should be noted that the actual velocity of aircraft do not change in our model, and hence they are always those of the planned trajectories (except in case of re-routing

where the velocity is extrapolated on the new segment). In practice and in the absence of learning processes, incorrect forecasts or stochastic changes of the trajectories are indistinguishable.

The *Sectors workload* module is used to set up the sectors configuration of the considered airspace and to determine the number of aircraft present in each ATC sector. The ACC we are considering is divided into a number of sectors. Each sector is characterized by its geographical location and by a proxy for its capacity, defined by us as inferred capacity and estimated as the maximum number of aircraft that are simultaneously present in a sector within a time window of one hour [94]. This information is obtained from the flight plans of the AIRAC used to start simulations. We want to emphasize that the inferred capacity is just a raw approximation of the real capacity. However the ABM can be set up with the real capacities if they are available.
In addition to the inferred capacity of a sector we dynamically estimate its workload. Specifically, we estimate sector workload by assigning a numerical flag to each navigation point of the planned flight trajectories for each sector. We define workload of a sector the number of flights planned to cross it during the time window of an hour. At each time-step the ABM evaluates the workload of each sector of the ACC.

## 3.5 Priority list of controllers' actions

At each time step we create a list of flights active in the considered time-step. The list is randomly ordered. The order of the list is followed by the controller in her attempt to solve potential conflicts and to issue directs. Specifically, the $i$-th aircraft trajectory in the list is checked against the trajectories of previous listed $i-1$ flights. For example, the first aircraft in the list will perform its planned trajectory whereas the trajectory of the second one will be checked with respect to the trajectory of the first one. The trajectory of the third aircraft will be checked with respect to the trajectories of the second and the first ones and so on. Indeed, to speed computation, the trajectory check between two aircraft is not performed when the two trajectories are too far to interact within the look-ahead time interval.

The random reordering of the flight priority list is done in order to be sure that the

trajectories to be deviated are not always the same ones. If a conflict involving the $i-th$ aircraft is not solved by one of the procedures followed by the controller, then the list is modified by putting the $i-th$ aircraft in the first position of the list and the trajectory analysis of the time step is repeated from the beginning. When this redefinition of the priority list is repeated more than 50 times for a time step the simulation is aborted. It is worth reporting that in the simulations performed to obtain the results of this work we never had to abort a simulation.

## 3.6 Conflict Detection module

The collision detection module calculates the minimum distance for each pair of aircraft positions between the flight $i$ and the flights labeled as $i-1$ in the priority list. This operation is repeated for all the times $t + k\delta t$ with k ranging from 1 to N such that $t + N\delta t \equiv t + \Delta t_m$ where $\Delta t_m$ is equal to $\Delta t_l$ or $\Delta t_d$ depending whether the conflict detection module has been activated by a re-routing procedure or by a direct procedure. For each flight $i$ the algorithm computes an array of flight positions $p_{i,k}$, $k = 1, \cdots N$ given the flight positions at different time $t + k\delta t$.

Suppose we are now checking if the $i$-th flight trajectory is conflicting with all other $f_j$ trajectories, with $j < i$. For each of the $N$ elementary time-increments, we compute a matrix of distances $d^i_{j,k}$ with j rows and N columns. For all aircraft flying at the same flight level all distances are computed by using the Haversine distance [95] between each pair of flight positions[4]. For pairs of aircraft flying at different flight levels at time $t+k\delta t$ the distance is set to infinity because aircraft flying at different flight level are not raising minimum separation issues. For each column we select the minimum value and obtain a vector $d^i_{min}(k)$ of length $N$. A possible conflict between two aircraft flying at the same flight level is detected at time $t + k\delta t$ whenever the elements of $d^i_{min}(k)$ are smaller than the safety distance threshold $d_{thr}$ that is usually set to 5 NM. This reference value is the standard value used in ATM for conflict detection, see Ref. [96].

[4]The computation of the Haversine distance is particularly time-consuming. Therefore we have also implemented in the code the possibility that in some specific cases the Euclidean distance is used instead of the Haversine one. This is for example advised when it is necessary to perform a very large number of simulations in a limited portion of the airspace.

In order to mimic some heuristics typically used by air traffic controllers in detecting conflict we introduce in the ABM a linear growth of the safety threshold $d_{thr}$ as a function of the time interval from the present time. In fact when an air traffic controller forecasts the position of an aircraft at a far future time he uses an additional space of separation between the aircraft to be safe in the forecast. Our model therefore uses a safety distance threshold defined as:

$$d_{thr}(k) = d_{thr} + \Delta d_{thr} k \tag{3.1}$$

where $\Delta d_{thr}$ is one of the model parameters.

When a conflict is detected the algorithm proceeds to the next module that performs the de-conflicting of flight trajectories.

## 3.7 Conflict Resolution module

After the conflict detection module has detected a conflict, this module searches for a new conflict free trajectory. It is conceived as a two-step algorithm that acts on the search of a new trajectory. The first step attempts to perform a re-routing of the flight trajectory. When the re-routing is successful the new trajectory is accepted. If the re-routing module fails to find an appropriate new trajectory the algorithm move to the second step that require a change of flight level for the aircraft.

### 3.7.1 Re-rerouting submodule

The procedure of the re-routing attempt is illustrated in Fig. 3.3. We first identify the position $B$ (not necessarily a navigation point) defined by $k = 0$ at the considered time step. We then identify the navigation point $A$ which is the first navigation point after the area of the potential collision (filled circle in the figure). The procedure is to attempt to re-route the trajectory such that all navigation points that are in the conflict area plus the $A$ navigation point are avoided. These navigation points are replaced by a temporary navigation point (see T point in Fig. 3.3). The temporary navigation point is selected from several possibilities (see grey points in Fig. 3.3) by choosing the navigation point solving the conflict that presents the shortest path between position B and navigation

point E, i.e. the navigation point where the flight trajectory is re-routed. Another constraint about the re-routing trajectory is the request that the deviated trajectory from the planned one cannot exceed an angle $\alpha_M$ both for the $\alpha_{in}$ and $\alpha out$ angles observed between the planned and the re-routed trajectories (see Fig. 3.3). If the re-routing trajectory is not able to find a solution the re-routing submodule attempts to re-route the flight trajectory by moving forward the navigation point E and by looking again for a re-routing trajectory. When a possible solution is found, the result of the search is accepted if the re-routing trajectory deviates from the planned trajectory for less than a maximal time $T_{max}$. $T_{max}$ is a model parameter that represents the maximal time that an aircraft can spend away from its planned trajectory each time it is deviated. If the solution found has a deviation time longer than $T_{max}$ the re-routing submodule is not selecting any new trajectory and the resolution of the conflict is passed to the flight level module. In the right panel we show the distance between the two aircraft for the planned trajectory (blue dots) and the ones considered by the ABM module (gray lines). Amongst those, the trajectory that satisfies the requirement of minimum separation distance is highlighted in red, as in the left panel.

### 3.7.2 Flight level change submodule

The second step of the conflict resolution module involves changes of flight level. A flight level (FL) is a unit measure defined as altitude above sea-level in 100 feet units measured according to a standard atmosphere. Allowed flight levels are separated by 1000 feet, i.e. 10 flight levels (separation levels). This is the standard separation vertical distance between any pair of aircraft, see Ref. [96]. Moreover, in our model the semicircular rule has been considered, meaning that aircraft flying in opposite directions are allowed to fly only along odd or even levels respectively. Therefore when an aircraft needs to be moved to another separation level, it will not be moved to the next first one but to the second one in order to respect the semicircular rule, thus performing a jump of 2000 feet or 20 FLs.

All flights are considered to be available in the planned trajectories. In our agent-based model aircraft can move two Flight Levels (FL) first upwards and, if the conflict cannot be solved by a move upwards, downwards. The model assumes that the flight

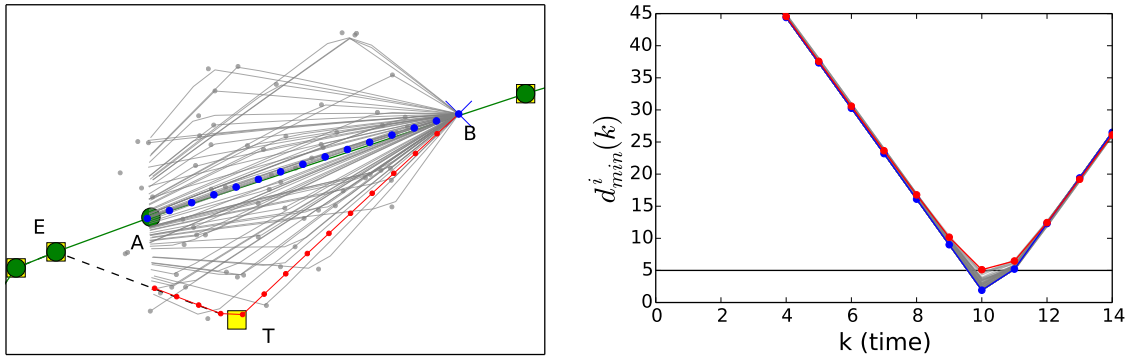


Figure 3.3: The figure illustrates the procedure of re-routing, see text for more details. The gray trajectories, although possible, are not selected because they do not guarantee the minimum separation of 5 NM required between two aircraft. The re-routing occurs between point B (blue cross of the left panel) and E (green circle of the left panel). The re-routing is performed by deviating the flight trajectory to the temporary navigation point $T$ (yellow square of the left panel) and then re-route back the trajectory to navigation point E. To find the best re-routing flight trajectory the ABM module explores trajectories passing through several different temporary navigation points (gray spots of the left panel). The distance between the two aircraft is shown in the right panel for the planned trajectory (blue dots), the ones considered by the ABM module (gray lines) and the selected one satisfying the requirement of minimum separation distance (red dots). In the left panel all trajectories are considered within the time of the look-ahead $\Delta t_l$.

level change is abrupt occurring when the conflict resolution is settled. If no flight level is available to solve the conflict then the list is reshuffled by moving the considered flight in the first position of the priority list.

When a flight level change is executed the flight remains in the new flight level for a time equals to $T_{max}$. After $T_{max}$ the aircraft goes back to the flight level of the planned flight.

## 3.8 Direct module

A direct, i.e. a change of the planned trajectory significantly shortening the flight path, is made by skipping one or more navigation points of the flight plan and flying straightly from the current navigation point to a distant navigation point of the flight plan. In our algorithm this module is executed with a probability that depends on the workload of sectors of initial and ending navigation points of the direct.

When the workload of sector exceeds its inferred capacity all directs that come from other sectors are not allowed, while re-routing due to safety issues are still allowed. Operationally this means that in a condition when the workload equal or exceeds inferred capacity any other incoming flight has to enter the sector from the navigation point specified in the flight plan.

Specifically, let $n_i$ be the first navigation point to be crossed of the current time step, and $n_m$ the navigation point where the flight will return on its original flight plan. By issuing a direct trajectory from $n_i$ to $n_m$ therefore $m - i - 1$ navigation points will be absent in the new trajectory, as illustrated in the left panel of Fig. 3.4.

The direct module first evaluates how many navigation points can be skipped with the constraint that the flight has to come back to the planned trajectory within a time interval equal to $T_{max} = 20$ min [5], and the direct is conditioned to the inferred sectors' capacity of the adjacent sectors.

After that the model evaluates if the new trajectory will be involved in conflicts. In order to do this check we use the Conflict Detection module of section 3.6 with a

[5]The choice of $T_{max}$ has been done in agreement with the indications of the air traffic controllers consulted within the ELSA project of SESAR.

different time-interval $\Delta t_d$. If the direct is safe and the angle between the new and original trajectory is larger then a sensitivity threshold value $\alpha_s = 1°$ then the new trajectory is accepted, otherwise the algorithm tries a suboptimal solution, see the left panel of Fig. 3.4.

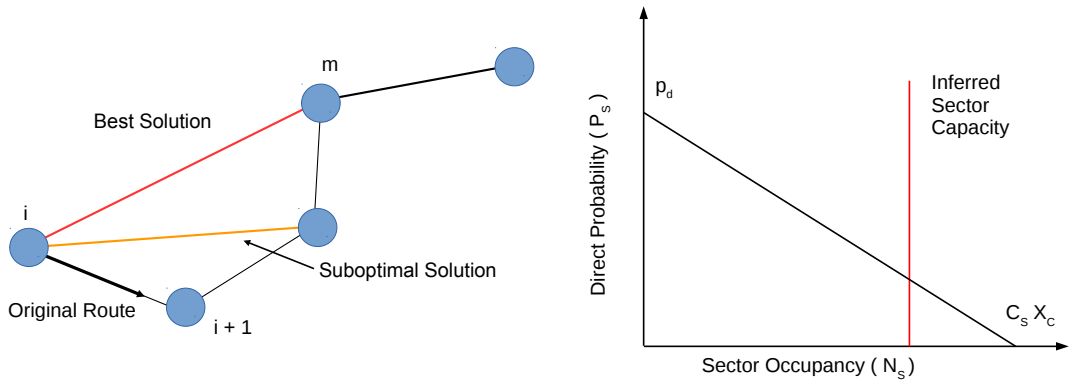


Figure 3.4: Left panel: illustration of the procedure implemented to issuing directs. Right panel: Probability function used in the procedure implemented to issuing directs.

The probability to issue a direct for an air controller operation on a sector $s$ is dependent by the workload and by the inferred capacity of the sector involved. Let $C_s$ be a constant of the $s$-sector that in our calibration procedure we fixed to be the inferred sector capacity obtained from real data [94]. Let $P_s(N_s)$ be the probability to issue a direct in the $s$-sector when the workload of sector $s$ is $N_s$. For the sake of simplicity we model $P_s(N_s)$ as a linear decreasing function of $N_s$, see the right panel of Fig. 3.4

$$P_s(N_s) = p_d \left(1 - \frac{N_s}{x_c\, C_s}\right) \tag{3.2}$$

The probability to attempt a direct is function of two parameters $p_d$ and $x_c$. The first $P_s(N_s = 1) = p_d$ is the probability to attempt a direct if just one flight is in the sector. The second parameter $x_c$ is used to control the slope of probability as a function of the workload, as illustrated in the right panel of Fig. 3.4. The $p_d$ parameter plays the role of a scale factor for the overall probability. The $x_c$ parameter measures the controllers confidence in approaching the maximum sector's inferred capacity. While $N_s$ and $C_s$ are

parameters depending on each specific sector, $p_d$ and $x_c$ are global parameters that are set across the whole considered ACC.

In the present version of the model, air traffic controllers behave in the same way in the different sectors. However, by introducing a direct probability $P_s$ that depends on the actual inferred capacity of each sector, see Eq. 3.2, we have actual a genuinely multi-sector ABM where directs are issued differently across the ACC and across the day. The choice of the use of the same parameters for different controllers and sectors (except inferred capacity) is done in order to make the ABM model as parsimonious as possible.

## 3.9 Disruptions

In the current version of the ABM the disruptions are modeled as circles of center $S_c$ and fixed radius $S_r$ and located at a flight level drawn from a random uniform distribution in the range $[FL_{min}, FL_{max}]$. Each disruption vertically extends over 1 separation level, i.e. 1000 feet. Each disruption has a duration drawn from a random uniform distribution in the range $[\Delta t_s, S_d\, \Delta t_s]$, where $S_d$ is an integer number. The area within these circles is inaccessible for the aircraft, and if a disruption appears along an aircraft flight trajectory, the aircraft has to be re-routed or change flight level because all maneuvers are interdicted inside the disruptions. We implemented the fact that there is an average number $S_m$ of disruptions per time-step per flight-level. In our model, the number of disruptions will follow a Poisson distribution with mean $S_m$.

The position of the disruptions is drawn from a list of points provided by the user. In this way the user can obtain a uniform distribution of the disruptions inside the ACC providing a uniform distribution of the points $S_c$, or he/she can obtain different spatial distributions by providing an appropriate list.

At the beginning of each time-step the controllers cannot forecast the disruptions. This means that they look at the current position of the disruptions and they operate assuming that the disruptions are fixed along the time horizon $\Delta t_d$ even if they could disappear within the $\Delta t_s$ time step.

This module is not used in the simulations of the present dissertation. For this reason,

the disruption parameters are not included in the summary Table:3.1.

## 3.10 Model's parameters

In Table 3.1 we summarize the model's parameters used in the different modules described above. In the third column of the Table we give a short description of the parameter and in the fourth column we give a categorization of the parameters describing whether the parameter is calibrated from data (CD) or it is set according to information obtained by interviewing ATM experts and ATCOs (CV). A more detailed description of the parameters is done in the following sections.

The parameters that need to be calibrated from data are a few. There are also several parameters (CV category) that can be inferred form the typical behavior of controllers. These are parameters that should be selected by consulting ATM experts and ATCOs. It is worth noting that by considering these variables as parameters our model allows to perform scenario simulations to test how changing a certain feature of air traffic controllers might affect ATM performances.

| ID | Parameter | Description | Type | Value |
|---|---|---|---|---|
| 1 | $\delta t$ | Length of the elementary time-interval. | | 10 s |
| 2 | $\Delta t_l$ | Length of the forecast for collision, controller's look-ahead. | CD | 7.5 m |
| 3 | $\Delta t_d$ | Length of the forecast for directs. | CV | 15 m |
| 4 | $\Delta t_s$ | Basic time step. | | 3 min. |
| 5 | $l_\epsilon$ | Aircraft velocity noise range | | 0 ; 0.1 |
| 6 | $d_{thr}$ | Safety Distance threshold. | CV | 5NM |
| 7 | $\Delta d_{thr}$ | Increment of the safety distance threshold in the forecast. | CV | 0; 0.33 in section 5.2.1 |
| 8 | $\alpha_M$ | Maximum angle of deviation between planned and re-routed trajectory. | CV | 27 deg. |
| 9 | $T_{max}$ | Maximum time spent outside the planned flight trajectory. | CV | 20 min. |
| 10 | $p_d$ | Unconditional probability to try to issue a direct. | CD | 0.24 |
| 11 | $x_c$ | Tolerance to the sector congestion. | CD | 0.63 |
| 12 | $\alpha_s$ | Minimal angle to issue a direct. | | 1° |
| 13 | $C_s$ | Sector inferred capacity. | CD | Sector's specific |

Table 3.1: Model parameters.

# 4 Input Data Generation

In this chapter we describe the modules of the model that we used to generate the input data to the model necessary in order to perform the simulations.

## 4.1 Using the real Flight Plans

We briefly recall here that the DDR files available for the ELSA project are mainly of three types: M1/M3 files containing information of the flight trajectories, and the NEVAC files containing information about the sectors, the ACCs and the navigation points. Specifically the M1 files contain the last filled flight plan submitted few hours before departure, whereas the M3 files contain the radar track of the aircraft. Both M1 and M3 have the same format, that is a sequence of 4-Dimensional points i.e. latitude, longitude, flight level (FL) and time-stamp for each NVP.
In the present dissertation, we have considered all flights in the enlarged ECAC airspace even if they departed and/or landed in airports external to the enlarged ECAC airspace. One of the main issues we had to tackle was cleaning the data. Indeed, there are many information in the database that we do not need. Hence, we decided to use standard filters to work on a well designed set of flights. Specifically we selected: i) flights performed with Landplanes (i.e. no helicopter, gyrocopter, only aircraft which can only operate from or alight on land), ii) scheduled flight, iii) flight having a IATA code, furthermore we excluded iv) flight having a duration shorter than 10 minutes, and v) military flight.
Additionally, with the aim to modelling the en-route air traffic flow on a specific ACC, we filter out that portion of the flight trajectory lower than 240 Flight Level (FL). Furthermore we exclude from the input flight plans such NVPs that are not contained

within considered ACC.

Finally by cross-checking our input flight plan with the NEVAC files, we are able to associate at each NVP the related sector of reference. As a result the M1 produced can be immediately used as ABM input files, or they can be send to the modules described in the following sections.

## 4.2 Flight Plan Generator 1 module: from M1 real trajectories

The first Flight Plan Generator produces M1 simulated file obtained by starting from real data. In fact, for the considered day and for the considered airspace, we select the flight plans according to the filters illustrated in the previous section and then we generate simulated flight plans that preserve:

- The distribution of flight between origin and destination. For an example, see the upper left panel in Fig. 4.1.
- The occupancy of flight levels (with odd rule). For an example, see the upper right panel in Fig. 4.1.
- The distribution of departure times. For an example, see green curve in lower right panel of Fig. 4.1.
- The median velocity of the aircraft, see lower left panel in Fig. 4.1.
- The unweighted navigation point network, see Ref:[43].

It is worth mentioning that the navigation point network is generated starting from real data. Then the trajectories of the simulated M1 flight plans are the best-path on the navigation point network. The generated trajectories are therefore relative to the CURRENT scenario by construction. One can use the correction procedure of section 4.3.1 or the correction procedure of section 4.3.2 to generate flight plans with larger efficiency up to the level of the SESAR scenario.

This module does not take into account capacity constraints. It will therefore be used in those simulations where we would like to emphasize the fact that in the SESAR scenario sectors will play a minor role.

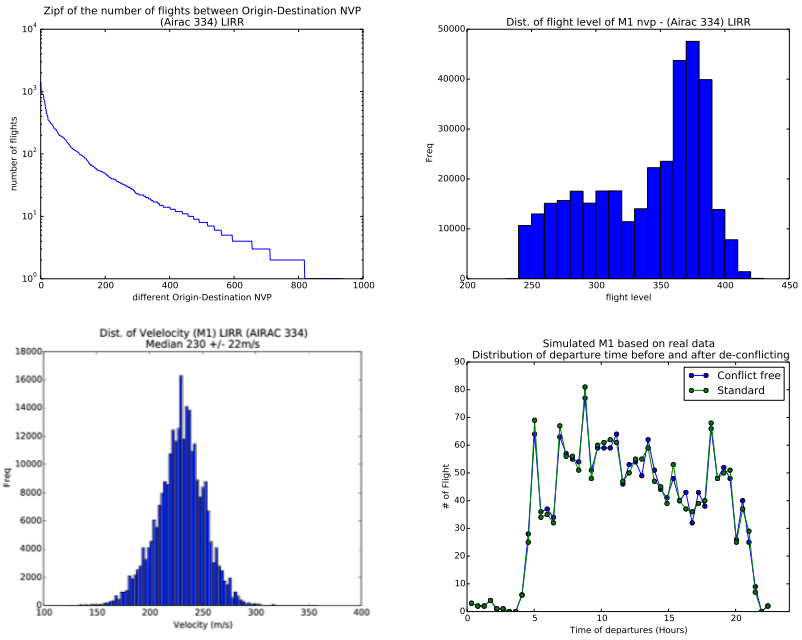


Figure 4.1: We show: the empirical probability distribution of the number of flights between origin and destination airports (upper left panel) and empirical probability distribution of flight level occupancy (upper right), the empirical distribution of the aricraft velocities (lower left) and the distribution of the departure times: the geen curve refers to the empirical values, the blue curve are the de-conflicted flight plans descrived in sec:4.4 (lower right). All figures refer to the day 06/05/2010, LIRR ACC.

### 4.2.1 Flight Plan Generator 2 module: Strategic Layer

The strategic layer is a full agent-based model where different agents, i.e. airlines and network manager, are collaborating or competing for the same resources, i.e. time slots and trajectories [94]. The strategic layer is designed to generate trajectories with a coarse level of description, suitable to study high level phenomena. In particular, the trajectories are kinematic and do not take into account winds, weight, etc.

In short, the strategic layer takes as input a network of navigation points with the legitimate paths and fills the airspace realistically, with airlines submitting flight plans and the network manager rejecting or accepting them on a capacity-constraint basis.

For the purposes of the present work, we consider the strategic layer as an external tool that produces a set of realistic trajectories, fulfilling some capacity constraints, which can be used as an input to our tactical layer. Since the agents can have different behaviors, the results depend also on the choices of the code user. Here we used some default values that were obtained by considering the results of the calibration procedure in [60].

As a result, the strategic layer, when used as a "traffic generator", generates synthetic traffic on a given network of navigation points and sectors. It allows to create traffic in a set of sectors given some airports and/or entry/exit points in a realistic way, making sure no sector is overloaded. The user can specify in particular the sector capacities. Other parameters, such as those specifying the type of airlines present in the considered airspace, are set to default values [60].

### 4.2.2 3-D trajectories

It is worth mentioning that both traffic generators give as an output 2-D trajectories, i.e. trajectories that lie on an horizontal plane. We aim in the future to overcome such limitation, working at a fork project of the strategic layer. However the current released version of the strategic layer [60] does not allow to manage 3-D trajectories.

In order to have 3-D trajectories we implemented the following procedure: (i) we first extract from the distribution of flight levels occupancy a number of flight level values equal to the number of navigation points of the considered trajectory; (ii) we then order the values so that the first third of them are in increasing order, the last third of values are in decreasing order the second third of values are mixed. This is a very simplistic procedure that nevertheless has the advantage to roughly capture the fact that aircraft have an ascending en-route and descending phase.

## 4.3 SESAR scenario trajectories

The model described above will be used to perform scenario simulations in order to investigate how predictability and capacity issues will change from the current to the SESAR scenario. To this end, we decided to model the SESAR scenario as the end-point of a spectrum of possible scenarios continuously ranging from the current to the SESAR scenario.

First of all we extended the definition presented in section 2.2 of the single flight efficiency to an airspace efficiency $E$ in order to measure how different a given network of routes is with respect to the situation where any pair of airports (Origin and Destination) is directly connected by straight route. We define such efficiency as:

$$E = \frac{\sum_{N_f} d(O,D)_i}{\sum_{N_f} d_{BP}(O,D)} \tag{4.1}$$

where $d(O,D)$ is shortest distance between Origin and Destination, while $d_{BP}(O,D)$ is the Best Path distance on the route network identified by the navigation points. The sum is over all planned flights recorded in the M1 files. In this way the more a route is congested, the more weight it has. Another possible way to have an unweighted efficiency is to extend the sum above all possible routes. This metric takes values in the range (0,1]. Of course, the value E=1 corresponds to the SESAR scenario.

### 4.3.1 A correction procedure

We will move in a controllable way from the current scenario to the SESAR scenario by generating surrogate route networks each identified by a certain value of efficiency. This will be done by introducing a *correction* of the current trajectories. This will allow us to study the transition between the current scenario and the SESAR scenario in a controlled way.

The algorithm requires as input a generic M1 file, i.e. a set of real planned trajectories, and produces as output another surrogate M1 with a larger target value of efficiency. At each step the algorithm evaluates the current efficiency and if it is less than the target efficiency performs the following steps:

- for any flight trajectory, the first and last point will not be modified, as they correspond to the origin $O$ and destination $D$ airports, see Fig. 4.2.
- then we randomly selects a navigation point $P_i$ of a certain trajectory flight between the $2^{nd}$ navigation point and the one before the last navigation point.
- we substitute $P_i$ with the medium point $M_i$ between the previous navigation point $P_{i-1}$ and the next one $P_{i+1}$, see Fig. 4.2. In some case, $P_{i-1}$ might coincide with the origin $O$ or $P_{i+1}$ might coincide with the origin $D$. This is not a problem given the fact that $P_{i-1}$ and $P_{i+1}$ are merely used as a reference.
- this procedure is iterated until the target efficiency is reached or all navigation points of all trajectories in the M1 files are modified.

At each iteration of the above steps the procedure maintains the number of navigation points present in the M1 files.

By using such procedure we can generate a set of M1 scenarios with increasing efficiency from the current scenario to the SESAR scenario characterized by unitary efficiency. We will therefore use the model described in the previous section to generate the corresponding sets of M3 files. We will be therefore able to investigate the modifications occurring from the current to the SESAR scenario in a controlled way.

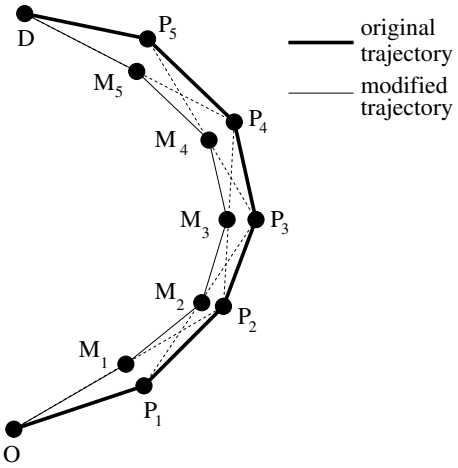


Figure 4.2: The figure illustrates the techniques of correction that we use in order to generate surrogate M1 scenarios with increasing efficiency.

### 4.3.2 A simplified correction procedure

The correction procedure described above may be rather time consuming from a computational point of view. We have therefore devised a simplified procedure that reveals to be less time consuming and therefore more appropriate when we will have to perform several sets of simulations.

The alternative correction is done in the following way. In a first step, a point $P_i$ is chosen at random on a trajectory, like previously. However, the point is simply removed from the trajectory instead of being moved, i.e. the flight goes from $P_{i-1}$ to $P_{i+1}$ directly. The procedure goes on until the target efficiency is met.

In a second time, we resample the trajectories by generating new points on the trajectory so as to ensure that the agent-based model works properly. We do this by keeping the same number of navpoints between the remaining points on the trajectories that there were originally. Hence, the number of navigation points per trajectory is kept constant too. Figure 4.3 illustrates the procedure.

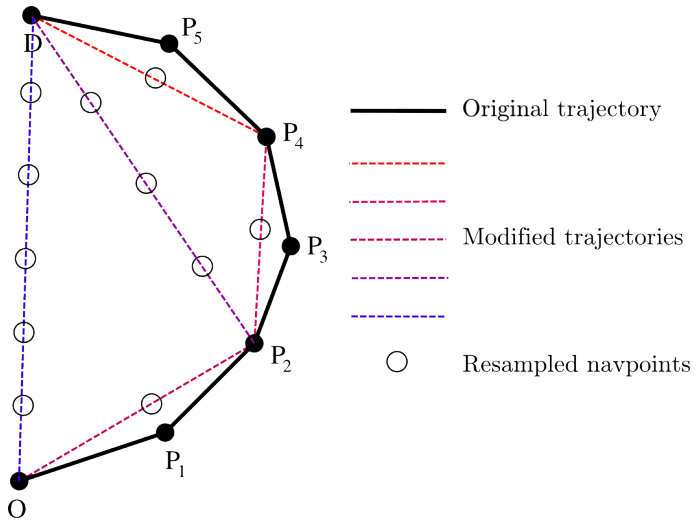


Figure 4.3: The figure illustrates the simplified technique of correction that we use in order to generate surrogate M1 scenarios with increasing efficiency.

By summarizing, our model will give us the possibility of performing simulations of the current and SESAR scenario each of them characterized by:

- **current scenario**: low efficiency, no conflict-free trajectories.

- **SESAR scenario**: unitary efficiency, conflict-free trajectories.

In both cases we can consider the possibility of giving or not directs ($p_d = 0$ or $p_d = 1$) and the possibility of having or not having sectors.

## 4.4 Pre-tactical de-conflicting module

The deconflicting module we describe here takes as input M1 real or surrogate trajectories. In other words, we start from M1 flight plans and try to make them conflict-free by using a *brute force* method.

In fact, it is assumed that in the SESAR scenario, differently from the current scenario, the flight-plan recorded in the M1 files will already be conflict-free, due to a better strategic planning of the different aircraft trajectories. Therefore in order to eliminate any possible bias due to this issue we decided that in some case it might be worth to consider M1 de-conflicted trajectories for all the networks with different efficiency values generated by using the procedures of section 4.3.

Specifically, we use the Conflict Detection Module of section 3.2 to detect possible conflicts. Starting from M1 files, we consider all flight trajectories active in the selected ACC and in the considered day. If a conflict is detected, we randomly shift in time the departure of the interested aircraft of an amount of time within the range [-5 min, 5 min]. We try this procedure until the flight trajectory is de-conflicted, for a maximum number of 100 iterations. If at the end of the 100 iterations the aircraft is still involved in a safety event we try to shift in time the departure of this aircraft of an amount of time within the range [-10 min, 10 min], then within the range [-15 min, 15 min] and finally in the range [-20 min, 20 min].

At the end of this process all M1 flight trajectories will be conflict-free. Indeed, in a few cases even enlarging the shift time interval to 20 min may be not enough to get conflict-free M1 flight trajectories. In this case, we start again the procedure starting from another flight-plan.

This module may be switched on and off, depending on the type of simulations we want to perform.

# 5 ABM Calibration, simulations and Scenarios Analysis

## 5.1 Calibration of the model

In this section we want to discuss the calibration activities that have to be performed in order to use our model.

We will here refer to the air-traffic of LIRR ACC (Rome, Italy) between 2010-05-06 and 2010-06-03, i.e. the 334 AIRAC. The input data of the model are taken from the database of DDR and NEVAC files developed within the ELSA [97] project. We consider as an input to the model the M1 flight plans with the constraints indicated in section 4.1. To focus our attention on the en-route phase we filtered out from the flight plans all navigation points crossed at an altitude lower then 240FL. After the filtering procedure 35714 flights were retained in the entire AIRAC. In order to include the local constrains of the sector capacities, it is important to remember that the sectors are not static geometric regions but they are merged together and split dynamically to fulfill the occupancy requirement. For the sake of simplicity we will refer to the collapsed sector defined in the reference [94]. These are a static bi-dimensional projection of the sectors higher than FL 350. The sectors capacity inferred from data is defined as the maximum number of flight expected within a time-window of a hour inside the collapsed sector.

In this section we describe our calibration procedure. In our simulations we consider the scheduled flights of the LIRR ACC (Rome, Italy) of the AIRAC 334 described in section 4.1. The calibration procedure is performed by choosing a specific stylized fact observed in real data and requesting that model simulations are able to reproduce them.

Indeed, there is some degree of arbitrariness in selecting the specific stylized fact. Dif-

ferent ones can be chosen depending on the specific aspects of the ATM researchers want to investigate. In the present work, in order to calibrate the models parameters related to controllers' behavior we choose as stylized fact a statistical regularity concerning the intraday pattern of directs issued by ATCOs. Specifically we calibrate our model to reproduce the intraday evolution of the deviation rate metric of section 2.3 that has been recently introduced in Ref. [50].

The deviation rate described in section 2.3 quantifies the deviations observed from the planned flight trajectories. We call *deviation* the event such that an aircraft passing over a scheduled navigation point does not go to the next planned one. The deviation rate is defined as the ratio between the observed number of deviations and the number of possible deviations in the airspace estimated in a one hour time window. The number of possible deviations is defined as the number of planned navigation points that are actually crossed by the aircraft. This metric is computed for each hour of the day by using the information about all planned and actual flight trajectories.

This metric describes an unknown mixture of ATCO operations, i.e. re-routing and direct. In section 2.3 it is shown that, in relative terms, directs are mainly issued during night-time i.e. in low traffic conditions while they are relatively less issued during day-time. Our choice is to reproduce this intraday statistical regularity. In the right panel of Fig. 5.1 we show (blue circles) the empirical behavior of the deviation rate estimated over the entire 334 AIRAC cycle as a function of the time of the day. The deviation rate presents a U-shape having higher values during night hours and lower values during day hours. The error bars are computed as the 95 % Wilson score interval [83] used to associate a confidence interval to a proportion in a statistical population.

Hereafter we detail the procedure we have used to calibrate $p_d$, $x_c$ and $\Delta t_l$ parameters. In our calibration procedure we considered $p_d \in [0.03, 0.5]$ with steps of 0.01567, $x_c \in [0.34, 1.5]$ with step of 0.03867 and $\Delta t_l \in [5, 15]$ minutes with steps of 2.5 minutes and for each triplet of parameters we performed one single simulation for each considered day in the AIRAC, totaling 20 days of simulations – with Saturday and Sundays excluded. From the output of the ABM we estimated the deviation rate with a time window of one hour. By using the results of simulations, we minimized the chi-squared $\chi^2$ computed starting from the deviation rates obtained with the ABM and the values estimated from

real data.

$$\chi^2 = \sum_T \frac{(dev_i^{(sim)} - dev_i^{(real)})^2}{dev_i^{(real)}}$$

The $\chi^2$ is therefore computed over 24 points. In the left panel of Fig 5.1 we are showing the average values of the $\chi^2$, as a function of $p_d$ and $x_c$ when $\Delta t_l = 7.5$ minutes. The lowest value of $\chi^2$ is associated to $p_d = 0.2465$ and $x_c = 0.6310$ and $\Delta t = 7.5$ min. This set of parameters corresponds to $\chi^2 = 0.01294$. However, it is worth noticing that a larger region of parameters (see the magenta region) could still provide acceptable set of parameters. The solid green line in the right panel of Fig. 5.1 shows the deviation rate metric obtained by performing the simulation of the model with the selected parameters $p_d = 0.2465$ and $x_c = 0.6310$ and $\Delta t_l = 7.5$ min.

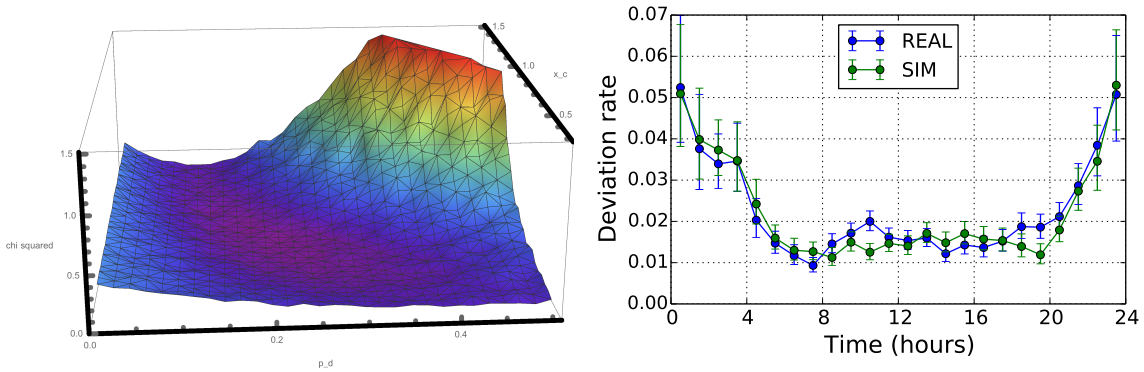


Figure 5.1: Illustration of the calibration procedure. Left Panel: we are showing the values of the $\chi^2$, as a function of $p_d$ and $x_c$ when $\Delta t = 7.5$ minutes. Right Panel: we show the empirical (blue circles) behavior of the deviation rate metric averaged over the entire 334 AIRAC cycle. The solid green line shows the deviation rate metric obtained by performing a simulation of the model with the selected parameters $p_d = 0.2465$ and $x_c = 0.6310$ and $\Delta t = 7.5$ min.

Here we want to assess the importance of the calibration procedure. In fact, in Fig. 5.2 we show results that can be obtained by our model by choosing sets of parameters different from the calibrated ones. The first example sets that no direct is issued (left panel of Fig. 5.2 ). The "No Directs" case is obtained by setting $p_d = 0$ and $\Delta t_l = 7.5$ min. The second example sets that the probability to issue a direct is independent from the sector workload (right panel of Fig. 5.2). This second example is obtained by setting

to the case when $p_d = 0.24$, $\Delta t_l = 7.5$, as in the calibrated case and $x_c = 1000$. Such a value of $x_c$ ensures that the sector workload plays no role when directs are issued. With the chosen parameters we have that the deviations rate simulated during night-time corresponds to the empirical case.

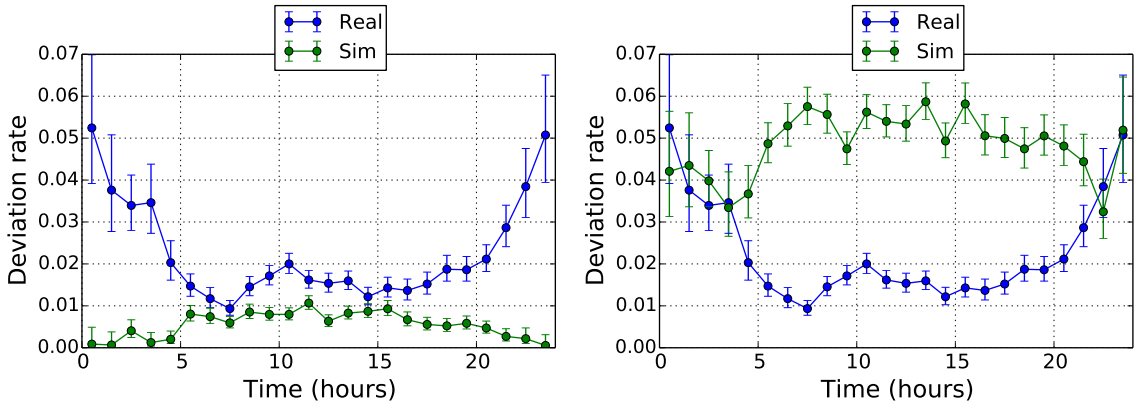


Figure 5.2: Left panel: deviation rates in the "No Directs" case. Right panel: deviation rates in the "No Sector Directs" case.

## 5.2 Statistical regularities of ABM simulations

In this section we give some examples of the simulation outputs of our model obtained with the parameters of the calibration procedure of section 5.1 for the evolution of the planned flight trajectories of the LIRR ACC (Rome, Italy) of the AIRAC 334.

In Fig. 5.3 we show the fraction of the different decisions taken by controllers. The three decisions controllers can take are (i) issuing a direct, (ii) re-routing a flight trajectory, and (iii) temporary change the flight level of a trajectory. We label the total number of operations in a given one hour interval as $N_O$. $N_D$ is the number of directs issued by controllers in the time interval. Similarly, $N_R$ is the number of re-routings and $N_F$ is the number of flight level changes. In Fig. 5.3 we show the ratio of directs $N_D/N_O$ (blue circles), the ratio of re-routings $N_R/N_O$ (green circles), and the ratio of flight level changes $N_F/N_O$ (red circles). The error bar is to the 95% Wilson confidence interval. The ratio of flight level changes (red circles) and the ratio of re-routings (green circles) issued to solve possible conflicts are larger during day-time rather than during

night-time. It is worth noting that the number of re-routing is always higher than the number of flight level changes. This is a satisfactory outcome of our model consistent with the feedback we have received from ATM experts. The ratio of directs (blue circles) behaves in the opposite way. This is again expected, given the fact that lower traffic conditions during night allows for the possibility of optimizing trajectories more easily [50]. During day-time, the sector workload can be different for different sectors and therefore maximal sector capacity is not reached at the same time for all sectors. This can be an explanation why directs are also issued during day-time.

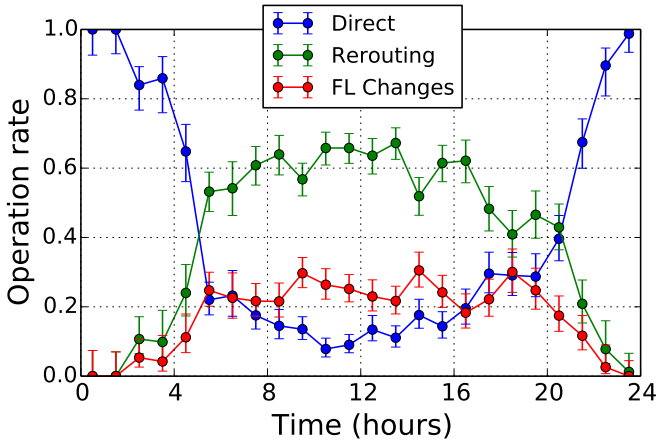


Figure 5.3: Controllers' operation rate: the ratio $N_F/N_O$ between the number $N_F$ of flight level changes (red circles) and the total number of operations $N_O$, the ratio $N_R/N_O$ between the number $N_R$ of re-routings (green circles) issued to solve possible conflicts and $N_O$, the ratio $N_D/N_O$ between the number $N_D$ of directs (blue circles) and $N_O$, where $N_O = N_F + N_R + N_D$. The error bar correspond to the 95% Wilson confidence interval.

### 5.2.1 Conflict resolution in the ABM

In this section we discuss the ability of our model in performing conflict resolution by investigating the distance observed between all pairs of aircraft flying during a given day.

In Fig. 5.4 we show the cumulated distribution of the distance between any pair of aircraft for a simulation performed for the first day of AIRAC 334. The red curve shows

the distribution of the planned trajectories, the blue curve (labeled as simulation I) is the cumulated distribution of the flight trajectories simulated with our model by using the safety threshold of 5 NM. The green curve (labeled as simulation II) is the cumulated distribution of the flight trajectories simulated with our model by using a safety threshold that increases with the look-ahead, as described in section 3.6. Specifically, in the second simulation we set $\Delta d_{thr} = 0.33$.

In the figure we highlight as a vertical line the value of 5 NM. It is worth noting that both the blue and the green lines show values that are on the right of the vertical line. This means that our ABM solves all conflicts that were present in the planned flight of the day. The blue line presents values that are quite close to the 5 NM threshold whereas, as expected, the green line has lower values for distances slight above 5NM, thus indicating that aircraft are more separated.

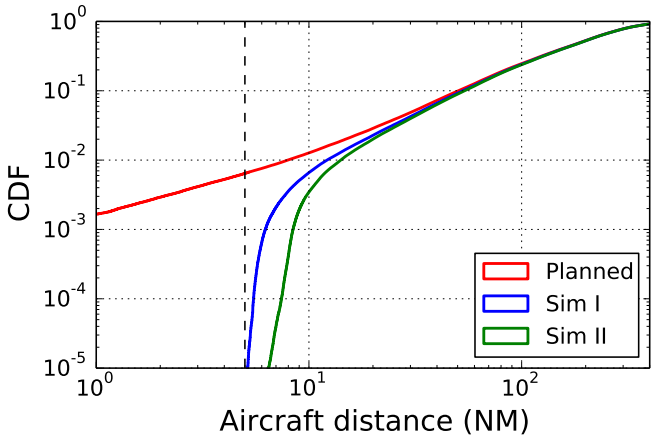


Figure 5.4: Cumulative distribution of the distance between any pair of aircraft. The red curve shows the cumulative distribution of the planned trajectories, the blue curve (simulation I) is the cumulative distribution of flight trajectories simulated with our model by considering a fixed safety threshold of 5 NM. The green curve (simulation II) is the cumulative distribution of flight trajectories simulated with our model when the safety threshold increases with the look-ahead by setting $\Delta d_{the} = 0.33$. The cumulative distribution is obtained by considering all flights of AIRAC 334 and the associated simulations.

The parameter $\Delta d_{thr}$ therefore allows the model to fine tune the probability of ob-

serving a pair of aircraft with a given minimal distance in a given day. As also recalled in Table 3.1, $\Delta d_{thr}$ is a parameter that might in principle reflect the ATCOs behavior when managing traffic with a large look-ahead. In fact, a large $\Delta d_{thr}$ would indicate that human controllers tend to be overly safe when managing trajectories with a large look-ahead and tend to separate aircraft pairs more than it is needed. The model shows that this might end up in having aircraft separated more the 5 NM and therefore in a non-optimal usage of the available airspace that in turn leads to a reduction of the maximal sector capacity. On the other hand, a small $\Delta d_{thr}$ would indicate that human controllers are rather confident about their procedures even for aircraft that are far away. In this case our simulations indicate that all available airspace is used which might lead to an optimal assessment of sector capacity.

### 5.2.2 Spatial heterogeneity of the operations

In Fig. 5.5 we show the map of navigation points with the information about the type of operations controllers do in proximity of such navigation points. In the left panel we show re-routings. In the central panel we show flight level changes, while in the right panel we show directs. In all panels the size of of circles is proportional to the number of operations performed. All values refer to the 334 AIRAC. Interestingly, the navigation points with the highest number of re-routings are aligned along the route between Milan and Rome, which shows the highest traffic levels, as indicated in Fig. 5.6. On the other hand the highest number of directs is issued either in central Italy (most probably in proximity of Fiumicino airport) or in the Thyrrenian Sea, between Naples and Sicily, where traffic levels are less pronounced than in the northern region, as indicated in Fig. 5.6. The location of flight level change operations highlights those navigation points where controllers have difficulties in solving conflicts and use flight level change as the last resort for conflict solution.

A similar result also holds for operations performed by real ATCOs. Indeed, the ATCO operations do not uniformly affect the flux of aircraft in the airspace. Rather, ATCOs typically concentrate their operations on specific segments of flight trajectories (i.e. on the path joining two neighboring navigation points). This is clearly shown by the results summarized in Fig.5.6 where we show the distribution of the difference

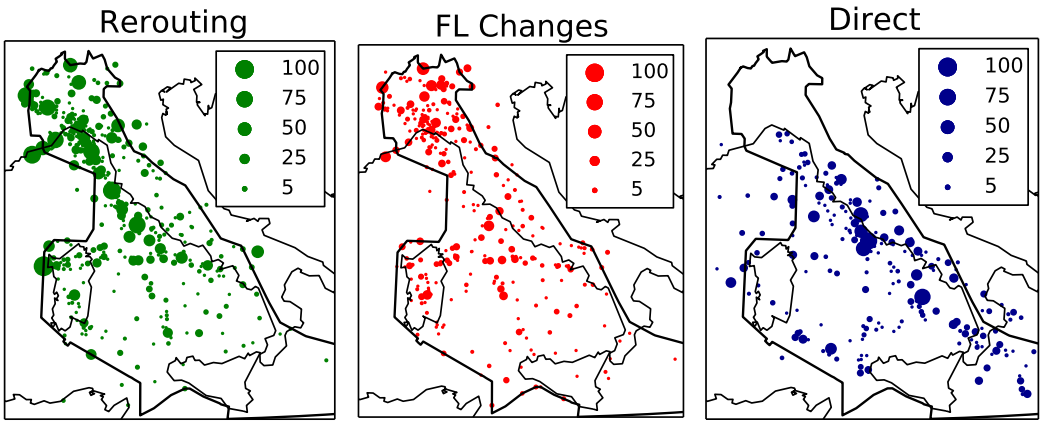


Figure 5.5: Map of navigation points with the information about the type of operations controllers have to do in their neighboring. Left panel (green): the size of each circle is proportional to the number of re-routings. Central panel (red): the size of each circle is proportional to the number of flight level changes. Right panel (blue): the size of each circle is proportional to the number of directs

$M = M_{pp} - M_{pr}$ between the number of planned flights that should have passed through a certain trajectory segment $M_{pp}$ and the number of these flights that actually passed through that trajectory segment $M_{pr}$. The blue line shows empirical data, while the green line refers to data obtained through numerical simulations of our ABM. The red line refers to a random allocation of $M$ values the missed flight in each trajectory segment. This random allocation preserves $(i)$ the planned number of flights in each trajectory segment $M_{pp}$ and $(ii)$ the sum $\sum_{link} M$ for the whole ACC. Such random sampling therefore preserves the planned heterogeneity of the system as well as the global number of operations done by the controllers.

Two comments are in order. On one hand, one can notice that the ABM well reproduces the empirical observations. On the other hand, it is worth noticing that these two distributions show tails that are fatter than those of the distribution obtained with the random sampling. This indicates that there are trajectory segments where the number of operations done by the controllers is higher that what should be expected by the random null model. This clearly suggests that ATCO operations tend to be focused

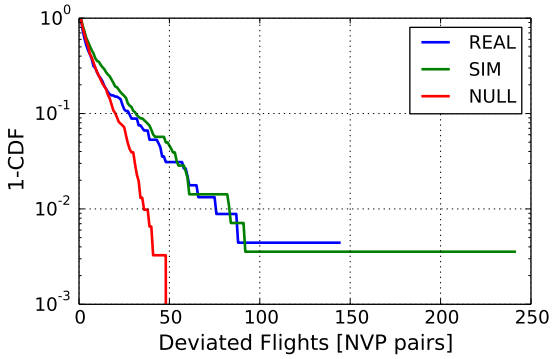


Figure 5.6: Complementary cumulative distribution of the difference $M = M_{pp} - M_{pr}$ between the number of planned flights that should have passed through a certain trajectory segment $M_{pp}$ and the number of these flights that actually passed through that trajectory segment $M_{pr}$. The blue line refer to empirical data, while the green curve refer to data obtained through numerical simulations of our ABM. The red curve refer to data obtained by performing a random sampling of the missed flight in each trajectory segment.

on specific regions of the ACC. The comparison with such simple random null model therefore allow us to highlight the presence of specific regions in the airspace that cannot be explained just with the heterogeneity of the flux of aircraft: it is therefore a genuine effect produced by the ATCOs and it is quite well reproduced by the ABM.

However, although the ABM well reproduces the existence of regional heterogeneity, it is worth emphasizing that there are airspace regions where the ABM and human ATCOs manage traffic in a different way. In Fig. 5.7 we show the difference M in a specific region of the ACC located close to Genoa and characterized by high traffic conditions. The left panel refers to the empirical case while the right panel refers to numerical simulations performed with our ABM. The difference M is here shown through a color scale reported on the right of each panel. One can see that there are trajectory segments where ATCOs do not modify planned trajectories (lighter colors) that are instead quite heavily affected by the ABM (darker colors) and viceversa.

In fact, this should not be surprising given the fact that ATCOs have to deal with tactical conditions (weather events, aircraft problems, ....) that our ABM does not take

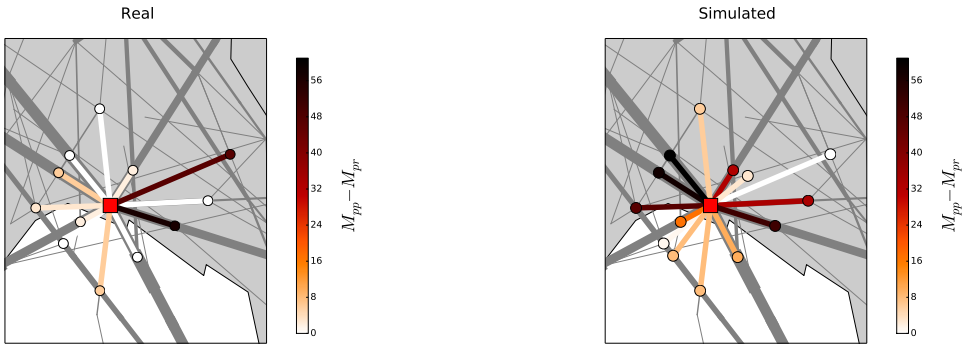


Figure 5.7: Difference M in a specific region of the ACC located close to Genoa, Italy. The left panel refers to the empirical case while the right panel refers to numerical simulations performed with our ABM. The difference M is here shown through the color-code reported on the right of each panel.

into account. Moreover, this different behavior might also be due to the fact that human controllers tend to be overly safe and therefore have a conservative style in managing the aircraft trajectories.

## 5.3 Dependence of directs and conflict resolution rates from model parameters

Finally, we report on how our model performs under parameters different from the ones chosen for calibration. Specifically, we evaluate the performances of our model with respect to model decisions concerning directs and conflict resolutions as a function of procedures followed by air traffic controllers and air traffic conditions of sectors.

Results of our investigation are summarized in Fig. 5.8. In the left panel of Fig. 5.8 we show the number of actions that the controllers perform in order to solve conflicts, i.e. re-routings and flight level changes, as a function of the number of directs for the five values of $\Delta t$ shown in the legend. Each point in the plot corresponds to the result of a simulation of the ABM performed with a pair $(p_d, x_c)$ of parameters selected in the range $p_d \in [0.03, 0.5]$ (with step of 0.01567), $x_c \in [0.34, 1.5]$ (with step of 0.03867). The figure suggests the existence of a linear negative relation between the number of

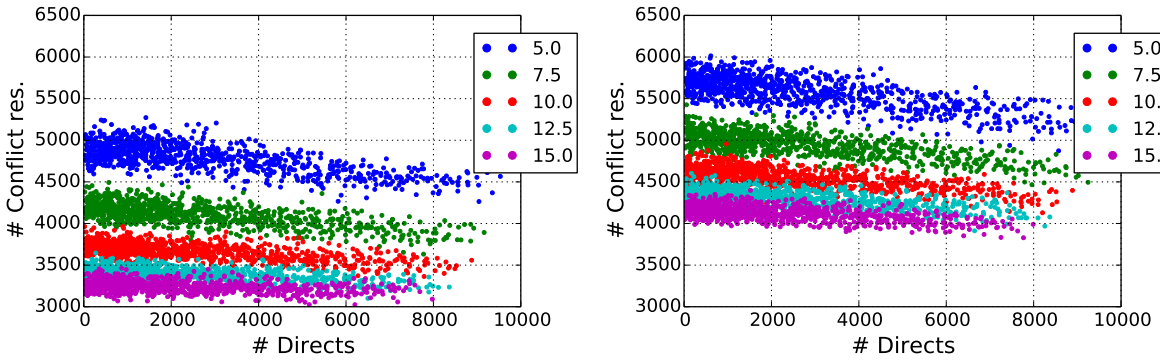


Figure 5.8: Number of conflict resolutions as a function of the number of issued directs. Each point in the plot corresponds to the result of a simulation of the ABM performed with a pair $(p_d, x_c)$ of parameters selected in the range $p_d \in [0.03, 0.5]$ (with step of 0.01567), $x_c \in [0.34, 1.5]$ (with step of 0.03867). Different colors refers to different values of the look-ahead $\Delta t_l$. In all simulations $\Delta t_d = 15$ min.The simulations on the left panel are made with a perfect forecast. The simulations on the left panel are done by introducing a noise in the velocity of aircraft ($l_\epsilon = 0.1$). This noise strongly affects the reliability of forecast of flight trajectories.

operations needed to solve conflicts and the number of directs, thus indicating that the number of unsolved conflicts decreases when the number of directs issued increases.

These results refer to ATCOs able to do a perfect forecast within the look-ahead used when directs are issued $\Delta t_d$. In reality, many unexpected factors can contribute to make uncertain a forecast. Uncertainty can result for example from a flight entering the airspace within $\Delta t_d$ unexpectedly or a weather event, or some errors in the forecast of aircraft positions. We evaluate the performance of our ABM model with respect to this type of uncertainty by performing a series of simulations in the presence of a source of noise. Specifically, the source of noise is introduced in the velocity of aircraft. In the right panel of Fig. 5.8 we show the results of a numerical simulation obtained by introducing noise in the velocity estimation of the aircraft. The parameter used is $l_\epsilon = 0.1$ which is a quite large value. This produces the effect of increasing the number of needed conflict resolutions especially for simulations with a high value of the look-ahead.

In Table 5.1 we report the result of a linear fitting procedure on the five sets of

| look-ahead (min) | noise | slope | intercept | correlation coef. | p-value | std err |
|---|---|---|---|---|---|---|
| 5.00 | 0.0 | -0.052 | 4939 | -0.691 | $10^{-128}$ | 0.002 |
| 7.50 | 0.0 | -0.040 | 4215 | -0.653 | $10^{-110}$ | 0.002 |
| 10.0 | 0.0 | -0.028 | 3734 | -0.571 | $10^{-79}$ | 0.001 |
| 12.5 | 0.0 | -0.021 | 3444 | -0.522 | $10^{-64}$ | 0.001 |
| 15.0 | 0.0 | -0.013 | 3273 | -0.342 | $10^{-26}$ | 0.001 |
| 5.00 | 0.1 | -0.060 | 5749 | -0.719 | $10^{-144}$ | 0.002 |
| 7.50 | 0.1 | -0.046 | 5073 | -0.694 | $10^{-130}$ | 0.002 |
| 10.0 | 0.1 | -0.039 | 4650 | -0.685 | $10^{-125}$ | 0.001 |
| 12.5 | 0.1 | -0.030 | 4370 | -0.582 | $10^{-82}$ | 0.001 |
| 15.0 | 0.1 | -0.027 | 4186 | -0.555 | $10^{-74}$ | 0.001 |

Table 5.1: Summary statistics of the result of a linear fitting procedure on the five sets of simulations obtained with different values of $\Delta t_l$. Other parameters are changed as described in the text. The upper part of the table refers to simulations with perfect forecast whereas the lower part refers to simulations in the presence of noise. The simulations in the presence of noise are obtained by setting $l_\epsilon = 0.1$.

simulations obtained for different values of $\Delta t_l$ and shown in Fig. 5.8 as points of different colors. The upper part of the table refers to simulations with perfect forecast whereas the lower part refers to simulations in the presence of noise. The $p - value$ reported in a column is the two-sided $p - value$ of the null hypothesis that the slope of the linear relationship is zero. Indeed, the low $p - values$ observed support the existence of a linear relationship between directs and conflict resolution events, although the slope value can be quite small in all considered cases. In fact, the correlation values reported in the fourth column are indicating a statistically robust negative relationship between directs and conflict resolution events.

It is worth noting that slopes observed in the presence of noise are systematically higher in absolute value that in the case of perfect forecast. This seems to suggest that also in the presence of enhanced uncertainty issuing directs reduces the number of conflicts to be resolved.

## 5.4 Results relating to the SESAR scenario

In this section we show that our model predicts that in the SESAR scenario potential conflicts will be less frequent than in the current scenario although they will be more widespread over all the entire airspace. This in principle increase the complexity controllers will have to face in the SESAR scenario.

The data we will consider below were obtained by first selecting the first day of AIRAC 334 (06 May 2010) and the LIRR ACC which covers most of Central Italy. We then generated synthetic M1 trajectories by using the Flight Plan Generator with no capacity constraints of section 4.2.1. We generated N=100 realizations of the given day. These trajectories are subsequently rectified by using the module described in section 4.3.1 in order to generate sets of flight-plans corresponding to different level of efficiency ranging from a low value of $E = 0.973$ corresponding to the current scenario to the highest value of $E = 0.999$ corresponding to the SESAR scenario. Moreover, such trajectories were deconflicted by using the module described in section 4.4. That was done in order to discard any effect due to the resolution of possible conflicts, given the fact that in the SESAR scenario it is assumed that the flight trajectories released by the Network Manager will be conflict-free. Trajectories were generated for different number of aircraft present in the airspace. These values ranged from $N_f = 1500$ to $N_f = 2200$. From real data, we can observe that the number of aircraft actually present in the considered airspace, given the applied filters, is approximately $N_f = 1800$. After, in each simulation we perturbed each flight trajectory by randomly assigning a delay on departure to a percentage $f_d$ of the flight trajectories. The maximum amount of delay on departure was 600 sec and the percentage of delayed flight trajectories was $f_d = 0.20$.

### 5.4.1 Going from the Current Scenario to SESAR Scenario

In Fig. 5.9 we show the average number of conflicts detected in the LIRR ACC, for different values of efficiency (horizontal axis) and for different values of the number of aircraft present in the ACC (different lines in the plot). All the curves have been normalized with $N_f^2$, i.e. with the maximum number of pairs of conflicting aircraft in an environment with $N_f$ aircraft. The average number of conflicts is here measured as

the average number of actions that the controller has to perform in order to avoid the conflicts detected by the Conflict Detection Module described in section 3.6. Therefore, these measures are performed on the surrogate M3 flight trajectories generated by our model. [1]. Indeed, the figure shows two interesting features: on one side we have that all curves seem to collapse in a single curve when the number of conflicts is rescaled with $N_f^2$. This is expected in a stable environment (same airspace, same departure times distribution). Indeed, adding a flight at random on an airspace has a constant probability – because of the stable environment – of triggering a conflict with each other flight. Hence, adding a flight adds on average $p \times N_f$ conflicts, where $p$ is the probability to have a conflict. If, on average, a flight creates $k$ conflicts, then the total number of conflicts will grow as $kp(N_f - 1)/N_f/2 \sim N_f^2$. Moreover, the number of detected conflicts decreases when the efficiency increases, thus indicating that in the SESAR scenario we would observe less conflicts and therefore a smaller workload for controllers.

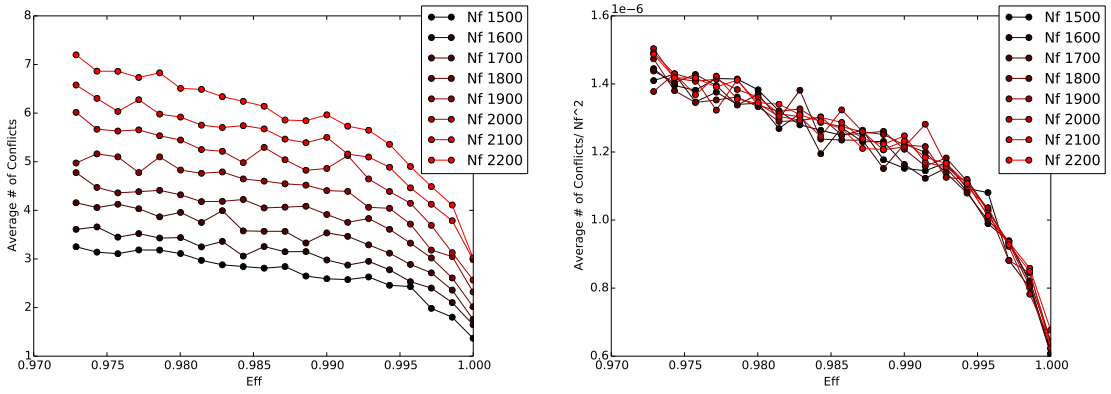


Figure 5.9: In the left panel we show the average number of conflicts detected in the surrogate M3 flight trajectories of the LIRR ACC, for different values of efficiency (horizontal axis) and for different numbers aircraft present in the ACC (different lines in the plot). In the right panel, each of the curve has been normalized with $N_f^2$ that represents the maximum possible number of conflicts in an environment with $N_f$ aircraft.

We have also devised a simple procedure to compute what is the expected number of

[1] We recall that our trajectories only concern the en-route part and do not include the airports proximities or the terminal maneuvering area (TMA) sectors, as described in section 4.1.

possible safety events (PSE), i.e. potential conflicts we should expect if all flights were to stick exactly to their flight plans. Indeed, since we add some noise on the departure times of the flights, the expected conflicts might not occur, and others non-expected events can take place. Moreover, we can also understand whether the fact that we observe less conflicts is already present at the level of planning or if it is mainly due to the management of trajectories done by the controllers. We start from the M1 deconflicted trajectories and we implement the following procedure:

- We perform a very fine spatial sampling of all flight trajectories, taking one point every meter along the trajectories.
- Starting from the original flight plans we associate to each of these sampled points a timestamp. This is done by assuming that between two navigation points the velocity of the aircraft is constant.
- We select those sampled points $P_i^{(a)}$ in the $a$-th flight trajectory and $P_j^{(b)}$ in the $b$-th flight trajectory such that the Euclidean distance $d(P_i^{(a)}, P_j^{(b)})$ between the two points is smaller than the safety threshold distance $d_{thresh} = 5$ NM.
- We further select the points such that the times $t_i^{(a)}$ at which the $a$-th aircraft crosses $P_i^{(a)}$ and $t_j^{(b)}$ at which the $b$-th aircraft crosses $P_j^{(b)}$ are below a certain time threshold $T_{thresh}$.

By using such procedure we are able to show what are the points of the ACC that are likely to attract the controller attention as a source of possible conflicts. Of course, the number of PSEs thus defined is strictly dependent on the threshold $T_{thresh}$ considered. In Fig. 5.10 we show the PSEs detected in the LIRR ACC, for different values of efficiency (horizontal axis) and for different values of the number of aircraft present in the ACC (different curves in the plot). As above, each of the curves has been normalized by $N_f^2$. In the figure we show the results for $T_{thresh} = 5.0$ min. Also in this case, the figure shows two interesting features. First, all curves collapse in a single curve when the number of PSEs is rescaled by $N_f^2$. Second, the number of PSEs decreases with the efficiency, thus indicating that in the SESAR scenario we would expect less potential conflicts.

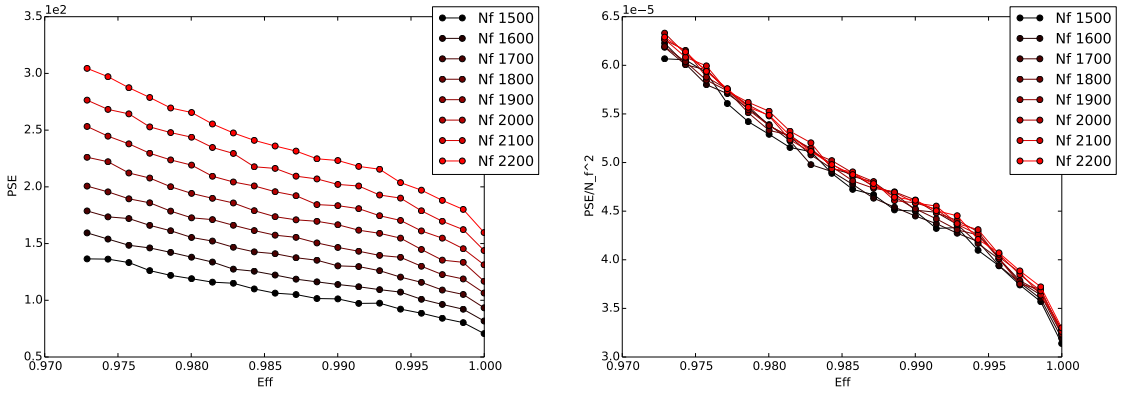


Figure 5.10: In the left panel we show the average number of PSEs detected in the M1 flight trajectories of the LIRR ACC, for different values of efficiency (horizontal axis) and for different numbers of aircraft present in the ACC (different curves in the plot). In the right panel each of the curve has been normalized with $N_f^2$ that represents the maximum possible number of conflicts in an environment with $N_f$ aircraft.

In Fig. 5.11 we show a scatter plot between the normalized PSEs detected from the M1 files with $T_{thresh} = 5.0$ min (horizontal axis) and the normalized number of conflicts detected from the surrogate M3 files (vertical axis) for different values of efficiency. The figure shows the existence of two different regimes. For values of efficiency close to unity, the points can be fitted with a linear relationship, with a slope around 0.05, while for lower values of efficiency, we have a linear relationship with a slope around 0.01. In any case, the fact that the slope is higher for high values of efficiency indicates that a small variation in the PSEs translates into a larger variation of the number of detected conflicts. This means that the SESAR scenario might turn out to be less flexible with respect to variations in the planning of the trajectories.

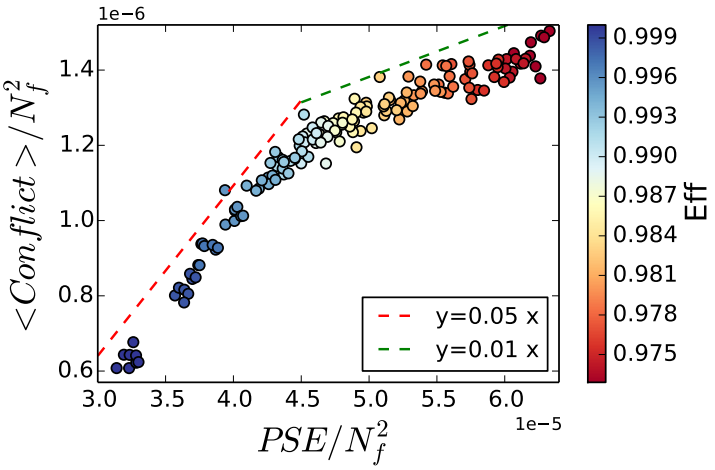


Figure 5.11: Scatter plot of the average number of conflicts detected in the surrogate M3 flight trajectories versus the average number of possible safety events (PSE) of the LIRR ACC. Different points represent different values of efficiency and different values of the number of aircraft present in the ACC. In dashed line we added the linear fits corresponding to the first and second part of the curve.

### 5.4.2 Heterogeneity

The above results show that in the SESAR scenario one should expect to observe less conflicts than in the current scenario. We now investigate their spatial locations. In fact, the main reason for having a navigation point grid is that it helps the controllers in monitoring the air traffic, since they need to do it only in specific portions of the airspace. We are therefore interested in understanding whether or not this feature will be maintained in the SESAR scenario.

In Fig. 5.12 we show a density map of the PSEs detected when considering three different values of efficiency and $T_{thresh} = 5.0$ min. In the left panel we show the PSEs detected starting from the real M1 trajectories, which correspond to an efficiency value of $E = 0.973$. In the right panel we show the PSEs detected starting from the M1 trajectories corresponding to the SESAR scenario, i.e. with an efficiency value of $E = 0.999$. In the central panel we show the PSEs detected starting from the M1 trajectories corre-

sponding to the intermediate value of efficiency $E = 0.980$. As expected, when efficiency increases, the possible conflicts are more spread all over the airspace, rather than being concentrated in specific regions. In fact, flight trajectories are more distributed over the entire airspace and therefore the probability of conflicting is smaller. This explains why the number of detected conflicts decreases when the efficiency increases. This also implies that the controller activity in the SESAR scenario will change, moving from a situation where he/she has to give attention to a high number of conflicts concentrated in specific points, to a situation where he/she will have to manage less conflicts spread over a much larger portion of the airspace.

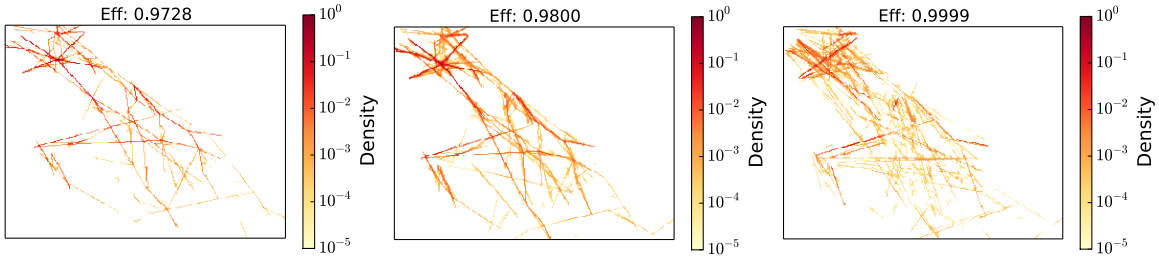


Figure 5.12: Density map of the PSEs detected when considering three different values of efficiency and $T_{thresh} = 5.0$ min in the LIRR ACC. In the left panel we show the PSEs detected starting from the real M1 trajectories, i.e. of $E = 0.973$. In the right panel we show the PSEs detected starting from the M1 trajectories corresponding to the SESAR scenario, i.e. with an efficiency value of $E = 0.999$. In the central panel we show the PSEs detected starting from the M1 trajectories corresponding to the intermediate value of efficiency $E = 0.980$. To enhance readability, we first take the logarithm of the number of PSEs and then we normalize by dividing all values of the maximum value found in the three graphs (which is reached in the left panel).

Indeed, controllers are obviously sensitive not only to the number of conflicts or the number of flights, but to other factors. In fact, to our knowledge there is no consensus about what is a complex situation for controllers. In literature [98] there are examples of several metrics that capture specific aspects of the complexity typically faced by the controllers. These metrics are quite diverse and are linked to time to conflicts, distances

between aircraft, geometry of conflicts, etc. They are computable with the planned trajectories, which allows to see at each point in time what is the expected complexity for the controller. On the other hand, we also have our own measure of complexity, directly coming from the model. In fact, the number of actions done by the controllers can be viewed as a complexity measure where our (super-)controller gradually meets more complex situations and thus makes more actions to solve the conflicts. As a consequence, we investigated in Ref.[60] whether the number of actions can be related to the complexity metrics already known in literature.

### 5.4.3 Complexity Scaling

In this subsection, it is worth understanding better what is the relationship between the complexity and its most simple component, the density.

To investigate this issue we perform simulations on the same airspace, but varying the sectors capacities. We first produce a fixed number of trajectories with the strategic layer, and then we change the capacities in three different ways:

- In the first scenario, we decrease uniformly the capacities of all sectors.
- In the second one, we "impair" severely three central sectors, increasing the capacities of the surrounding sectors to have the same average capacity. Then we decrease all capacities uniformly like in the previous point.
- The last one is the witness in which we remove the capacity constraint and change the number of flights submitting a flight plan.

After that, we use the tactical layer to solve all conflicts in each simulation and we track the number of actions of the controllers. Figure 5.13 shows the output. For each of the scenarios, we performed a power-law regression with the function $N_f \mapsto bN_f^a$. For the red line – without capacity constraints – we obtain $a = 2.0 \pm 9.0e-5$ and $b = 8.4e-5 \pm 3.0e-11$, i.e. a pure quadratic law. This is expected, because the number of conflicts should scale with the number of pairs of aircraft, i.e. $\sim N_f(N_f-1)/2 \sim N_f^2$, as already noted before.

Interestingly, the regression for the two other scenarios yield different scalings. With the same regression, the violet line yields: $a = 2.4 \pm 1.0e-4$ and $b = 3.6e-6 \pm 8.0e-14$

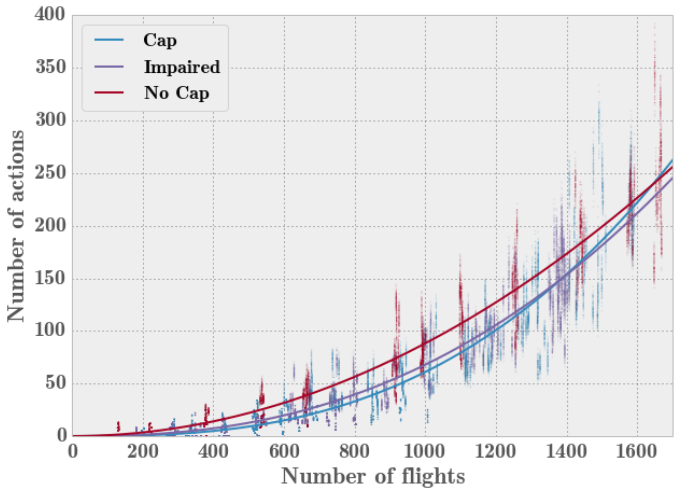


Figure 5.13: Different scaling for different scenarios. The scatter plots have been obtained with a uniform reduction of the capacities (light blue), with some sectors severely impaired (violet) and without any capacity (red). The solid lines are the result of power law regressions for each set of data (see text for the values of the coefficients).

and the blue line gives: $a = 2.8 \pm 2.0e-4$ and $b = 3.4e-7 \pm 1.0e-15$. In other words, they are clearly displaying super-quadratic behaviours. But before explaining why, we comment on the fact that despite this behaviour, these two cases usually need less actions than the unconstrained capacity case for the same number of flights. This is due to the fact that capacities tend to spread the flights during the day. Hence the concentration in time of flights decreases during peaks, which decreases the number of potential conflicts (flights are flying at different times).

The same argument explains the super-quadratic behaviour. Indeed, due to our experimental procedure, when the number of flights increases, it means that the capacities have less relative influence, since we keep the number of flights fixed as input to the strategic layer. Hence, when the number of flights increases, the number of potential conflicts increases more quickly than $N_f^2$, because more flights are flying at similar times. Finally, note that the same kind of simulations in free-routing yields the same kind of results (not shown here).

The conclusion is that sectors play a major role in the complexity of the airspace, and that complexity heavily depends on the pairs of flights simultaneously present in the airspace. All the variance is not explained by the density though, and other factors are important, especially to human controllers.

## 5.5 Results: The Heterogeneity of the Network among Different ACCs

In this section we decided to consider many different ACCs in order to investigate whether the results obtained in section 5.4 might depend on the features of the starting network of navigation points. Also in this case, we here considered as a starting point the real data relative to AIRAC 334 and day 06/05/2010.

We model the flights trajectories within a set of 15 ACCs: LFFF, EGPX, LECB, LFMM, LECM, LECS, LFRR, LIPP, LECP, EGCC, LIMM, LFEE, EGTT, LIBB, LIRR. The main features of these ACCs are reported in Table 5.2.

In the previous section we used the Conflict-Free Flight Plan Generator of section 4.2 which makes use of the shortest path route on the considered navigation points network,

| ACC | ACC name | number of flights | Area (km$^2$) | Number of sectors |
|---|---|---|---|---|
| LIRR | **Rome** | 2122 | 501732 | 10 |
| LIMM | Milan (I) | 1066 | 73234 | 5 |
| LIPP | Padova (I) | 1083 | 95360 | 5 |
| LIBB | Brindisi (I) | 448 | 244179 | 3 |
| LFFF | **Paris** | 639 | 171702 | 4 |
| LFMM | Marseille (F) | 1494 | 299525 | 11 |
| LFEE | Reims (F) | 1799 | 98989 | 5 |
| LFRR | Brest (F) | 1886 | 400217 | 11 |
| EGTT | **London** | 2854 | 3648975 | 18 |
| EGCC | Manchester (UK) | 786 | 47959 | 3 |
| EGPX | Scotland | 614 | 6838031 | 12 |
| LECM | **Madrid** | 2203 | 442101 | 10 |
| LECB | Barcelona (ES) | 1366 | 266783 | 9 |
| LECP | Palma (ES) | 321 | 51173 | 6 |
| LECS | Sevilla (ES) | 660 | 182051 | 15 |

Table 5.2: Main features of the 15 considered ACCs.

while in this section the routes generated with the module described in sec. 4.2.1 not always correspond to a shortest paths.

We performed a this set of simulations by using the rectification procedure of section 4.3.2 and the Conflict-Free Flight Plan Generator of section 4.2.1. The aim of this test is the same as in section 5.4.

For each ACC we generated 100 surrogate M1 flight plans preserving four stylized facts observed in the real M1 files:

- The distribution of departure times.
- The distribution of flight levels for each navigation point (also with the constraint of the odd rule),
- The same fraction of number of flights between each origin-destination pair.

- The same total number of flights in the ACC.

After generating such M1 trajectories, for each ACC we performed 10 simulations. In each simulation we perturbed each flight trajectory by randomly assigning a delay on departure to a percentage $f_d$ of the flight trajectories. The maximum amount of delay on departure was 600 sec and the percentage of delayed flight trajectories was $f_d = 0.20$.

Furthermore, we performed two types of simulation. The first one was made without the direct modules (i.e. $p_d = 0$), the second one with the direct module with $p_d = 1$ $x_c = 1000$. This is done because we want to investigate the extreme situation occurring when either we do not have directs or a direct is issued whenever it is possible. For each of the 15 ACCs mentioned above we made simulations for its real efficiency value (current scenario) and the ideal unitary efficiency value corresponding to the SESAR scenario. In a few cases we also considered intermediate values of efficiency. The considered cases are summarized in Table 5.3. In the table, all ACCs are ordered according to their original efficiency value.

In Fig. 5.14, for each of the 15 ACCs and in the two extreme cases of $p_d = 0$ (blue circles) and $p_d = 1, x_c = 1000$ (red circles), we show a scatter-plot of the efficiency obtained after running the ABM versus the original efficiency measured in the ACC. In both cases, there exists a linear relationship between the M3 and the M1 efficiency. However, the efficiency obtained by issuing a direct is larger than the one obtained by generating flight trajectories where no direct is issued. Such result is of course expected. The importance of these two curves lies in the fact that they constitute the boundaries between which our simulations will have to stay.

| ACC | original efficiency | target efficiency 1 | target efficiency 2 | target efficiency 3 |
|---|---|---|---|---|
| EGTT | 0.9145 | 0.954 | 0.98 | 0.999 |
| LIMM | 0.9278 | 0.954 | 0.98 | 0.999 |
| LIRR | 0.9448 | 0.98 | 0.999 | |
| LFRR | 0.9509 | 0.98 | 0.999 | |
| LFFF | 0.9524 | 0.98 | 0.999 | |
| EGPX | 0.9550 | 0.98 | 0.999 | |
| LECP | 0.9623 | 0.98 | 0.999 | |
| LECM | 0.9744 | 0.999 | | |
| LECS | 0.9751 | 0.999 | | |
| LECB | 0.9756 | 0.999 | | |
| LFMM | 0.9781 | 0.999 | | |
| LFEE | 0.9813 | 0.999 | | |
| EGCC | 0.9848 | 0.999 | | |
| LIBB | 0.9849 | 0.999 | | |
| LIPP | 0.9850 | 0.999 | | |

Table 5.3: Efficiencies values used in the numerical simulations for the 15 ACCs. Such values have been obtained starting from the data relative to AIRAC 334 and day 06/05/2010. The efficiency value for LIRR is different from the one used in section 5.4, due to the fact that the Conflict-Free Flight Plan Generator of section 4.2 considers shortest paths, while the Conflict-Free Flight Plan Generator of section 4.2.1 considers real trajectories.

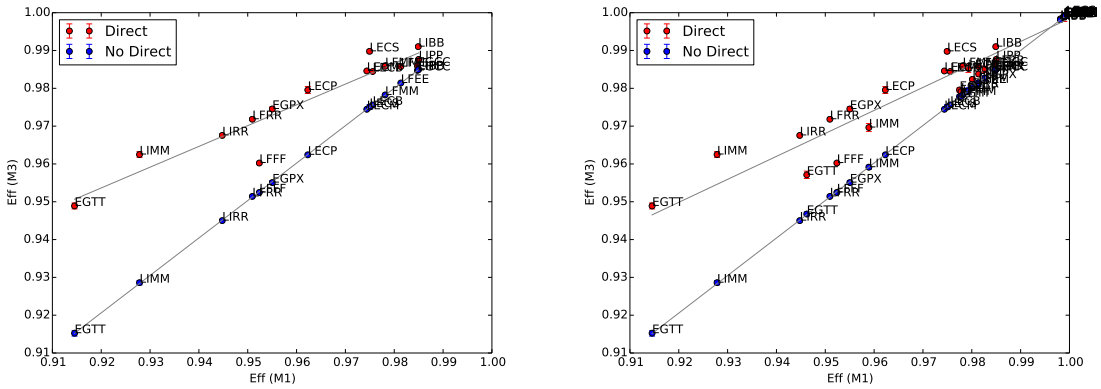


Figure 5.14: In the left pannel is the scatter-plot of the efficiencies of the M3 surrogate trajectories obtained after running the ABM versus the original efficiency measured for each of the 15 ACCs and in the two extreme cases of $p_d = 0$ (blue circles) and $p_d = 1$ (red circles). In the right panel we show all the 39 target efficiencies of Table 5.3

In Fig. 5.15, for each of the 15 ACCs and in the two extreme cases of $p_d = 0$ (right panels) and $p_d = 1$ (left panels), we show the number of re-routing (top panels) and the number of flight level changes (bottom panels) for the 15 ACCs. In this case we considered the original navigation points networks with their efficiency and the networks obtained by using the rectification procedure of section 4.3.2 with a few new target efficiencies. The figures show that in all cases the number of re-routing decreases as long as efficiency increases. However, the number of flight level changes might increase in some cases. In the bottom panels we show the total number of actions done by the ABM, i.e. we consider both re-routings and flight level changes. In this case, we number of actions generally decreases as long as efficiency increase, as already observed in Fig. 5.9.

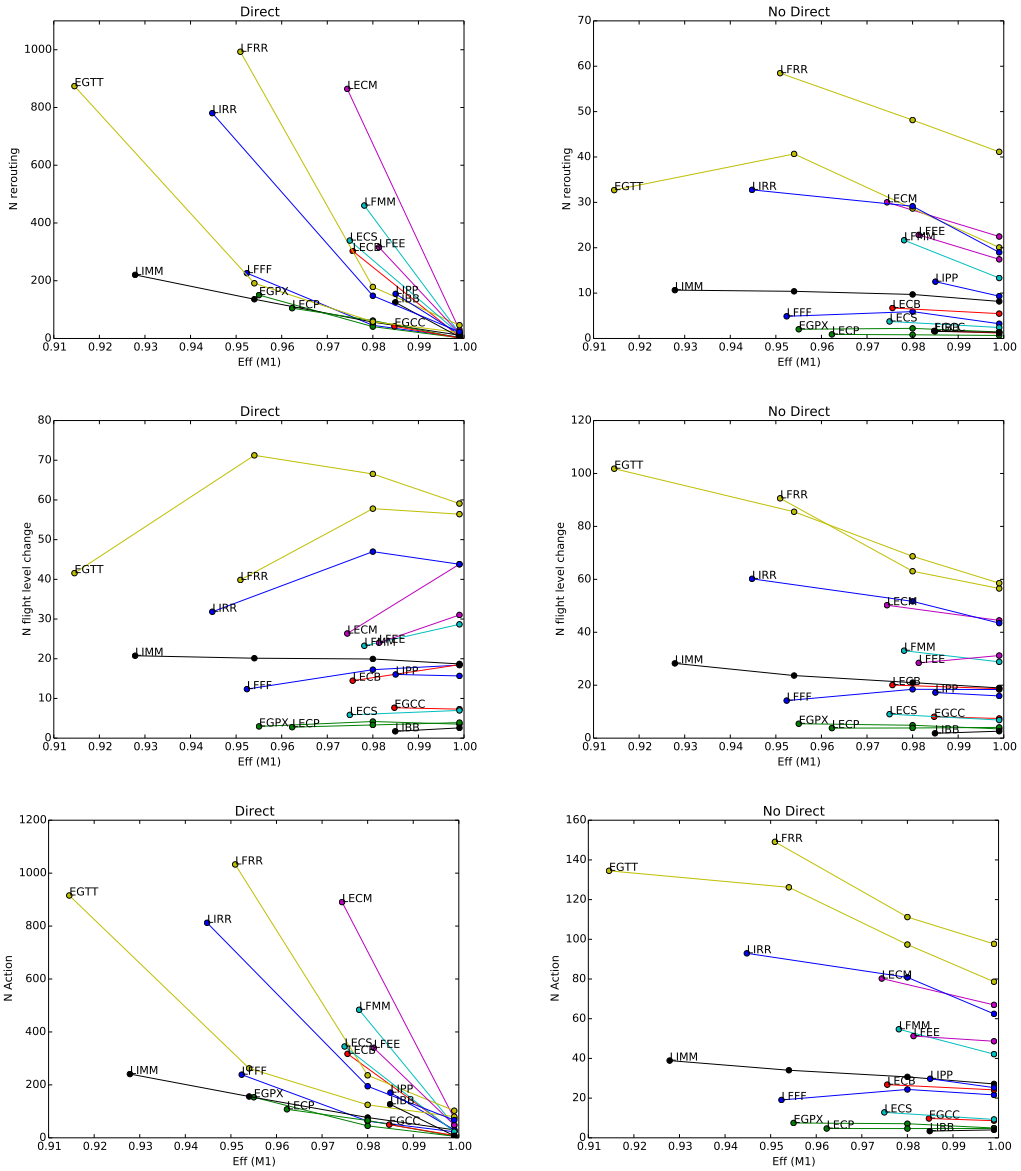


Figure 5.15: Number of re-routings (top panels) and number of flight level changes (central panels) and total number of actions (bottom panels) for each of the 15 ACCs and in the two extreme cases of $p_d = 0$ (right panels) and $p_d = 1$ (left panels).

For each of the 15 ACCs, let us consider the Gain metric defined as:

$$G = \frac{N(E_S) - N(E_C)}{N(E_C)} \tag{5.1}$$

where $E_S = 0.9999$ is the target efficiency relative to the SESAR scenario and $E_C$ is the

efficiency of the considered ACC in the current scenario. $N$ here indicates the number of re-routing actions done by the ABM. The G metric should indicate how much, in percentage, we gain in terms of number of re-routings when we move from the current to the SESAR scenario. In Fig. 5.16 we show the Gain for the case when $p_d = 1$ (top panel) and $p_d = 0$ (bottom panel). As expected the Gain is larger when directs can be issued. However we were not able to see any dependance of the gain $G$ from variables such as the original efficiency $E_C$ or other ACC metrics as those reported in Table 5.2.

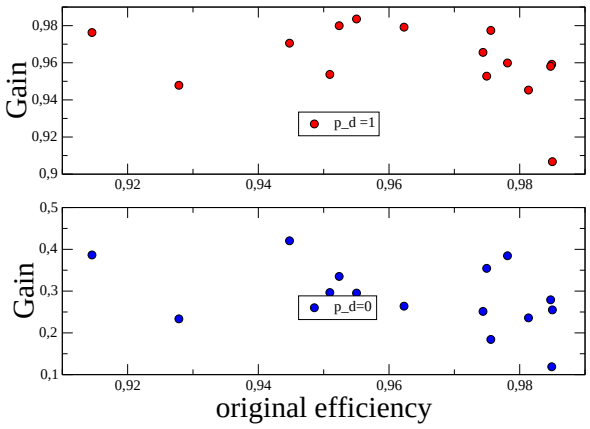


Figure 5.16: Gain metric of Eq. 5.1 computed for each of the 15 ACCs and in the two extreme cases of $p_d = 0$ (bottom panel) and $p_d = 1$ (top panel).

In Table 5.4 we show the average number of reroutings and flight level changes in the SESAR scenario (E=1) for the two extreme cases $p_d = 0$ and $p_d = 1$. The correlation between flight level changes and re-routings is 0.85 when $p_d = 1$ and 0.80 when $p_d = 0$. The values of re-routings and flight level changes are quite similar in the two cases when $p_d = 0$ and $p_d = 1$, thus indicating that trajectories are really linearized in the SESAR scenario and therefore issuing directs does not play a big role, as already notice in Fig. 5.14.

In Fig. 5.17 we show the number of re-routings versus the number of flight level changes for the case $p_d = 1$ (left panel) and the when $p_d = 0$ (right panel). In the figure the blue points correspond to the 15 ACCs considered with their original efficiency values, i.e. the one corresponding to the scenario (see Table 5.3). The figure indicates

| ACC | original efficiency | average # of reroutings (no directs) | average # of flight level changes (no directs) | average # of of reroutings (directs) | average # of flight level changes (directs) |
|---|---|---|---|---|---|
| LFFF | 0.9524 | 3.248 | 18.74 | 4.537 | 18.392 |
| EGPX | 0.9550 | 1.432 | 3.5 | 2.471 | 3.525 |
| LECB | 0.9756 | 5.477 | 18.693 | 6.846 | 18.508 |
| LIPP | 0.9850 | 9.326 | 15.953 | 14.414 | 15.672 |
| LFEE | 0.9813 | 17.447 | 31.207 | 17.288 | 31.028 |
| LECM | 0.9744 | 22.469 | 44.493 | 29.752 | 43.817 |
| LFRR | 0.9509 | 41.137 | 56.547 | 45.975 | 56.419 |
| LECS | 0.9751 | 2.423 | 6.844 | 16.014 | 6.981 |
| LFMM | 0.9781 | 13.326 | 28.829 | 18.473 | 28.672 |
| LECP | 0.9623 | 0.661 | 4.059 | 2.186 | 3.913 |
| EGCC | 0.9848 | 1.198 | 7.434 | 1.765 | 7.304 |
| LIMM | 0.9278 | 8.169 | 18.977 | 11.485 | 18.695 |
| EGTT | 0.9145 | 20.062 | 58.569 | 20.731 | 59.093 |
| LIBB | 0.9849 | 1.372 | 2.621 | 5.11 | 2.581 |
| LIRR | 0.9448 | 18.985 | 43.458 | 22.993 | 43.804 |

Table 5.4: average number of reroutings and flight level changes in the SESAR scenario (E=1) for the two extreme cases $p_d = 0$ and $p_d = 1$

the existence of a positive correlation between number of re-routings and number of flight level changes, although there seems to exist no linear relation between the two variables. In fact, we observe a correlation of 0.879 for the current scenario when $p_d = 1$ and 0.908 for the current scenario when $p_d = 0$. The lack of a linear law indicates that the starting navigation points network and the other metrics such as those of Table 5.2 might play a role. The red points correspond to the 15 ACCs considered with their unitary efficiency values, i.e. the one corresponding to the SESAR scenario. Also in this case a positive correlation between number of re-routings and number of flight level changes. For the SESAR scenario we observe a correlation of 0.840 when $p_d = 1$ and 0.910 when $p_d = 0$. Moreover, in the SESAR scenario when $p_d = 1$ we observe an increase on flight level changes and a decrease of the number of re-routings, while in the case when $p_d = 0$ the differences between future SESAR and current scenario are negligible. This goes in the direction by which the rectification of trajectories (with direct, in this case) is again beneficial for the general efficiency of the system. The green points correspond to the intermediate values of efficiency reported in Table 5.3.

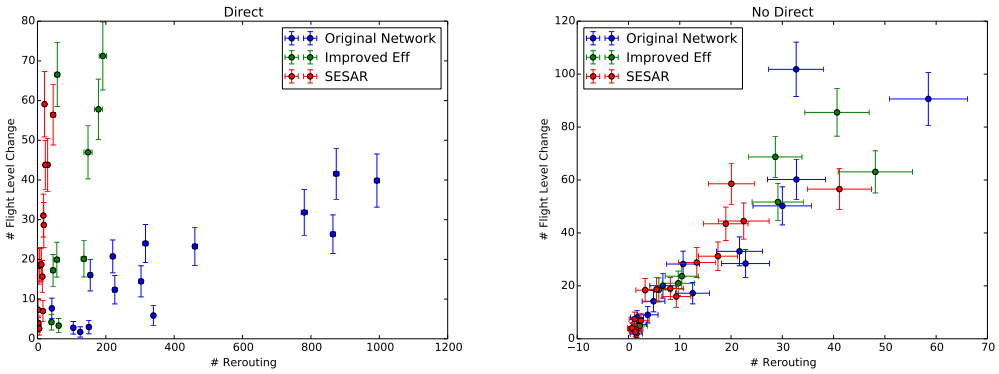


Figure 5.17: Scatter-Plot of the number of flight level changes versus the number of re-routings. The blue points correspond to the 15 ACCs considered with their original efficiency values, i.e. the one corresponding to the scenario. The red points correspond to the 15 ACCs considered with their unitary efficiency values, i.e. the one corresponding to the SESAR scenario. The green points correspond to the intermediate values of efficiency reported in Table 5.3.

In Fig. 5.18 we show the number of re-routings with respect to the number of flights in the ACC for the case $p_d = 1$ (left panel) and when $p_d = 0$ (right panel). The blue points correspond to the 15 ACCs considered with their original efficiency values, i.e. the one corresponding to the scenario. The red points correspond to the 15 ACCs considered with their unitary efficiency values, i.e. the one corresponding to the SESAR scenario. The green points correspond to the intermediate values of efficiency reported in Table 5.3. The relationship between number of re-routings and number of flights is approximatively linear. However, we recall that in Fig. 5.9 we had observed that the number of re-routings might rescale with $N_f^2$. In fact, the two empirical facts are not contrasting with each other. Indeed, in Fig. 5.9 we were considering a given ACC with an arbitrarily changing number of flights. In the present case, we are considering different ACCs each with its own number of flights. Moreover, when looking at the points relative to the SESAR scenario with $p_d = 0$ we do not see any clear relationship between number of re-routings and number of flights in the ACC, thus indicating that the specific features of the ACC might still play a role in the SESAR scenario. This is in a sense unfortunate. Had we observed a common behaviors in all ACCs in the SESAR scenario, this would have been a strong support to the idea of having more standard management procedures in the SESAR scenario. As shown in Fig. 5.19 similar considerations can be done for the relationship between number of flight level changes and number of flights in the ACC.

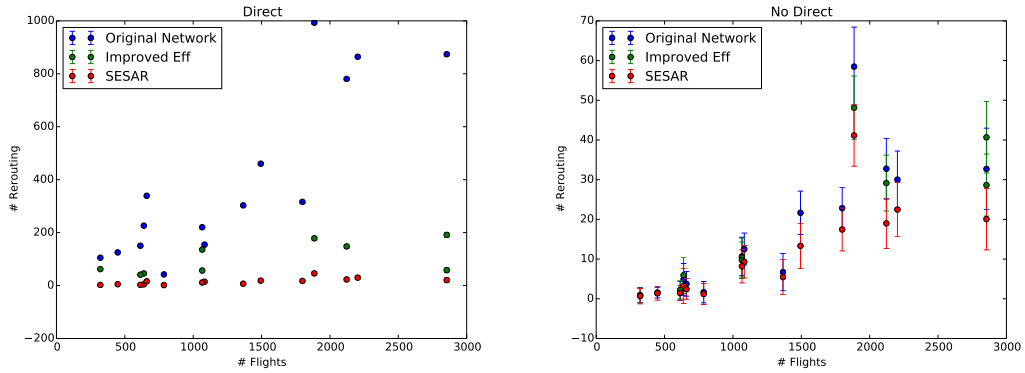


Figure 5.18: Number of re-routings as a function of the Number of Flights. The blue points correspond to the 15 ACCs considered with their original efficiency values, i.e. the one corresponding to the scenario. The red points correspond to the 15 ACCs considered with their unitary efficiency values, i.e. the one corresponding to the SESAR scenario. The green points correspond to the intermediate values of efficiency reported in Table 5.3.

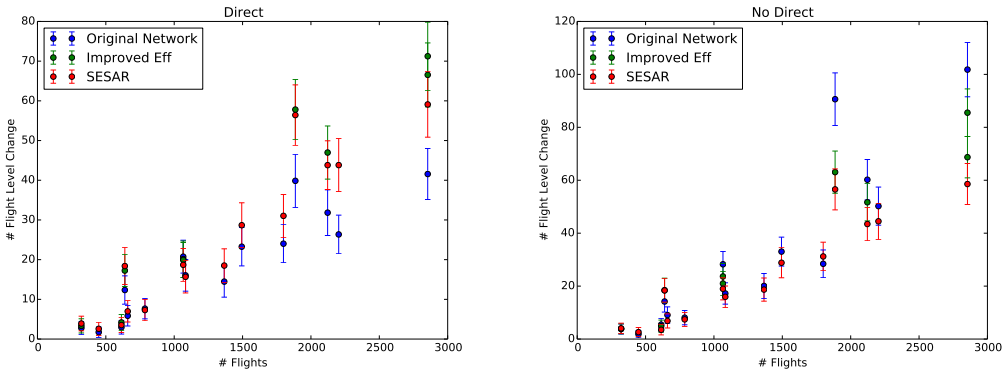


Figure 5.19: Number of Flight level changes as a function of the Number of Flights. The blue points correspond to the 15 ACCs considered with their original efficiency values, i.e. the one corresponding to the scenario. The red points correspond to the 15 ACCs considered with their unitary efficiency values, i.e. the one corresponding to the SESAR scenario. The green points correspond to the intermediate values of efficiency reported in Table 5.3.

# 6 Conclusions

In this dissertation we highlighted the complex nature of the air transportation management system by focusing on the activities of the air traffic controllers. Despite the difficulties in understanding the pilot/controller interaction at the level of the single aircraft, we observed that the statistical proprieties of flight trajectory deviations have typical patterns. Such regularities were modelled by our ABM that was built by using a minimal set of rules. We want to stress that agent-based modelling nowadays is the only technique that allows a genuine modelling of emerging phenomena starting from the microscopic level of interaction of agents. In our case, the complexity of the flight plans network, together with the heterogeneity of the sector geometry, makes virtually impossible to write down fundamental equations for such system. Moreover, even if it were possible, the high uncertainty due to both unforeseeable meteorological events and other sources of uncertainty would vanish such efforts. Differently, our ABM shows a good agreement of ABM simulations with empirical data and a non-trivial behaviour in modelling the transition towards the future SESAR scenario.

The air transportation system is a complex system with a pronounced within-day dynamics and a marked spatial heterogeneity. For example, by using traffic data, we have verified that day flights and night flights present a different value for their average length and a different distribution of flight length. In the air traffic management procedures, the interaction between pilots and air traffic controllers is primarily devoted to conflict resolutions aiming to prevent safety issues. Once safety problems are positively avoided or solved the interaction between pilots and air traffic controllers focuses on possible improvement of the efficiency of the air transportation system. To analyze the effect on the efficiency improvement of the system of their interaction we have considered a very

simple measure of flight efficiency based on the comparison between the length of planned or actual flight trajectory with the great circle distance. Our results show that night-time flights (in particular during the time interval from 8:00 pm to 4:00 am) are on average more efficient than day-time flights. Moreover, the gain of average efficiency obtained in the actual trajectories is systematically larger during night-time. Our results show an asymmetry in the change of efficiency of flights during night-time. Specifically for large changes in absolute value the improvement is more evident than the deterioration. This asymmetry is not detected during day-time when efficiency improvement is quite balanced by efficiency deterioration.

The tactical interaction present between pilots and air controllers is also reflected in the observation that flight trajectory deviations preferentially occur near the origin rather than close to destination of the flight. Moreover, flight trajectory deviations occur at an angle-to-destination that is a non monotonic function of the angle with a maximum observed close to 20 degree. Pilots and air controllers are most probably solving on average different kind of problems during day and night. In fact we observe that the fraction of flight trajectory deviations is higher during night-time than during day-time intraday time windows. We also detect that the fraction of flight trajectory deviations is an inverse function of the number of flights observed in the investigated time window.

Our study shows that the time of the day plays an important role in setting the most probable type of interaction between pilots and air controllers. Indeed, in addition to time there is also a role of the specific geographical location of the considered navigation point pair. To clarify this point we introduced a new metric called di-fork that is useful to track the trajectory deviations at the level of single navigation point pairs. By making use of this metric, we can detect the set of navigation point pairs presenting a number of flight trajectory deviations that are over-expressed or under-expressed with respect to a statistical null hypothesis assuming ($i$) that deviations occur randomly over the day and ($ii$) taking into account the heterogeneous number of flights planned to fly through the navigation point pair over the day. The detected set of over-expressed and under-expressed navigation point pairs is persistent over a time period spanning 5 successive AIRACs, i.e. up to 140 days. This result quantitatively shows that the fraction of

deviations occurring during the day is not a random variable. Rather, it corresponds to the effort of making the system more efficient under certain constraints due, for example, to safety and capacity issues.

We believe that these results present a clear statistical evidence of the ability of the air traffic management system of improving air traffic performances on average with respect to the set of planned flight trajectories. The improvement of performance is relatively more evident during night-time time windows when constraints related to the capacity of air sectors are less stringent. As a consequence the interaction between pilots and air controllers is a complex interaction that is the result of a learning process aiming not only at the prevention and resolution of safety problems but also to the improvement of the performances of each single airline and of the entire air transportation system.

In this thesis I presented an agent-based model of the ATM system that aims at modeling the interactions between aircrafts and ATC controllers at a tactical level. Specifically, We have presented in detail the different modules of the model whose core is given by the conflict detection and resolution module and by the directs module. We have given an example of the calibration of our model done in order to obtain simulations describing the statistical regularities about the rate of flight trajectory deviations observed in empirical data. We explicitly show that the calibrated model is able to reproduce the existence of regional localization of ATM operations, i.e. the fact that ATCO operations tend to be focused on specific points of the ACC. Finally, we have shown scenario simulations results about the relationship between directs and conflict resolution events conditioned to model parameters.

Our model can be used to give useful insights about the functioning of the ATM system. We are aware that our model is very basic. For example, our agent-based model does not implement any learning mechanism as done for example in other models [52] or uses specific fitness measures. The way our model solves conflicts is fast from a computational point of view but provides solutions that are not optimized at a global level. However we implemented such a solution because we wanted to develop a parsimonious ABM mimicking the way air traffic controllers work in reality.

Indeed, we believe that such solution might be quite effective in the SESAR scenario

simulations. In fact with a simple variant of the ABM, we might simulate a scenario where controllers have a role less preeminent than in the current scenario and some basic conflict-resolution actions are left to aircraft interactions. In this respect, our model might mimic a scenario where pilots, that clearly have not a global vision of the system, endowed with a set of policy rules assigned by their airlines, will perform an *active* conflict resolution at a tactical level, thus realizing a sort of self-organization amongst aircraft.

Following on from this, we specifically studied the free-routing solutions envisioned by SESAR. First, we focused our analysis on a single Italian ACC (LIRR). The result of this SESAR scenario simulations was that we showed controllers can be expected to perform a smaller number of operations but that these operations will be dispersed over a larger area of airspace.
Next we investigated the transition to the SESAR scenario for 15 different ACCs. We observed an overall decreasing of the operations performed, in agreement with what we initially found. However, differences between the ACCs emerged during the transition to SESAR, probably due to the traffic and the geometry specificity of these ACCs. The maximum gain of efficiency achieved with direct operations shows a universal stability governed by a linear law. In other words: the maximum improvements that are possible to obtain with local optimization are constrained by the global efficiency of the airways.

Moreover it appears impossible to use a simple law to describe the transition of airways to a high level of global efficiency. This is because the gain in safety due to increased efficiency is an emerging phenomenon strongly dependent upon the specificity of the structure.

Taking our research forward, we aim to better understand the challenges of the transition to SESAR for heterogeneous Area Control Centers (ACCs) by using synthetic ACCs. With a view to highlight the most important potential variables in the SESAR transition, we aim to analyse the geometry of the intersections of routes, the occupancy of flight levels and the transportation flow on the network. It must be remembered, of course, that the SESAR scenario will not be implemented immediately; instead a

lengthy transition period between the current scenario and the new SESAR scenario should be expected. We believe that our model could be a useful tool to explore possible intermediate scenarios. In the present work we explored such intermediate scenarios in which high efficiency areas grow homogeneously in airspace. However, we think that a more reasonable transition should be dis-homogeneous i.e. a scenario where the airspace has both high efficiency areas and also a smaller number of low efficiency areas, where the traffic conditions require more careful management by the ATCs. In this intermediate scenario, the ABM could help us discover areas where the SESAR scenario could be implemented easily thus creating highly efficient areas of airspace. To achieve this potentially important result further work on the ABM is required, specifically: we are looking to employ a Network Designer agent that creates and modifies the NVP structure. Such modification will be a local correction procedure driven by an utility function. Our belief is that such function will be able to take into account both the network efficiency and the workload of the ATCOs, nevertheless airline and passenger utilities could be taken into account too.
Additionally, in the future development of the ABM, we want to include a function that manages the Terminal Manoeuvring Areas (TMA) – the airspace close to the airports. The specific procedures used in TMAs, and the effects these have on the en-route areas, are of great significance simply by merit of their quantity: there are a huge number of airports (and thus TMAs) in European airspace.
It is worth mentioning that the modular structure of the code could allow us, in the next future, to improve the aircraft cinematic description. Therefore, the future release of the code could include for example: smooth flight level changes, winds, different aircraft models, pilot agency etc.

Finally, we will include in future versions of our ABM the memory of the ATC agents. This important feature can help us to discover new protocols required to solve conflicts. In future scenarios, the standard procedures may no longer be applicable. By including the memory of ATC agents, the new adaptive agents will perform their actions on the basis of previous knowledge of problematic areas. As a result the new protocol created will be an emerging bottom-up effect.

In conclusion, the current and future challenges facing Airport Transport Management

are numerous and complex: they exist at the level of infrastructure, i.e. navigation point network structures and route structure; at the level of sector dynamic configuration and at the level of strategic trajectory planning. We believe that the introduction of our agent-based modelling approach will be extremely useful in solving these challenges at all three levels.

# Bibliography


[1] Claudio Castellano, Santo Fortunato, and Vittorio Loreto. Statistical physics of social dynamics. *Reviews of modern physics*, 81(2):591, 2009.

[2] Gabor Forgacs and Stuart A Newman. *Biological physics of the developing embryo*. Cambridge University Press, 2005.

[3] Andrew Cook and Damián Rivas. *Complexity science in air traffic management*. Routledge, 2016.

[4] Yaneer Bar-Yam. General features of complex systems. *Encyclopedia of Life Support Systems (EOLSS), UNESCO, EOLSS Publishers, Oxford, UK*, 2002.

[5] Philip W Anderson et al. More is different. *Science*, 177(4047):393–396, 1972.

[6] Pier Luigi Luisi. *The emergence of life: from chemical origins to synthetic biology*. Cambridge University Press, 2006.

[7] Michael Batty. *Cities and complexity: understanding cities with cellular automata, agent-based models, and fractals*. The MIT press, 2007.

[8] Giorgio Parisi. Complex systems: a physicist's viewpoint. *Physica A: Statistical Mechanics and its Applications*, 263(1):557–564, 1999.

[9] RB Levien and SM Tan. Double pendulum: An experiment in chaos. *American Journal of Physics*, 61:1038–1038, 1993.

[10] Steven H Strogatz. *Nonlinear dynamics and chaos: with applications to physics, biology, chemistry, and engineering*. Westview press, 2014.

[11] Raymond-Alain Thietart and Bernard Forgues. Chaos theory and organization. *Organization science*, 6(1):19–31, 1995.

[12] J Doyne Farmer, Fabrizio Lillo, et al. On the origin of power-law tails in price fluctuations. *Quantitative Finance*, 4(1):7–11, 2004.

[13] Michelle Girvan and Mark EJ Newman. Community structure in social and biological networks. *Proceedings of the national academy of sciences*, 99(12):7821–7826, 2002.

[14] Rosario N Mantegna. Hierarchical structure in financial markets. *The European Physical Journal B-Condensed Matter and Complex Systems*, 11(1):193–197, 1999.

[15] Fusakichi Omori. *On the after-shocks of earthquakes*, volume 7. The University, 1894.

[16] Joshua M Epstein and Robert Axtell. *Growing artificial societies: social science from the bottom up*. Brookings Institution Press, 1996.

[17] Eric Bonabeau. Agent-based modeling: Methods and techniques for simulating human systems. *Proceedings of the National Academy of Sciences*, 99(suppl 3):7280–7287, 2002.

[18] Pedro Domingos. The role of occam's razor in knowledge discovery. *Data mining and knowledge discovery*, 3(4):409–425, 1999.

[19] J Doyne Farmer, Paolo Patelli, and Ilija I Zovko. The predictive power of zero intelligence in financial markets. *Proceedings of the National Academy of Sciences of the United States of America*, 102(6):2254–2259, 2005.

[20] Thomas C Schelling. Dynamic models of segregation†. *Journal of mathematical sociology*, 1(2):143–186, 1971.

[21] Alison J Heppenstall, Andrew T Crooks, Linda M See, and Michael Batty. *Agent-based models of geographical systems*. Springer Science & Business Media, 2011.

[22] Andrei Borshchev and Alexei Filippov. From system dynamics and discrete event to practical agent based modeling: reasons, techniques, tools. In *Proceedings of the 22nd international conference of the system dynamics society*, volume 22. Citeseer, 2004.

[23] Alessandro Troisi, Vance Wong, and Mark A Ratner. An agent-based approach for modeling molecular self-organization. *Proceedings of the National Academy of Sciences of the United States of America*, 102(2):255–260, 2005.

[24] Dimitrios M Tsangaris and Juan José de Pablo. Bond-bias simulation of phase equilibria for strongly associating fluids. *The Journal of chemical physics*, 101(2):1477–1489, 1994.

[25] Marta Luisa Ciofi Degli Atti, Stefano Merler, Caterina Rizzo, Marco Ajelli, Marco Massari, Piero Manfredi, Cesare Furlanello, Gianpaolo Scalia Tomba, and Mimmo Iannelli. Mitigation measures for pandemic influenza in italy: an individual based model considering different scenarios. *PloS one*, 3(3):e1790, 2008.

[26] Marco Ajelli, Bruno Gonçalves, Duygu Balcan, Vittoria Colizza, Hao Hu, José J Ramasco, Stefano Merler, and Alessandro Vespignani. Comparing large-scale computational approaches to epidemic modeling: agent-based versus structured metapopulation models. *BMC infectious diseases*, 10(1):1, 2010.

[27] Lutz Schimansky-Geier, Michaela Mieth, Helge Rosé, and Horst Malchow. Structure formation by active brownian particles. *Physics Letters A*, 207(3):140–146, 1995.

[28] Werner Ebeling and Frank Schweitzer. Swarms of particle agents with harmonic interactions. *Theory in Biosciences*, 120(3-4):207–224, 2001.

[29] Gerardo Beni and Jing Wang. Swarm intelligence in cellular robotic systems. In *Robots and Biological Systems: Towards a New Bionics?*, pages 703–712. Springer, 1993.

[30] Marco Dorigo, Mauro Birattari, and Thomas Stutzle. Ant colony optimization. *IEEE computational intelligence magazine*, 1(4):28–39, 2006.

[31] Craig W Reynolds. Flocks, herds and schools: A distributed behavioral model. *ACM SIGGRAPH computer graphics*, 21(4):25–34, 1987.

[32] Gavin Fullstone, Jonathan Wood, Mike Holcombe, and Giuseppe Battaglia. Modelling the transport of nanoparticles under blood flow using an agent-based approach. *Scientific reports*, 5, 2015.

[33] Joshua M Epstein, Ramesh Pankajakshan, and Ross A Hammond. Combining computational fluid dynamics and agent-based modeling: a new approach to evacuation planning. *PloS one*, 6(5):e20139, 2011.

[34] Anirban Chakraborti, Damien Challet, Arnab Chatterjee, Matteo Marsili, Yi-Cheng Zhang, and Bikas K Chakrabarti. Statistical mechanics of competitive resource allocation using agent-based models. *Physics Reports*, 552:1–25, 2015.

[35] W Brian Arthur. Inductive reasoning and bounded rationality. *The American economic review*, 84(2):406–411, 1994.

[36] Damien Challet, Matteo Marsili, and Riccardo Zecchina. Statistical mechanics of systems with heterogeneous agents: Minority games. *Physical Review Letters*, 84(8):1824, 2000.

[37] Massimiliano Zanin and Fabrizio Lillo. Modelling the air transport with complex networks: A short review. *The European Physical Journal Special Topics*, 215(1):5–21, 2013.

[38] Jiaoe Wang, Huihui Mo, Fahui Wang, and Fengjun Jin. Exploring the network structure and nodal centrality of china's air transport network: A complex network approach. *Journal of Transport Geography*, 19(4):712–721, 2011.

[39] Chi Li-Ping, Wang Ru, Su Hang, Xu Xin-Ping, Zhao Jin-Song, Li Wei, and Cai Xu. Structural properties of us flight network. *Chinese physics letters*, 20(8):1393, 2003.

[40] Alain Barrat, Marc Barthelemy, Romualdo Pastor-Satorras, and Alessandro Vespignani. The architecture of complex weighted networks. *Proceedings of the National Academy of Sciences of the United States of America*, 101(11):3747–3752, 2004.

[41] LP Chi and X Cai. Structural changes caused by error and attack tolerance in us airport network. *International Journal of Modern Physics B*, 18(17n19):2394–2400, 2004.

[42] Wei Li and Xu Cai. Statistical analysis of airport network of china. *Physical Review E*, 69(4):046106, 2004.

[43] Gérald Gurtner, Stefania Vitali, Marco Cipolla, Fabrizio Lillo, Rosario Nunzio Mantegna, Salvatore Miccichè, and Simone Pozzi. Multi-scale analysis of the european airspace using network community detection. *PloS one*, 9(5):e94414, 2014.

[44] Eurocontrol. Challenges of Growth 2013. Technical report, Eurocontrol, 2013.

[45] SESAR. SESAR definition phase D3: The ATM target concept. Technical Report September, SESAR, 2007.

[46] EC. COMMISSION REGULATION (EU) No 691/2010. Technical Report 11, European Commission, 2010.

[47] Eurocontrol. Eurocontrol final report on european commission's mandate to support the establishment of functional airspace blocks (FABs). Technical Report May, Eurocontrol, 2005.

[48] EUROCONTROL. Free Route Developments in Europe. (February), 2012.

[49] Eurocontrol. European free route airspace developments. Technical report, Eurocontrol, 2015.

[50] C Bongiorno, G Gurtner, F Lillo, RN Mantegna, and S Micciché. Statistical characterization of deviations from planned flight trajectories in air traffic management. *Journal of Air Transport Management*, (58C):152–163, 2017.

[51] James K Kuchar and Lee C Yang. A review of conflict detection and resolution modeling methods. *IEEE Transactions on intelligent transportation systems*, 1(4):179–189, 2000.

[52] Adrian K Agogino and Kagan Tumer. A multiagent approach to managing air traffic flow. *Autonomous Agents and Multi-Agent Systems*, 24(1):1–25, 2012.

[53] Karen M Feigh, Amy R Pritchett, AP Shah, SA Kalaver, A Jadhav, DM Holl, RC Bea, and AZ Gilgur. Analyzing air traffic management systems using agent-based modeling and simulation. 2005.

[54] Nicolas Durand, Jean-Marc Alliot, and Geraud Granger. Optimal resolution of en route conflicts. In *Procceedings of the 1rst USA/Europe Seminar*, 1997.

[55] Karl D Bilimoria. A geometric optimization approach to aircraft conflict resolution. In *AIAA guidance, navigation, and control conference and exhibit*, pages 14–17. AIAA Reston, VA, 2000.

[56] Martin S Eby and Wallace E Kelly. Free flight separation assurance using distributed algorithms. In *Aerospace Conference, 1999. Proceedings. 1999 IEEE*, volume 2, pages 429–441. IEEE, 1999.

[57] Karen Harper, Sean Guarino, Aaron White, Mark Hanson, Karl Bilimoria, and Daniel Mulfinger. An agent-based approach to aircraft conflict resolution with constraints. *AIAA Paper*, 4552, 2002.

[58] Géraud Granger, Nicolas Durand, and Jean-Marc Alliot. Optimal resolution of en route conflicts. In *ATM 2001, 4th USA/Europe Air Traffic Management Research and Development Seminar*, 2001.

[59] C Bongiorno, S Miccicè, G Gurtner, F Lillo, L Valori, M Ducci, B Monechi, and S Pozzi. An agent based model of air traffic management. *Proceedings of the SESAR Innovation Days, EUROCONTROL*, 2013:N40, 2013.

[60] Gérald Gurtner, Christian Bongiorno, Marco Ducci, and Salvatore Micciché. An empirically grounded agent based simulator for the air traffic management in the sesar scenario. *Journal of Air Transport Management*, (59C):26–43, 2017.

[61] C Bongiorno, S Micciché, and Rosario N Mantegna. An empirically grounded agent based model for modeling directs, conflict detection and resolution operations in air traffic management. *arXiv preprint arXiv:1609.08030*, 2016.

[62] Roger Guimera, Stefano Mossa, Adrian Turtschi, and LA Nunes Amaral. The worldwide air transportation network: Anomalous centrality, community structure, and cities' global roles. *Proceedings of the National Academy of Sciences*, 102(22):7794–7799, 2005.

[63] Vittoria Colizza, Alain Barrat, Marc Barthélemy, and Alessandro Vespignani. The role of the airline transportation network in the prediction and predictability of global epidemics. *Proceedings of the National Academy of Sciences of the United States of America*, 103(7):2015–2020, 2006.

[64] Michele Guida and Funaro Maria. Topology of the italian airport network: A scale-free small-world network with a fractal structure? *Chaos, Solitons & Fractals*, 31(3):527–536, 2007.

[65] Ganesh Bagler. Analysis of the airport network of india as a complex weighted network. *Physica A: Statistical Mechanics and its Applications*, 387(12):2972–2980, 2008.

[66] Zengwang Xu and Robert Harriss. Exploring the structure of the us intercity passenger air transportation network: a weighted complex network approach. *GeoJournal*, 73(2):87–102, 2008.

[67] Alessio Cardillo, Jesús Gómez-Gardenes, Massimiliano Zanin, Miguel Romance, David Papo, Francisco del Pozo, and Stefano Boccaletti. Emergence of network features from multiplexity. *arXiv preprint arXiv:1212.2153*, 2012.

[68] Marcelo FC Gomes, Ana Pastore y Piontti, Luca Rossi, Dennis Chao, Ira Longini, M Elizabeth Halloran, and Alessandro Vespignani. Assessing the international spreading risk associated with the 2014 west african ebola outbreak. *PLOS Currents Outbreaks*, 2014.

[69] Paolo Malighetti, Stefano Paleari, and Renato Redondi. Connectivity of the european airport network:"self-help hubbing" and business implications. *Journal of Air Transport Management*, 14(2):53–65, 2008.

[70] Lucas Lacasa, Miguel Cea, and Massimiliano Zanin. Jamming transition in air transportation networks. *Physica A: Statistical Mechanics and its Applications*, 388(18):3948–3954, 2009.

[71] Soufian Ben Amor and Marc Bui. A complex system approach in modeling airspace congestion dynamics. *Editorial and Advisory Board*, 3(1):39, 2012.

[72] Cai Kai-Quan, Zhang Jun, Du Wen-Bo, and Cao Xian-Bin. Analysis of the chinese air route network as a complex network. *Chinese Physics B*, 21(2):028903, 2012.

[73] Andrew Cook, G Tanner, S Cristóbal, and M Zanin. New perspectives for air transport performance. *Policy*, 1:P1, 2013.

[74] Pablo Fleurquin, José J Ramasco, and Victor M Eguiluz. Systemic delay propagation in the us airport network. *Scientific reports*, 3, 2013.

[75] Nikolas Pyrgiotis, Kerry M Malone, and Amedeo Odoni. Modelling delay propagation within an airport network. *Transportation Research Part C: Emerging Technologies*, 27:60–75, 2013.

[76] Alessio Cardillo, Massimiliano Zanin, Jesús Gómez-Gardenes, Miguel Romance, Alejandro J García del Amo, and Stefano Boccaletti. Modeling the multi-layer nature of the european air transport network: Resilience and passengers re-scheduling under random failures. *The European Physical Journal Special Topics*, 215(1):23–33, 2013.

[77] B Campanelli, P Fleurquin, VM Eguíluz, JJ Ramasco, A Arranz, I Etxebarria, and C Ciruelos. Modeling reactionary delays in the european air transport network. *Proceedings of the Fourth SESAR Innovation Days, Schaefer D (Ed.), Madrid*, 2014.

[78] Massimiliano Zanin. Network analysis reveals patterns behind air safety events. *Physica A: Statistical Mechanics and its Applications*, 401:201–206, 2014.

[79] Andrew Cook, Henk AP Blom, Fabrizio Lillo, Rosario Nunzio Mantegna, Salvatore Micciche, Damián Rivas, Rafael Vázquez, and Massimiliano Zanin. Applying complexity science to air traffic management. *Journal of Air Transport Management*, 42:149–158, 2015.

[80] JU SESAR. Sesar concept of operations step 1, 2012.

[81] EUROCONTROL. Ddr reference manual 1.5.8, ddr version: 1.5.8. `http://www.eurocontrol.int/services/demand-data-repository-ddr`, 2010.

[82] Performance Review Commission. Performance review report. `http://www.eurocontrol.int/sites/default/files/publication/files/prr-2013.pdf`, 2013.

[83] Edwin B Wilson. Probable inference, the law of succession, and statistical inference. *Journal of the American Statistical Association*, 22(158):209–212, 1927.

[84] C Bongiorno, S Miccichè, RN Mantegna, G Gurtner, F Lillo, and S Pozzi. Adaptative air traffic network: statistical regularities in air traffic management. In *presented at the 11$^{th}$ USA/Europe ATM R&D Seminar, 23-26 June 2015, Lisbon, Portugal.*

[85] Ronald A Fisher. On the interpretation of $\chi$ 2 from contingency tables, and the calculation of p. *Journal of the Royal Statistical Society*, 85(1):87–94, 1922.

[86] Isabelle Rivals, Léon Personnaz, Lieng Taing, and Marie-Claude Potier. Enrichment or depletion of a go category within a class of genes: which test? *Bioinformatics*, 23(4):401–407, 2007.

[87] Sture Holm. A simple sequentially rejective multiple test procedure. *Scandinavian journal of statistics*, pages 65–70, 1979.

[88] Shannon Zelinski and Michael Jastrzebski. Defining dynamic route structure for airspace configuration. *Proceedings of the Institution of Mechanical Engineers, Part G: Journal of Aerospace Engineering*, 226(9):1161–1170, 2012.

[89] Sergio Ruiz, Miquel A Piera, Jenaro Nosedal, and Andrea Ranieri. Strategic de-confliction in the presence of a large number of 4d trajectories using a causal modeling approach. *Transportation Research Part C: Emerging Technologies*, 39:129–147, 2014.

[90] Supatcha Chaimatanan, Daniel Delahaye, and Marcel Mongeau. A hybrid metaheuristic optimization algorithm for strategic planning of 4d aircraft trajectories at the continental scale. *IEEE Computational Intelligence Magazine*, 9(4):46–61, 2014.

[91] Adrian Agogino and Kagan Tumer. Regulating air traffic flow with coupled agents. In *Proceedings of the 7th international joint conference on Autonomous agents and multiagent systems-Volume 2*, pages 535–542. International Foundation for Autonomous Agents and Multiagent Systems, 2008.

[92] S Wolfe, P Jarvis, F Enomoto, Maarten Sierhuis, B Putten, and K Sheth. A multi-agent simulation of collaborative air traffic flow management. *Multi-agent Systems for Traffic and Transportation. IGI Global Publishing*, 2009.

[93] Brian W Kernighan and Dennis M Ritchie. The c programming language. 2006.

[94] Gérald Gurtner, Luca Valori, and Fabrizio Lillo. Competitive allocation of resources on a network: an agent-based model of air companies competing for the best routes. *Journal of Statistical Mechanics: Theory and Experiment*, 2015(5):P05028, 2015.

[95] William Marshall Smart. *Text-book on spherical astronomy*. CUP Archive, 1947.

[96] ICAO Doc. 4444–procedures for air navigation services–air traffic management. *Montreal, QC, Canada: The International Civil Aviation Organization (ICAO)*.

[97] ELSA project. *E.02.18-ELSA D1.3 Statistical Regularities in ATM - final draft*. Version: 21/12/2012, (Restricted audience).

[98] Jonathan M Histon, R John Hansman, Blake Gottlieb, Howard Kleinwaks, Sarah Yenson, Daniel Delahaye, and Stéphane Puechmorel. Structural considerations and cognitive complexity in air traffic control. In *Digital Avionics Systems Conference, 2002. Proceedings. The 21st*, volume 1, pages 1C2–1, 2002.